9-3-2013

Dynamic vegetation Roughness in the riparian zone

Tyler Gillihan

Tyler Gillihan
Candidate

Civil Engineering
Department

This thesis is approved, and it is acceptable in quality and form for publication.

Approved by the Thesis Committee:

Dr. Mark Stone, Chairperson

Dr. Julie Coonrod

Dr. Kerry Howe

Dynamic Vegetation Roughness in the Riparian Zone

BY

Tyler Gillihan

Bachelor of Science
Department of Civil Engineering
University of New Mexico, 2011

Submitted in Partial Fulfillment of the
Requirements for the Degree of

Master of Science
Civil Engineering

The University of New Mexico
Albuquerque, New Mexico

July, 2013

Dynamic Vegetation Roughness in the Riparian Zone

BY

Tyler Gillihan

B.S. CIVIL ENGINEERING, UNIVERSITY OF NEW MEXICO, 2011

M.S. CIVIL ENGINEERING, UNIVERSITY OF NEW MEXICO, 2013

ABSTRACT

Vegetation in the floodplain plays an important role in dictating the hydraulics of an open channel river system. While vegetation is beneficial to the biological productivity of the river system, it can also increase flood risk due to increased channel roughness. Traditional means of predicting flow hydraulics involve applying a constant roughness value, while neglecting change in roughness due to flow characteristics and variation of vegetation parameters. The objective of this research was to develop and demonstrate techniques to hydraulically model an open channel river system while taking into account dynamic roughness due to vegetation. The Sedimentation and River Hydraulics in Two-Dimensions (SRH-2D) model was enhanced to use measured vegetation parameters to calculate dynamic Manning's *n* values, referred to as effective *n* (n_e) values, while simulating the hydraulics of the system. Two approaches based on work by Järvelä (2004) and Baptist et al. (2007) were implemented into SRH-2D for roughness computations. Field and modeling work focused on a section of a restoration area along the San Joaquin River near Fresno, California. Both approaches were modeled at four different channel discharges: 31.2, 70.8, 113.3, and 212.4 m^3/s. A sensitivity analysis was also performed for both approaches at 113.3 m^3/s for parameters of uncertainty. A wide range of calculated n_e values showed that roughness is dependent

on velocity and flow depth. Both approaches underpredicted water surface elevation when compared to calibrated models. The difference in water surface elevations between the calibrated models and the roughness models varied with channel discharge, with both approaches performing equally. Both approaches overpredicted velocity in a similar fashion. The sensitivity analysis proved that both techniques are altered by their uncertain parameters. Further research of the uncertain parameters would increase the accuracy of the models and lead to a better understanding of dynamic roughness.

Table of Contents

List of Figures

List of Tables

Introduction

Vegetation plays an important role in the natural processes of open channel river systems. The biological productivity of vegetation in the flood plain is both beneficial to the river system and the human population surrounding the system (Poff et al. 1997). While vegetation along the floodplain is an integral part of maintaining the river's natural habitat, it also increases local flood risk. To reduce risk, it is preferred to minimize flow resistance in sites that are sensitive to flooding (Darby 1999). Roughness is also important for understanding other open channel flow characteristics such as velocity distribution, shear stress, and momentum exchange all of which are difficult to evaluate on a macro scale and require a require an understanding of local dynamic roughness to address areas of interest (Vermaas et al. 2011). For this reason it is important to understand friction imparted by vegetation in open channel systems.

The efforts to characterize roughness in natural open channel systems are complex. The majority of research that has been done on this topic does not focus on vegetated floodplains (Arcement and Schneider 1989). The equation developed by Robert Manning in 1891 is widely used to describe open channel flow (Fischenich 2000). The equation was developed empirically by taking the average velocity of the seven most common open channel equations at the time, and developing them further based on observations of the Mississippi River (Fischenich 2000). The Manning's equation is defined by $V = \frac{k_n}{n} R^{2/3} S^{1/2}$ where V is the average cross-sectional velocity, R is the hydraulic radius, S is the energy slope, k_n is a constant dependent on the units used, and n

is the Manning resistance coefficient. The Manning's resistant coefficient is dependent on the material type in the channel and is difficult to assign in a natural system.

Channel roughness is dependent on the hydrodynamics of the system. This includes both pressure and frictional forces caused by vegetative elements and the channel surface bed (Thompson and Roberson 1976). Typically a constant roughness value is estimated and assigned to a given length of channel. This estimation can be reasonable when friction dominates; meaning forces due to blunt bodies such as vegetation are minimal or non-existent. Unfortunately, this is not the case in many open channel systems. In densely vegetated open channels this typically does not apply because pressure forces imparted by the momentum absorbing area have a tendency to dominate (Kouwen and Fathi-Moghadam 2000).

Early methods focused on assigning unique constant values to various species of vegetation and land-use types. These methods were often based on observation and did not change dynamically with flow. Chow (1959) established a comprehensive list of constant Manning's *n* values for various land uses. This list is still often used in assigning Manning's *n* values for large open channel reaches. Currently there are more contemporary techniques that have been developed for the purpose of understanding roughness based on vegetation characteristics (Baptist et al. 2007; Darby 1999; Järvelä 2004; Kouwen and Fathi-Moghadam 2000; Nepf 1999). These techniques typically range from physical to empirical and have yielded accurate results in determining roughness. These techniques have yielded promising results on a small scale but have yet to be tested on a larger practical scale (Aberle and Järvelä 2013).

This research focuses on assessing vegetation roughness on a large scale. Two of the previously mentioned vegetation roughness approaches were implemented into hydraulic modeling software in an attempt to better understand the effects of hydraulic roughness. The objectives of this research were to: 1) develop and demonstrate a technique to hydraulically model river systems while taking into account dynamic roughness due to vegetation, 2) compare the results of the dynamic roughness models to highly calibrated traditional hydraulic models to assess accuracy, 3) determine which roughness approach developed is most appropriate for calculating roughness.

The technique developed involves measuring physical characteristics of various vegetation species in the field and implementing them into hydraulic modeling software. The Sedimentation and River Hydraulics in Two-Dimensions (SRH-2D) model was modified to use two different approaches based on work by Järvelä (2004) and Baptist et al. (2007) to calculate dynamic Manning's *n* values, herby referred to as effective *n* (n_e) values, and use them to model the hydraulics of the system. A reach along the San Joaquin River was chosen to demonstrate this modeling approach. Both the Järvelä and Baptist vegetation roughness hydraulic models were compared to previously developed calibrated models of the same reach to determine the best performing technique.

State of Knowledge

There has been significant research on the development of analytical and physical methods of quantifying vegetation roughness (Baptist et al. 2007; Darby 1999; Fathi-Maghadam and Kouwen 1997; Fischenich and Dudley 1999; Järvelä 2004; Kouwen and Fathi-Moghadam 2000; Nepf 1999; Thompson and Roberson 1976). As a result,

numerous techniques have been developed for the purpose of understanding and predicting vegetation induced roughness.

Thompson and Roberson (1976) developed one of the first analytical models to describe open channel roughness in channels lined with vegetation. The model uses small diameter cylinders to simulate roughness imparted by vegetation. Vegetation parameters such as height, diameter, and flexural rigidity were expressed in order to calculate roughness. Through a series of computations vegetation roughness, channel velocity, and shear stress were calculated and compared with experimental data with favorable results. Thompson and Roberson (1976) concluded that this model provides a theoretical basis for computing vegetation roughness.

Methods have been developed to model both vegetation and sediment roughness. Darby (1999) developed a model that would analyze roughness at each node of a created mesh. A total of six different empirically derived approaches were used to calculate roughness based on either two different types of sediment and four types of vegetation (Darby 1999). Empirically derived equations are used to calculate roughness and are based off of field measurements such as stem density, rigidity, height, and spacing. The model aids in determining stage-discharge curves and gives a better understanding of floodplain roughness. This method is limited due to difficult field measurements of rigidity and spacing.

Mathematical models derived by physical experiments have also been used in attempts at quantifying vegetation roughness. Fathi-Maghadam and Kouwen (1997) developed a model using pine and cedar tree saplings in a flume experiment to derive

physically based equations using dimensional analysis. This procedure allowed for the calculation of roughness in tall, woody, flexible, non-submerged vegetation. Results showed that, "Manning's *n* value increases proportionally to the square root of flow depth and inversely proportional to the mean velocity," (Fathi-Maghadam and Kouwen 1997). This model was later modified by Kouwen and Fathi-Moghadam (2000) to take into account vegetation parameters such as species, size, and density. The modified model assumed an increase in vegetation foliage area with height and thus showed that vegetation density is a crucial factor when calculating roughness (Kouwen and Fathi-Moghadam 2000).

Some techniques focus on estimation of drag forces in order to calculate roughness coefficients. Fischenich and Dudley (2000) developed simple field techniques for determining drag forces based on measuring vegetation geometry and leaf area index (LAI). Nepf (1999) presented a model relating drag, turbulence, and diffusion in emergent vegetation. Results of this work showed that turbulence is highly dependent on vegetative drag even in cases of sparse vegetation (Nepf 1999).

Baptist et al. (2007) introduced four analytical methods for determining vegetation roughness. The first method involved development of physically derived equations based on flow depth. The second was based on an analytical solution of the momentum equation. The third used a 1-DV turbulent model to describe resistance based on vegetation parameters. Finally, the last used genetic programming to modify the turbulent model based on synthetic data. Baptist et al. (2007) found that a genetic programming equation yielded the best results when compared to both laboratory flume experiments and previous values found in the literature.

A physical technique developed by Järvelä (2004) involves using field measurements of vegetation and physically derived equations to determine vegetation roughness. This technique is limited to emergent vegetation and low velocity (Juha Järvelä 2004). This technique and the physically derived method developed by Baptist et al. (2007) are the basis of the vegetation roughness computations in the newly developed SRH-2DV software used for this study.

Site Description

This research took place on a section of the San Joaquin River west of Fresno, California. A restoration area has been designated on the river that stretches from the Friant Dam to the confluence of the Merced River, for a total of 246 river kilometers (153 river miles) (SJRRP 2008). Field work was concentrated primarily in reach 1B with slight overlap in Reaches 1A and 2A. Reach 1A extends from the Friant Dam to the Highway 99 bridge, Reach 1B extends from the Highway 99 Bridge to Gravelly Ford, and Reach 2A extends from Gravelly Ford to the Chowchilla Bifurcation. These reaches were chosen due to their diverse vegetation. Figure 1 depicts an overview of the entire restoration area.

Figure 1: Restoration area designated by Reclamation, broken up into individual reaches (Reclamation 2012)

The restoration area has been classified by Moise and Hendrickson (2002) to have 30 different classes of vegetation along this stretch of the river. These include 11 types of vegetation based on Holland's system and consist of cottonwood riparian forest, herbaceous, mixed riparian forest, willow riparian forest, riparian oak forest, riparian scrub, river wash, wetland, willow scrub, exotic tree, and arundo (Holland 1986). To

further classify woody types, Moise added a numerical value from 1 to 6 to indicate branch density of the species based on Hink and Omhart's work (1984).

The field data measured represents the most common vegetation in reaches along the restoration area. Vegetation measured consisted of cottonwood riparian of branch density 3, cottonwood riparian low density of branch density 4, herbaceous, mixed riparian of branch density 1 and 3, mixed riparian low density of branch density 6, riparian scrub, willow riparian of branch density 3 and 4, willow scrub of branch density 5 and 6, and willow scrub low density of branch density 6. Field data measurements consisted of vegetation height, stem diameter, density, and Leaf Area Index (LAI). The unit less parameter LAI is defined as the ratio of the area of one side of leaf tissue to the unit ground area. A detailed description of field work can be found in Appendix A. Figure 2 shows different classes of vegetation represented by polygon areas near field site 3.

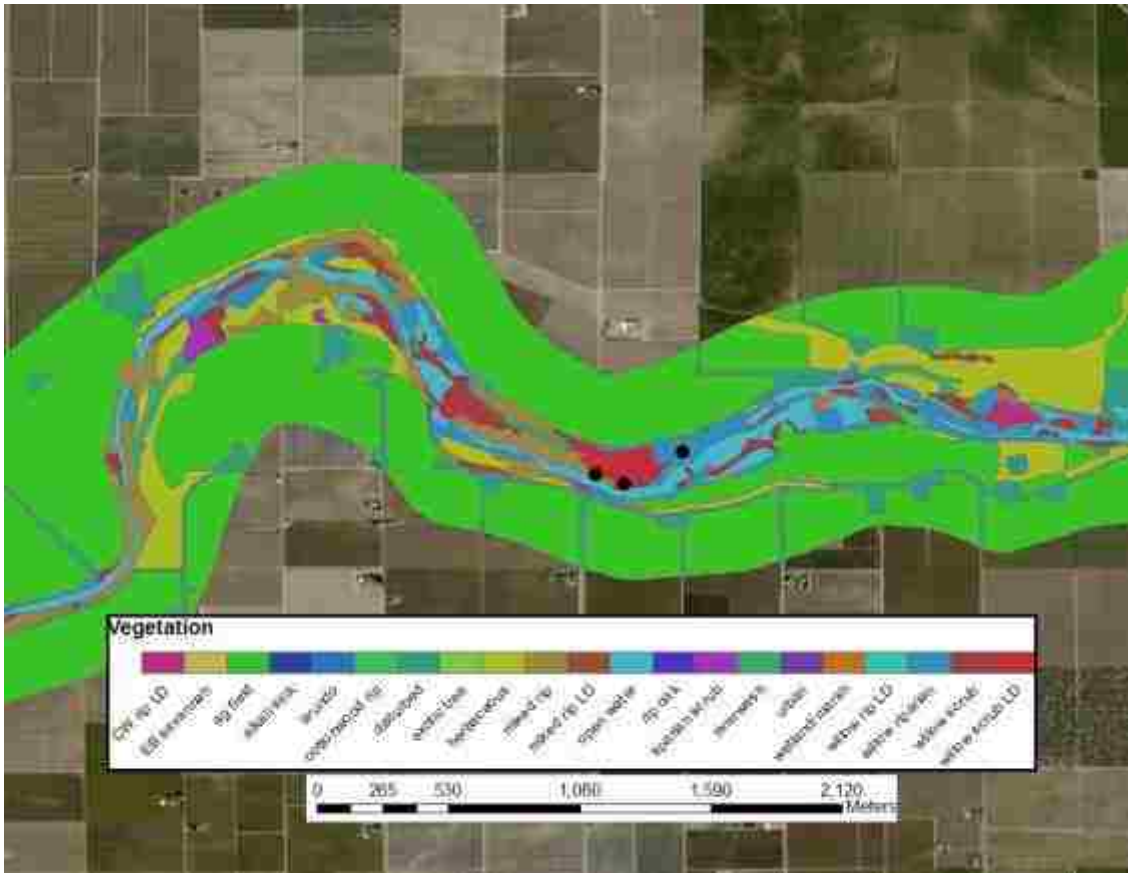

Figure 2: Vegetation classes near field site 3 indicated by the black dots

SRH-2DV

SRH-2D is a two dimensional hydraulic model developed by the United States Bureau of Reclamation. SRH-2D was designed to model flow hydraulics in open channel river systems by solving the two dimensional depth-averaged dynamic wave equations, otherwise known as the St. Venant equations (Lai 2008). The modeling software requires the use of a two dimensional mesh, created in the 3rd party program SMS (Surface-Water Modeling System), for spatial information. For more background information regarding the SRH-2D model, refer to Appendix C and Lai (2008).

The original SRH-2D was revised to calculate dynamic Manning's *n* values, referred to as effective *n* (n_e) values in this study, and hence affect the outcome of the solutions to the St. Venant equations. The resulting model is referred to as SRH-2DV, for vegetation. Reclamation developed the model to utilize techniques based on equations developed by Baptist et al (2007) and Järvelä (2004), to calculate channel roughness imparted by vegetation in the plain of flow. The model initially uses the default roughness values specified in the SRH-2D preprocessor based on the material properties (streambed sediments and vegetation) in the mesh. The model then proceeds to calculate a new roughness value at each mesh cell based on user specified vegetation parameters, along with parameters calculated by the St. Venant equations such as velocity and water depth. The model calculates these roughness values based on a user specified time step. While calculating roughness values at each cell, the model proceeds to recalculate the hydraulic flow depth, velocity, shear stress, and Froude number, hence entering an iterative cycle of hydraulic and roughness calculations. Eventually steady state is reached for both hydraulic and roughness calculations.

The Järvelä approach is based on descriptions of submerged or non-submerged, flexible, woody vegetation. Järvelä (2004) uses the equation below to describe channel roughness imparted by vegetation, where *f* is the Darcy's friction factor, $C_{d\chi}$ is the species specific drag coefficient developed by Järvelä (2004), *LAI* is the leaf area index, *U* is the two dimensional velocity magnitude expressed in meters per second, U_χ is the reference velocity in meters per second, χ is the species specific exponent, *h* is the flow depth in meters, and *H* is the vegetation height in meters.

$$f = 4C_{d\chi}LAI(\frac{U}{U_\chi})^\chi \frac{h}{H}$$

The model then converts Darcy's friction factor to Manning's *n* value by using the following equation.

$$n = h^{\frac{1}{6}} * \sqrt{\frac{f}{8g}}$$

Where *h* is flow depth, *g* is gravity, and *f* is Darcy's friction factor. The model requires parameters $C_{d\chi}$, *LAI*, U_χ, χ, and *H* to be specified. *LAI* and *H* are measured in the field. *U* and *h* are solved internally during model simulation. $C_{d\chi}$ and χ are unit-less values derived from prior work done by Fathi-Moghadam (1996) and are specific to different vegetation species. U_χ is typically used as the lowest velocity when used in determining the value of χ. This value is assumed to be 0.1 m/s (Järvelä 2004).

The Baptist approach is based on submerged or non-submerged cylindrical vegetation (Baptist et al. 2007). The equation below represents channel roughness where C_r is the roughness expressed as the Chezy coefficient, C_b is Chezy's coefficient for a channel bed without vegetation, C_D is the vegetation species drag coefficient, *m* is the

vegetation density specified as number of stems per square meter, *D* is vegetation stem diameter in meters, *h* is flow depth in meters, *g* is gravity expressed in meters per square second, and *H* is vegetation height expressed in meters.

$$C_r = \sqrt{\frac{1}{\frac{1}{C_b^2} + \frac{(C_D m D h)}{2g}}} + \frac{\sqrt{g}}{0.41} * \log(\frac{h}{H})$$

The model then converts C_r to Manning's *n* value using the following equation.

$$n = \frac{1}{C_r} h^{\frac{1}{6}}$$

The model requires C_b, C_D, *D*, *m*, and *H* to be specified prior to simulation. The parameter *h* is solved internally during simulation. The parameters *m*, *D*, and *H* are measured in the field. C_b and C_D are derived from literature or known knowledge of the vegetation's species.

The vegetation model needs additional files and data in to what is required for regular SRH-2D simulations. A GIS shapefile is needed for spatial data to reference the geographic location of each piece of vegetation. The vegetation classes must therefore be broken up into polygons using ArcGIS, as shown above in Figure 2. The software also requires a comma separated values spreadsheet containing numerical values to describe the physical parameters required by the Baptist and Järvelä approaches. One of the columns in the spreadsheet specifies what vegetation approach to use: "Jarvela", "Baptist" or "Default". If specified "Jarvela" or "Baptist", the program uses the respective approach to calculate n_e values for that particular vegetation polygon. If "Default" is specified, the program uses the original default Manning's *n* value applied to that polygon and no calculations are made for that type of vegetation. The spreadsheet's

rows must be numbered the same as the attributes table in the shapefile in order to apply the vegetation classes' parameters to the correct polygon.

Development of Models

The newly developed SRH-2DV model was demonstrated by comparing simulation results to the calibrated models developed by Reclamation for a fish habitat analysis report on the San Joaquin River (Reclamation 2012). The boundary conditions were identical to those used in the calibrated Reclamation models. This method was used for the purpose of consistency so the results of the study could be accurately compared to those of the Reclamation study. A detailed description of model development can be found in Appenix D. For the purpose of this study, modeling efforts focused on Reach 1B due to a larger vegetation density and the majority of field sites lying in the area. The 2D mesh and calibrated model for reach 1B were developed by Reclamation independent of this study (Reclamation 2012).

Calibrated Models

The reach 1B mesh was generated in SMS by Reclamation and was subsequently used for all further hydraulic modeling efforts, both for the fish habitat analysis report and this report. The mesh was generated by developing a topographic model surface using ArcGIS by combining filtered LiDAR data with rasterized channel surfaces based on SONAR data (Reclamation 2012). The 2D mesh was then created in SMS and the topographic model elevation data was imposed onto the mesh. Quadrilateral mesh elements were used in-channel, while tetrahedral elements were used along the floodplain. The average length scale was 9.45 meters for Reach 1B's quadrilateral elements (Reclamation 2012). Figure 3 below shows a section of the 1B mesh generated in SMS.

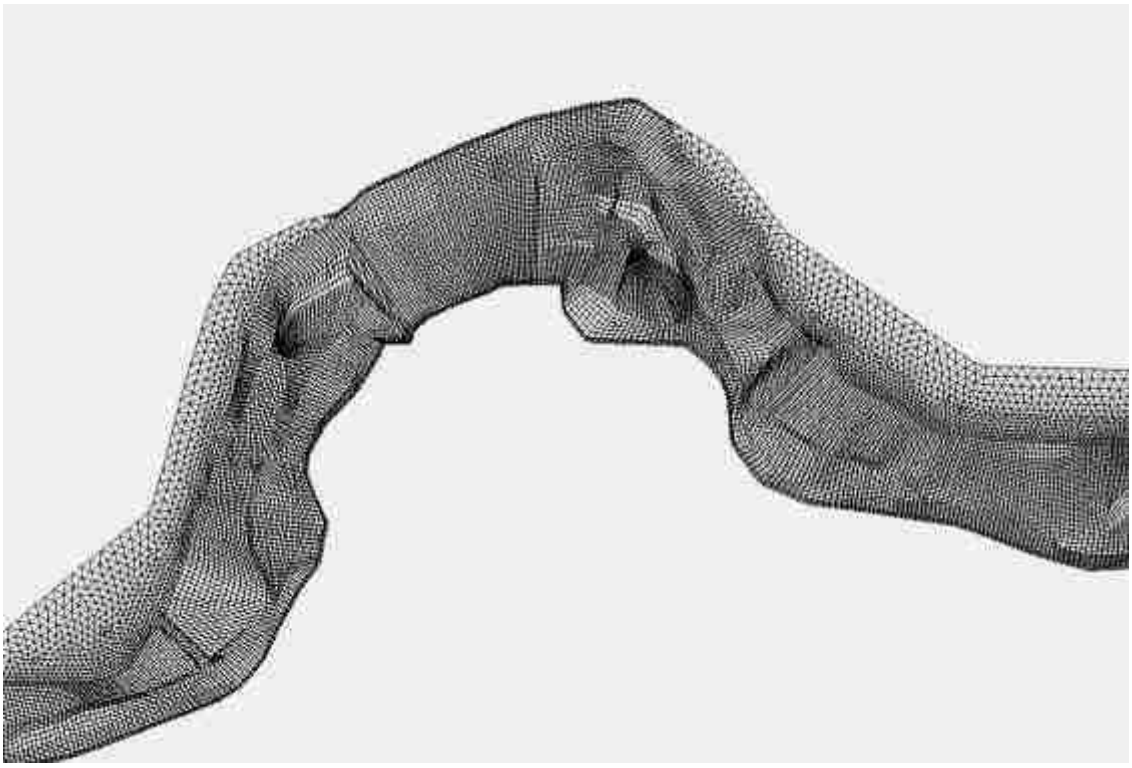

Figure 3: Section of 1B 2D mesh created in SMS

Boundary conditions for the Reclamation calibrated models were based on measured data and were calibrated accordingly. In SRH-2D, downstream boundary conditions are typically expressed as known water surface elevations, while upstream boundary conditions are typically defined by an input flow rate (Lai 2008). Downstream boundary conditions for the reach 1B calibrated models were based on water surface elevations along reach 1B measured by the California Department of Water Resources between the period of April 2010 and October 2011 (SJRRP 2010, 2011). Flow rates were also measured by the CDWR during this time. Discharges of 31.2, 70.8, 113.3, and 212.4 m^3/s (1100, 2500, 4000, 7500 ft^3/s) were chosen as the most appropriate for calibration purposes. Table 1 shows the four flow rates used for the calibrated models

and their corresponding downstream water surface elevations used as the downstream boundary condition for each model.

Table 1: Calibrated models' flow rate and corresponding downstream water surface elevation (WSE)

Flow (m^3/s) Upstream Boundary	WSE (m) Downstream Boundary
31.2	59.94
70.8	60.48
113.3	60.96
212.4	61.69

Channel roughness cannot be measured directly for practical purposes and therefore is typically used as a calibration parameter when developing hydraulic models. Reclamation started calibration with roughness values indicated in the Mussetter Engineering Inc. (2008) study and subsequently altered the values slightly to better meet measured water surface elevations. The mesh was broken into seven different material types, each of which varied in roughness, indicated as Manning's n values. Table 2 below displays the default Manning's n values used for the calibrated models. Figure 4 and Figure 5 display plan views of the Manning's n values mapped to the Reach 1B computational mesh.

Table 2: Manning's *n* values used for each calibrated model (Reclamation 2012)

Land Use Type	***n* Value**
Channel Bed/ Open Water	0.035
Agriculture	0.056
Open/Bare Ground/ Scattered Brush-Weeds	0.056
Scattered Trees/ Light Brush	0.075
Medium Density Trees/ Brush	0.1
Dense Trees/Brush	0.125
Urban/Industrial	0.1

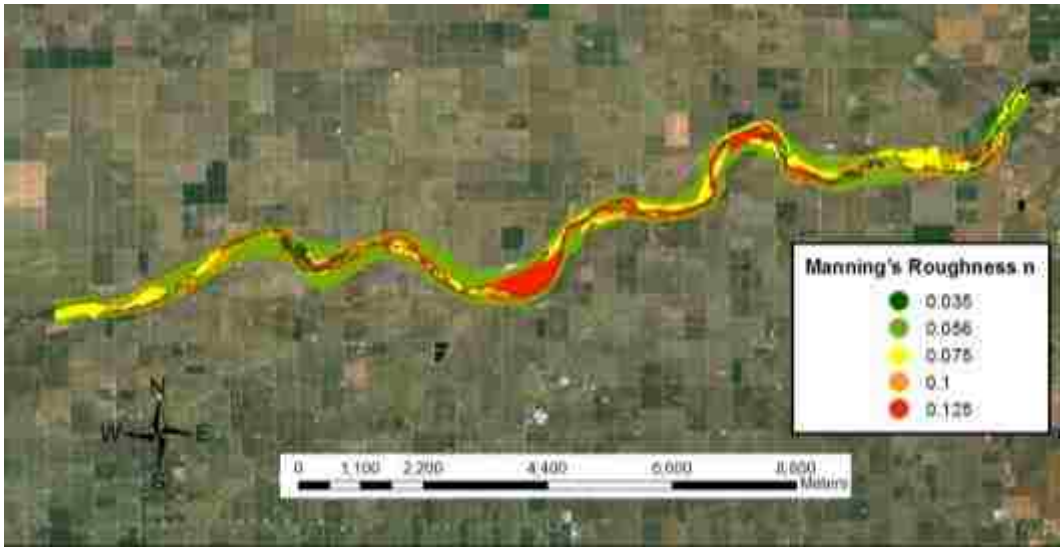

Figure 4: Reach 1B overview of default Manning's *n* values as provided by Reclamation (2012)

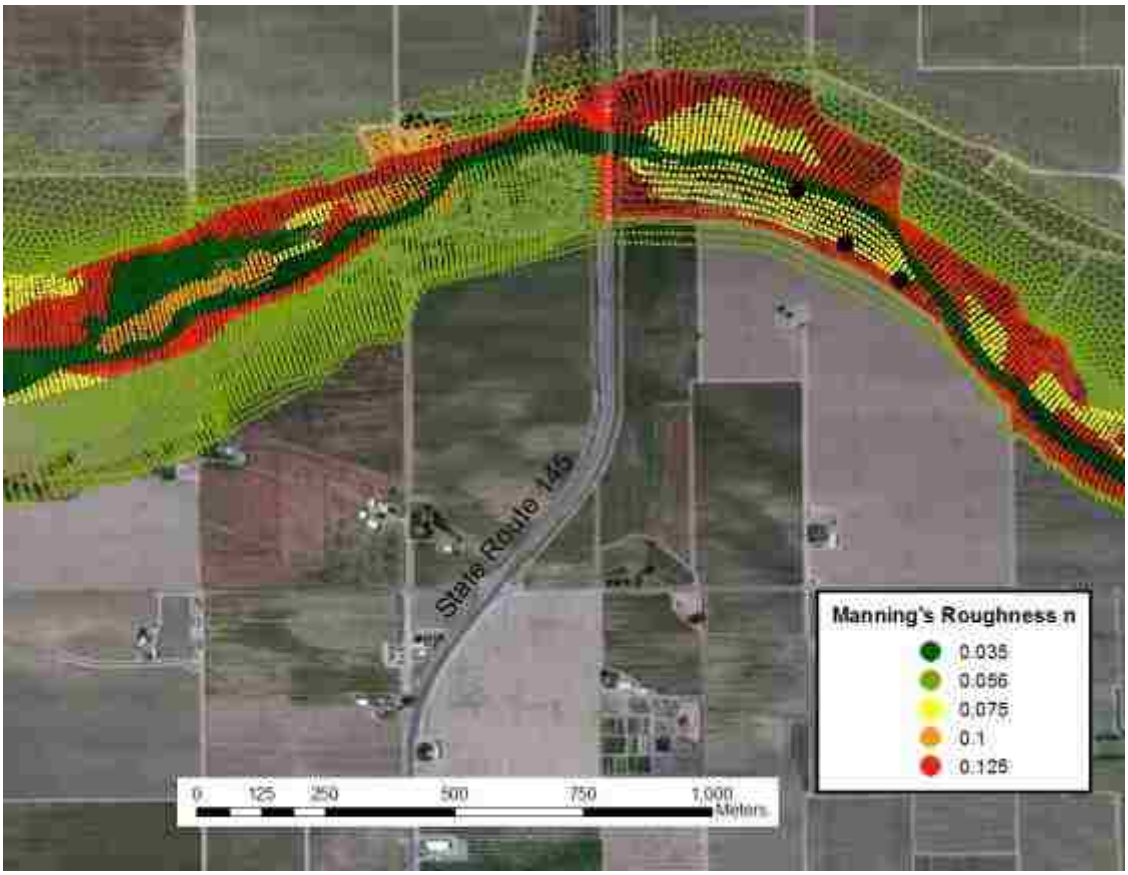

Figure 5: Default Manning's *n* values near field site 4

Calculated Roughness Models

Developments of the SRH-2DV models were created with comparison of the calibrated models in mind in order to have an accurate comparison. For this reason, all of the boundary conditions for these models are the same as the calibrated models. Discharges of 31.2, 70.8, 113.3, and 212.4 m3/s were chosen for these simulations to compare to the calibrated models. Corresponding water surface elevations from the calibrated models were used for the downstream boundary conditions. The specified Manning's n values listed in Table 2 above were used as the initial default roughness values in these models.

A shapefile, containing 5,641 vegetation polygons that span the entire San Joaquin Restoration Area, was provided by Reclamation to be used for this study. The reach 1B mesh only covers 663 of these polygons. The model only considers polygons located in the mesh domain for calculations, and therefore only these 663 were used. This shapefile contained 42 different vegetation classes. Twelve of the classes' parameters were measured directly in the field. See Appendix A for field work. These 12 classes consist of 57.8% of the vegetation polygons in Reach 1B. Five of the 42, accounting for 20.7%, consist of classes that do not involve vegetation and default to the original value of *n* provided. Agriculture consists of 12.1% of classes, of which rarely encountered flow during the simulations due to being too high on the floodplain. The remaining 24 classes that consisted of 9.5% of the reach were not measured in the field. They were assigned values based on their similarity to those measured in the field. For a complete list of vegetation parameters, see Appendix B.

Further boundary conditions had to be specified for the vegetation calculations. Simulations were performed using both the Järvelä and Baptist approaches. The key input parameters for the Järvelä approach involve specifying $C_{d\chi}$, *LAI*, U_χ, χ, and *H*. *LAI* and *H* were measured in the field and have a specific value for each vegetation type. $C_{d\chi,}$ U_χ, and χ had to be specified without field work that pertains to these parameters. Values of U_χ are typically specified as 0.1 m/s and therefore all simulations were performed using this value (Järvelä 2004). $C_{d\chi,}$and χ are species specific and must be chosen based on research. Researched values of $C_{d\chi,}$and χ are currently limited to a small number of vegetation species that include Cedar, Spruce, White Pine, Austrian Pine, and Willow (Fathi-Moghadam 1996). Values of $C_{d\chi}$ range from 0.43 to 0.69 while values of χ range

from -0.57 to -0.38. The vegetation dataset for this study contained a number of species in which these parameters have yet to be defined. For the purpose of this study, values of $C_{d\chi}$ equal to 0.5 and χ equal to -0.45 were used for every piece of vegetation. A sensitivity analysis was performed for these parameters at the 113.3 m^3/s discharge rate. Four extra simulations were performed in which $C_{d\chi}$ was increased and decreased by 0.1 and χ was increased and decreased by 0.1.

The Baptist approach requires specification of C_b, C_D, D, m, and H by the user, prior to simulation. D, m, and H were measured in the field and correspond to a specific vegetation type. C_D was chosen as a single value for all vegetation types in a similar fashion to the Järvelä approach. Determining drag coefficients requires both velocity and frontal area of the object in question (Fischenich and Dudley 1999). This is difficult to measure for natural vegetation in open channel flow, and is often estimated. For this reason, a drag coefficient of 1.0 was chosen for all vegetation types, which is the value often used for hydraulic analysis of vegetation in open channel flow to represent rigid cylinders (e.g. Baptist et al. 2007; Nehal et al. 2012; Petryk and Bosmajian 1975). Two sensitivity analyses were performed at the 113.3 m^3/s discharge by increasing and decreasing the drag coefficient by 0.5 for the two simulations. For the purpose of this study, it was assumed that channel roughness is dominated by vegetation as opposed to the channel bed; therefore C_b was set at a value of 80 for every simulation. This value corresponds to low roughness and results in negligible friction created by the channel bed in the Baptist approach equation (Julien 2002).

Each simulation was started from a hot start, meaning the bed is already wet and begins calculations with the hydraulic conditions of a previous run. Initial simulations at

each target flow were run for 480 hours simulation time, starting with a dry bed and without calculating the dynamic roughness values. The solutions to these runs were used as the hot start files for the vegetation roughness simulations. This was done to reduce the simulation time for the vegetation models. Simulations were run at appropriate lengths of time to reach a hydraulic steady state of: water surface elevations, velocity, and roughness. Each simulation was run for 200 hours. A detailed description of model development and boundary conditions can be found in Appendix D.

Results

The following tables represent the n_e values calculated by the vegetation models in comparison to the default *n* values used by the calibrated models. Five of the seven land use types are listed. Both categories of "Channel Bed/Open Water" and "Urban/Industrial" have not been included because the model does not calculate roughness values for these classes. The tables give minimum, maximum, and average values of n_e for the mesh cells that fall into each land use category. Table 3 displays values for the 31.2 m^3/s models and Table 4 displays values for the 212.4 m^3/s models. For the 70.8 m^3/s and the 113.3 m^3/s, see Appendix E.

Table 3: Summary of n_e values calculated by the vegetation models at 31.2 m^3/s

		Järvelä			Baptist		
Land Use Type	**Default *n***	**Minimum n_e**	**Maximum n_e**	**Average n_e**	**Minimum n_e**	**Maximum n_e**	**Average n_e**
Agriculture	0.056	0.002	0.153	0.056	0.006	0.098	0.056
Open/Bare Ground/ Scattered Brush-Weeds	0.056	0.008	0.152	0.049	0.012	0.098	0.049
Scattered Trees/ Light Brush	0.075	0.003	0.153	0.063	0.010	0.075	0.062
Medium Density Trees/ Brush	0.1	0.008	0.116	0.071	0.015	0.100	0.058
Dense Trees/Brush	0.125	0.003	0.157	0.069	0.010	0.125	0.058

Table 4: Summary of n_e values calculated by the vegetation models at 212.4 m^3/s

		Järvelä			Baptist		
Land Use Type	**Default n**	**Minimum n_e**	**Maximum n_e**	**Average n_e**	**Minimum n_e**	**Maximum n_e**	**Average n_e**
Agriculture	0.056	0.003	0.180	0.032	0.009	0.141	0.042
Open/Bare Ground/ Scattered Brush-Weeds	0.056	0.007	0.130	0.056	0.010	0.141	0.064
Scattered Trees/ Light Brush	0.075	0.003	0.185	0.049	0.011	0.147	0.054
Medium Density Trees/ Brush	0.1	0.005	0.197	0.078	0.012	0.157	0.061
Dense Trees/Brush	0.125	0.003	0.197	0.077	0.010	0.179	0.065

The following figures depict maps of n_e values plotted at cell points in the 2D mesh. These values were calculated using both the Järvelä and Baptist approaches in SRH-2DV and represent the steady state roughness value at the end of the 200 hour simulation time. The maps below focus on an area just downstream of field site 4 (represented by the red dots), located near the State Route 145 Bridge, approximately 14,800 meters downstream of the upstream end of the computational mesh. Maps of both approaches are shown at 31.2 m^3/s and 212.4 m^3/s models. For maps representing the remaining values at 70.8 m^3/s and 113.3 m^3/s, see Appendix E.

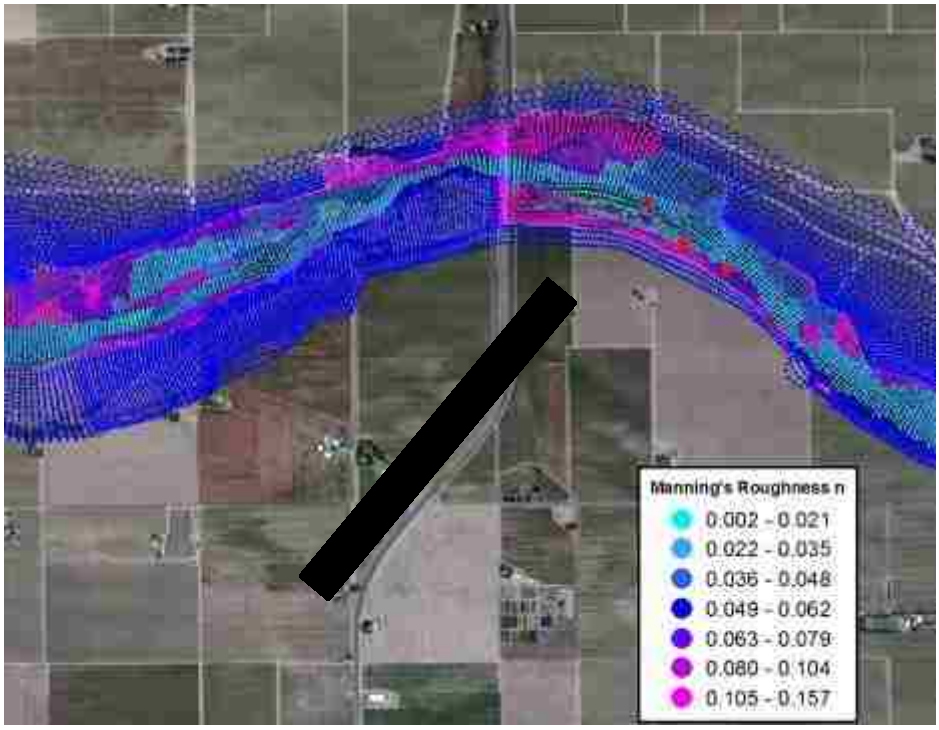

Figure 6: Manning's *n* values near field site 4 with the Järvelä approach at 31.2 m^3/s

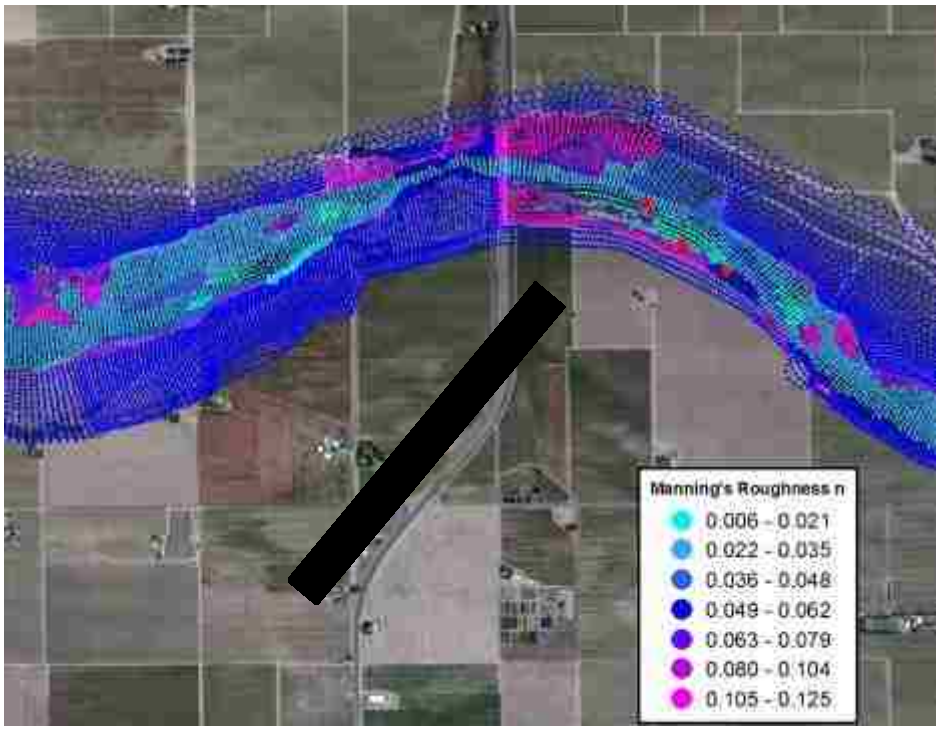

Figure 7: Manning's *n* values near field site 4 with the Baptist approach at 31.2 m^3/s

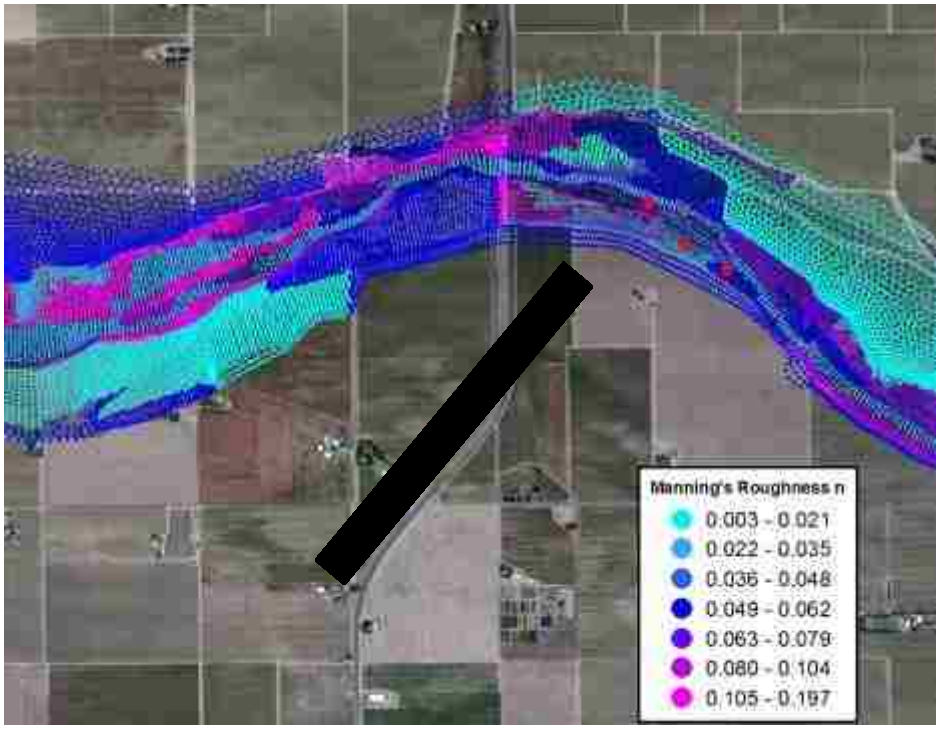

Figure 8: Manning's *n* values near field site 4 with the Järvelä approach at 212.4 m^3/s

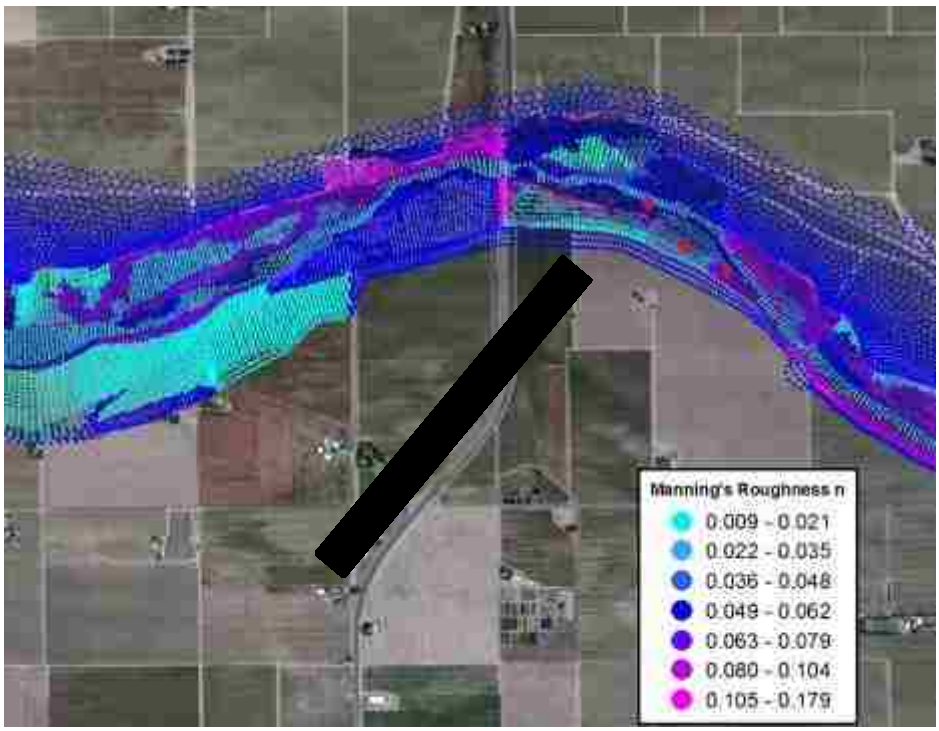

Figure 9: Manning's *n* values near field site 4 with the Baptist approach at 212.4 m^3/s

In order to quantify the results of this study, simulation water surface elevations were compared with both measured water surface elevations and water surface elevations generated from the calibrated models. The following figures represent water surface elevations along the center of flow of the San Joaquin River in Reach 1B. The plots are measured from the downstream end to the upstream end of the reach, represented by the x-axis. The y-axis represents the water surface elevation. In Figure 10, Figure 11, Figure 12, and Figure 13 plots of the water surface elevations for the Järvelä approach model, Baptist approach model, and the calibrated model are represented, as well as measured water surface elevations, for discharges of 31.2, 70.8, 113.3, and 212.4 m^3/s. Figure 14 represents a sensitivity analysis of the Järvelä approach by varying $C_{d\chi}$ by 0.1 at 113.3 m^3/s. Figure 15 represents a sensitivity analysis of the Järvelä approach by varying χ by 0.1 for the 113.3 m^3/s models. Figure 16 represents a sensitivity analysis of the Baptist approach by varying C_D by 0.5.

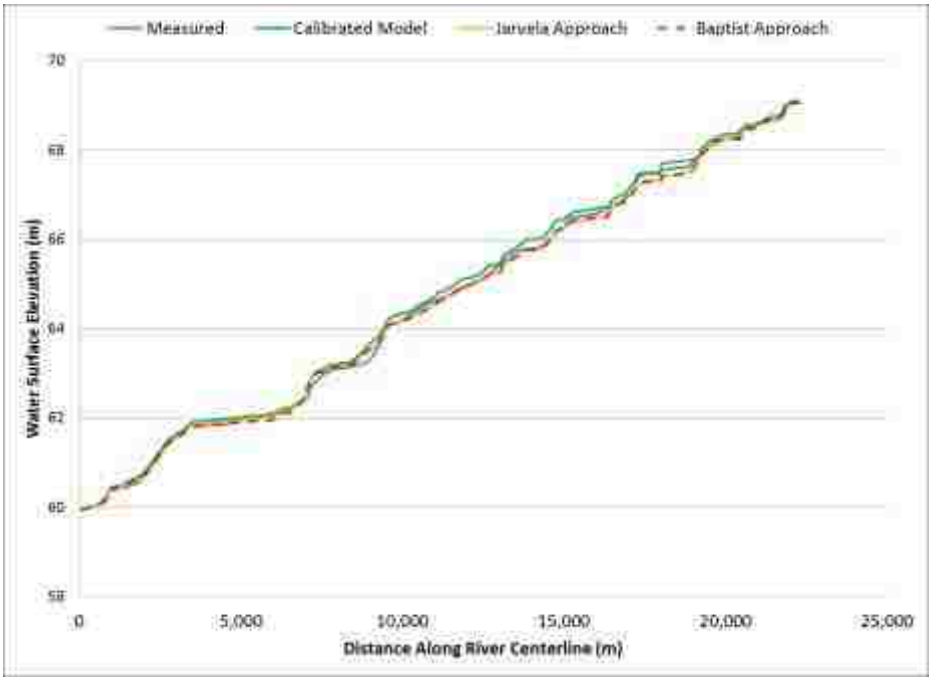

Figure 10: Simulated and measured water surface elevations at 31.2 m^3/s along Reach 1B centerline of flow

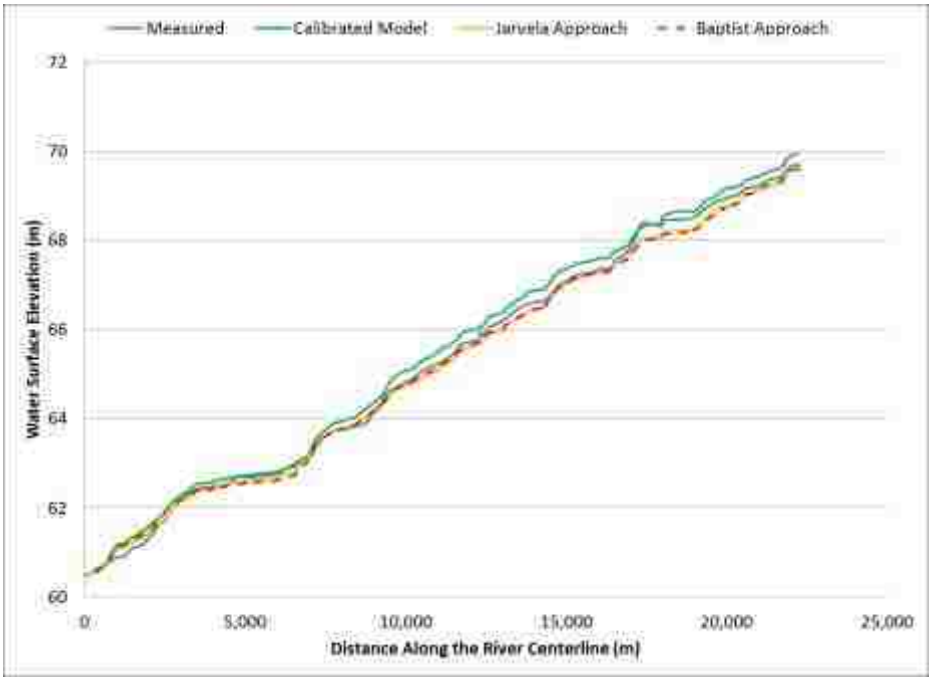

Figure 11: Simulated and measured water surface elevations at 70.8 m^3/s along Reach 1B centerline of flow

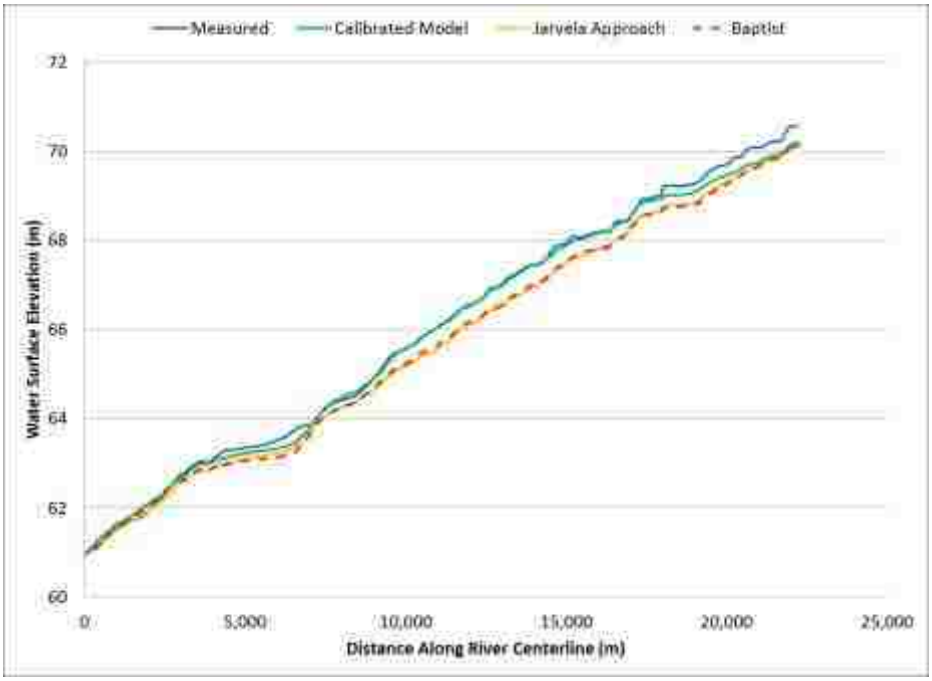

Figure 12: Simulated and measured water surface elevations at 113.3 m^3/s along Reach 1B centerline of flow

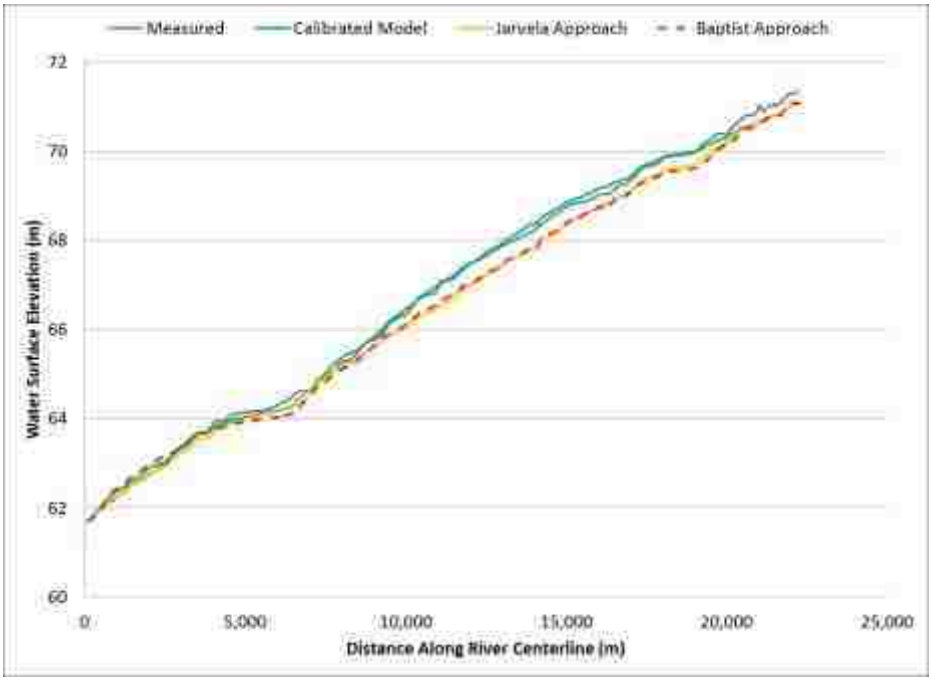

Figure 13: Simulated and measured water surface elevations at 212.4 m^3/s along Reach 1B centerline of flow

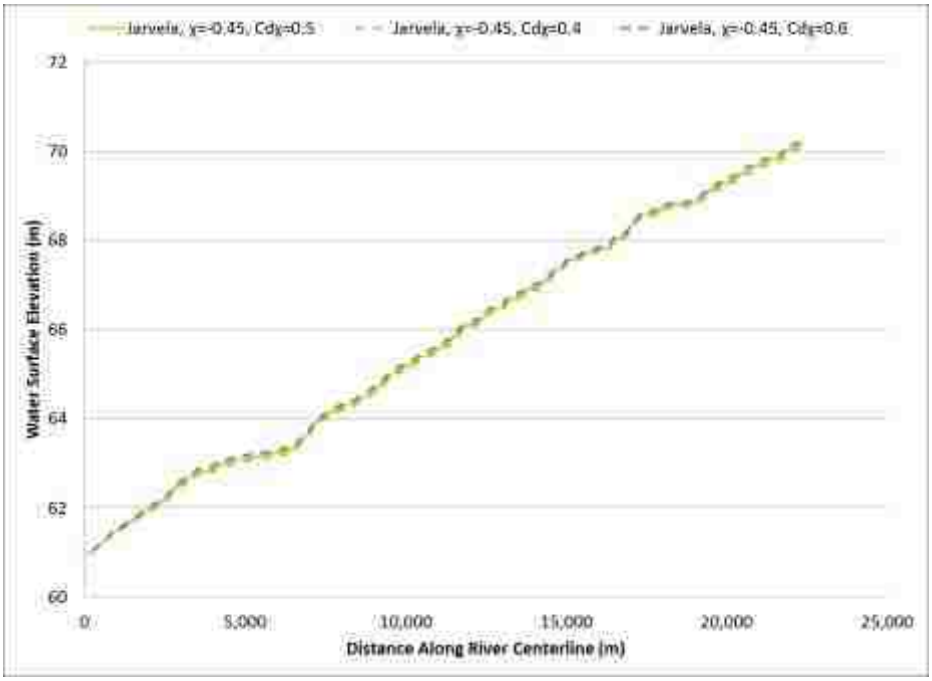

Figure 14: Water surface elevation sensitivity analysis using Järvelä approach, varying $C_{d\chi}$ by 0.1

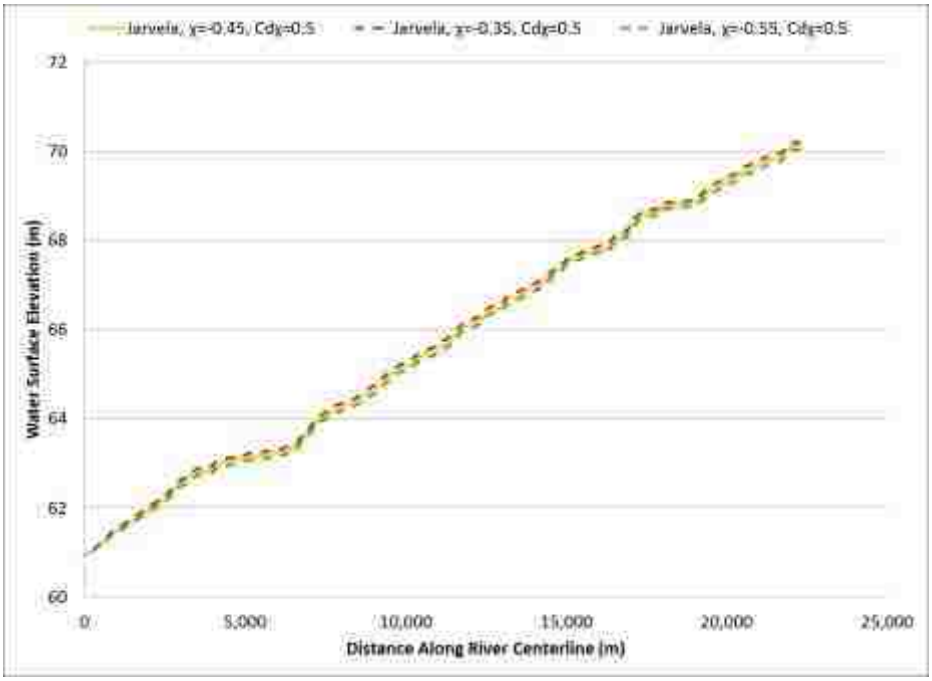

Figure 15: Water surface elevation sensitivity analysis using Järvelä approach, varying χ by 0.1

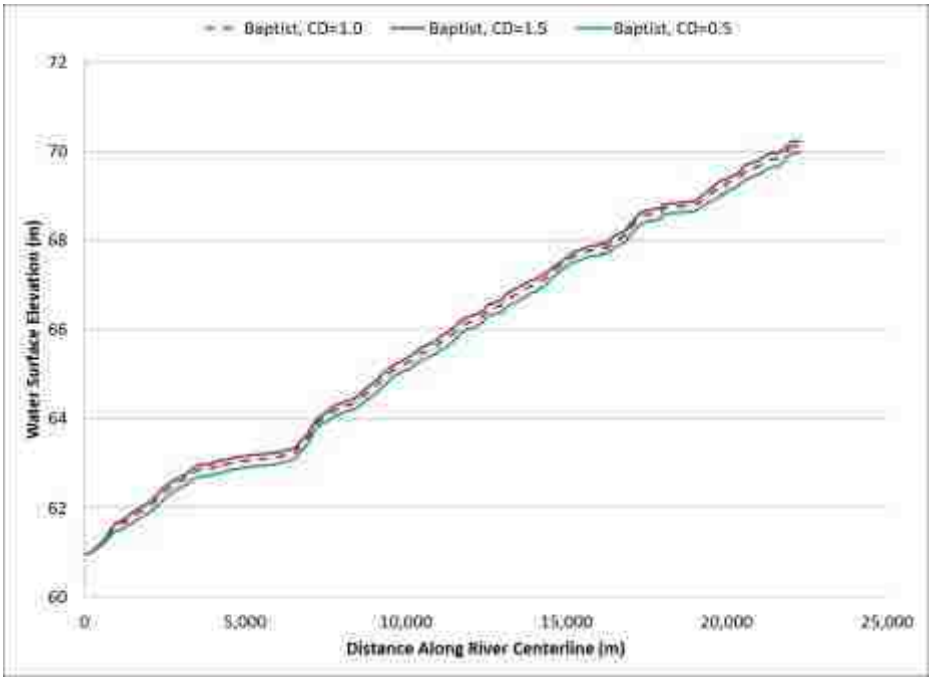

Figure 16: Water surface elevation sensitivity analysis using Baptist approach, varying C_D by 0.5

The root mean square error (RMSE) was applied to the models to try and measure accuracy. The calibrated models and the vegetation models were compared to the measured water surface elevations using this method. Table 5 represents the RMSE at the four discharges using the calibrated models, Järvelä, and Baptist models. Table 6 displays the RMSE between the sensitivity models at 113.3 m^3/s and the measured data.

Table 5: RMSE between all models and the measured water surface elevations

Flow (m^3/s)	RMSE (m)		
	Calibrated	Järvelä	Baptist
31.2	0.10	0.10	0.11
70.8	0.19	0.21	0.22
113.3	0.16	0.34	0.34
212.4	0.12	0.25	0.27

Table 6: RMSE between the Järvelä and Baptist sensitivity models and the measured water surface elevations

RMSE (m)							
Järvelä					Baptist		
$C_{d\chi}$=0.5 χ=-0.45	$C_{d\chi}$=0.4 χ=-0.45	$C_{d\chi}$=0.6 χ=-0.45	$C_{d\chi}$=0.5 χ=-0.35	$C_{d\chi}$=0.5 χ=-0.55	C_D=1.0	C_D=1.5	C_D=0.5
0.34	0.40	0.29	0.27	0.42	0.34	0.25	0.48

In addition to plotting the actual water surface elevations along the reach, the change in water surface elevations and velocity magnitude were plotted in histograms. The solutions to each simulation were subtracted from the calibrated models' solutions. The data was cleared of results that generated values of 0. Subtracting nodes that result in a value of 0 indicate that the node in the calibrated model and the vegetation model in question did not wet and therefore is not important to our analysis. Extraneous outliers of magnitude greater than 2 standard deviations away from the mean were removed to avoid

skewing the results. Twenty-five even interval bins were used for each histogram. The x-axis represents the change in the water surface elevation or velocity from the calibrated model. The y-axis represents frequency of each bin. The mean change in water surface elevation and velocity is plotted with the purple line. Figure 17 represents the difference in water surface elevations at 31.2 m^3/s between the Järvelä approach and the calibrated model. Figure 18 represents the difference between the Baptist approach and the calibrated model. Figure 19 represents the difference in water surface elevations at 212.4 m^3/s between the Järvelä approach and the calibrated model. Figure 20 represents the difference between the Baptist approach and the calibrated model. Figure 21 represents the difference in velocity magnitudes at 31.2 m^3/s between the Järvelä approach and the calibrated model. Figure 22 represents the difference between the Baptist approach and the calibrated model. Figure 23 represents the difference in velocity magnitudes at 212.4 m^3/s between the Järvelä approach and the calibrated model. Figure 24 represents the difference between the Baptist approach and the calibrated model. For the remaining models at 70.8 and 113.3 m^3/s, see Appendix E.

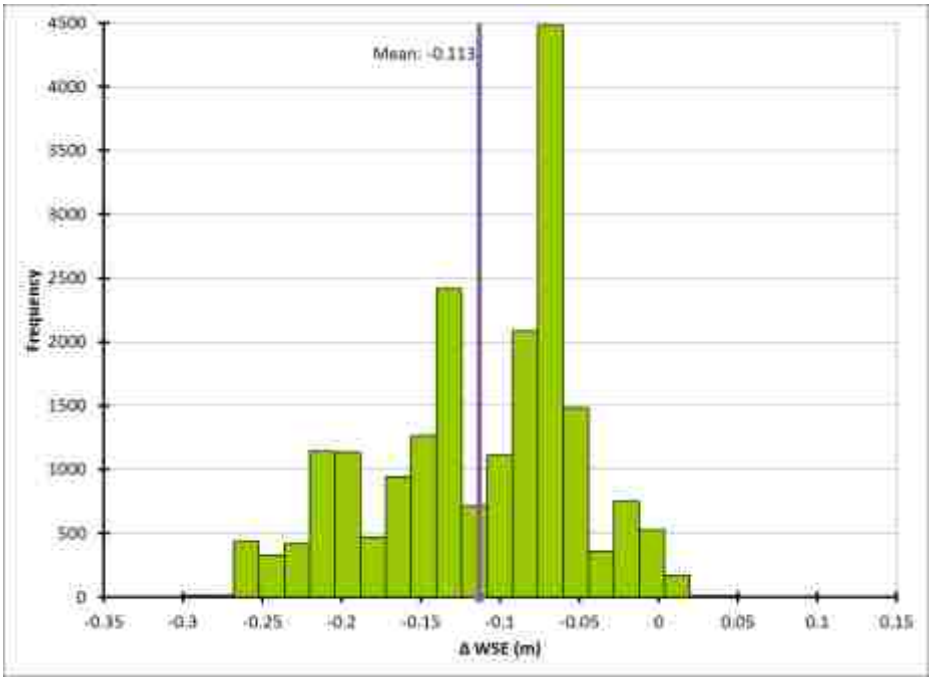

Figure 17: Change in water surface elevation at 31.2 m^3/s between the calibrated model and the Järvelä vegetation model

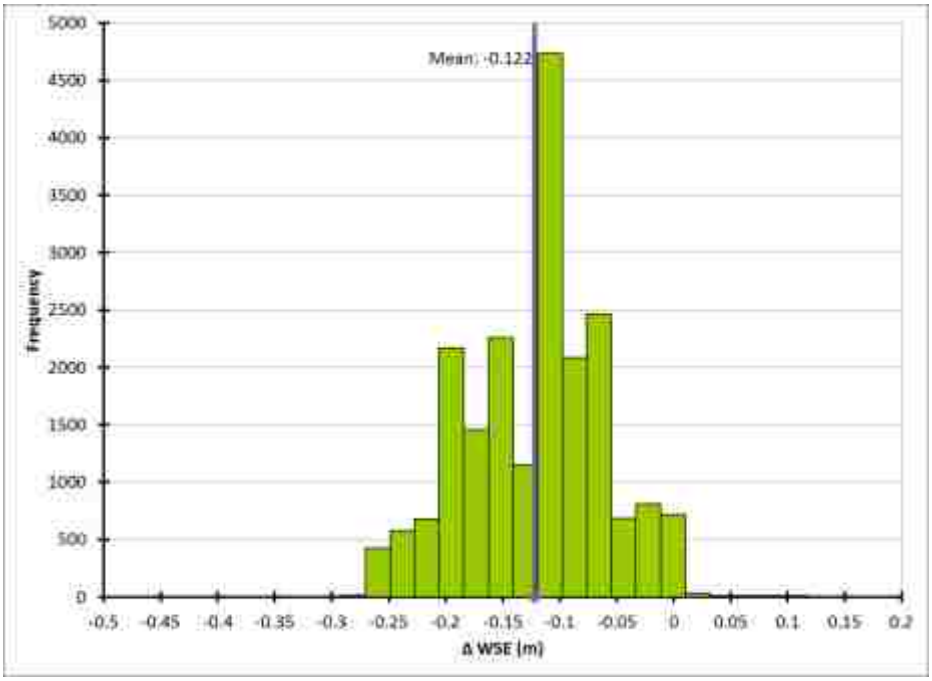

Figure 18: Change in water surface elevation at 31.2 m^3/s between the calibrated model and the Baptist vegetation model

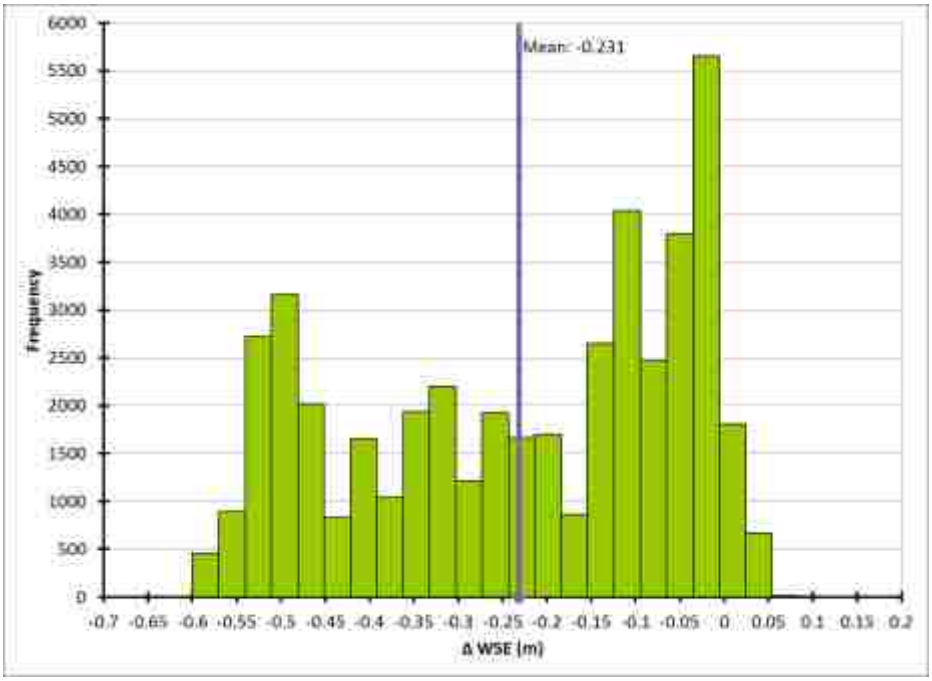

Figure 19: Change in water surface elevation at 212.4 m^3/s between the calibrated model and the Järvelä vegetation model

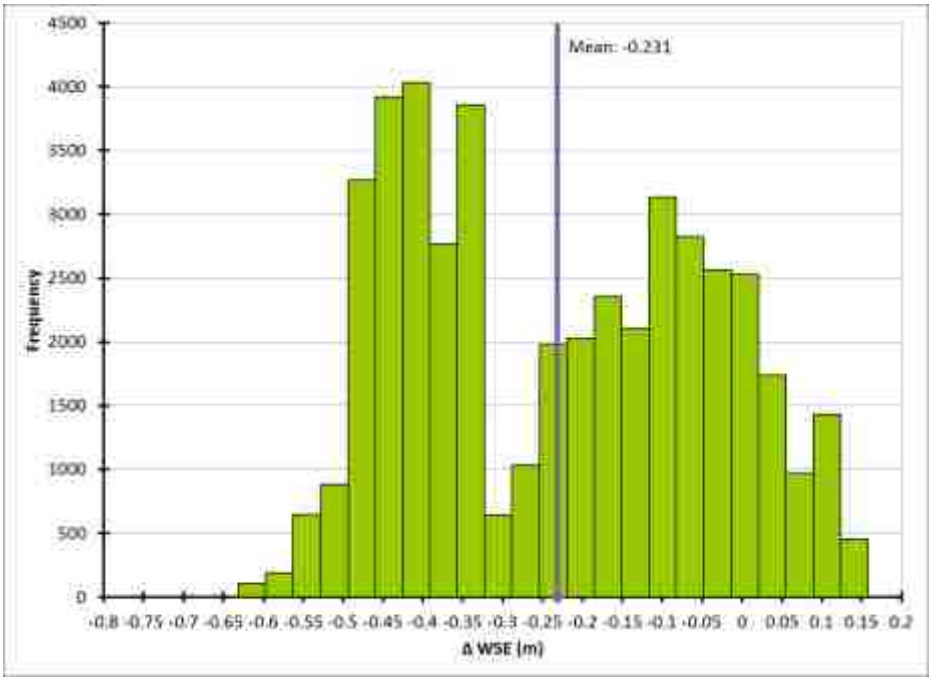

Figure 20: Change in water surface elevation at 212.4 m^3/s between the calibrated model and the Baptist vegetation model

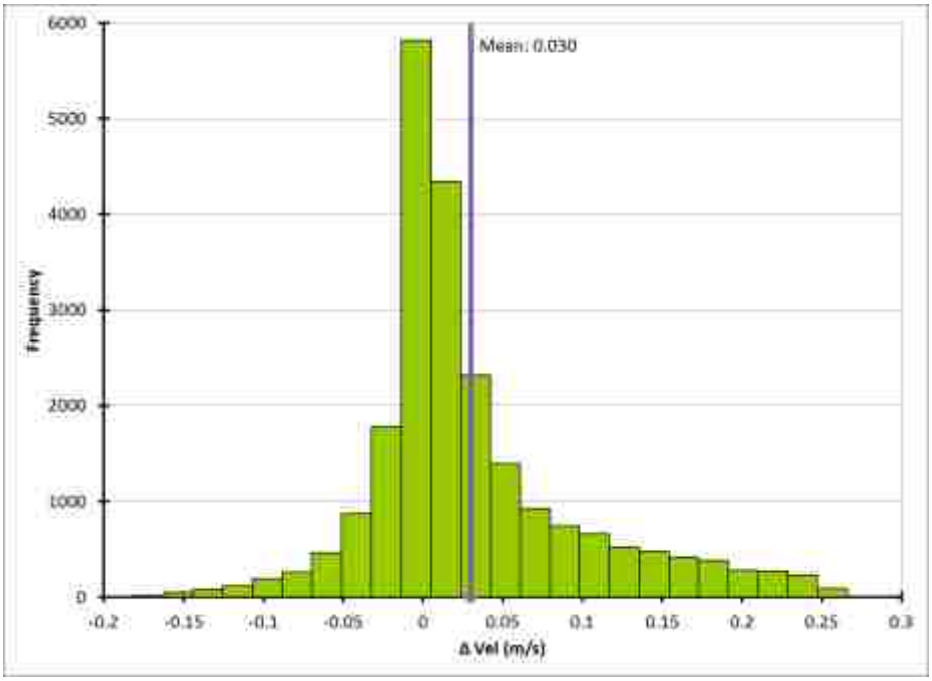

Figure 21: Change in velocity at 31.2 m^3/s between the calibrated model and the Järvelä vegetation model

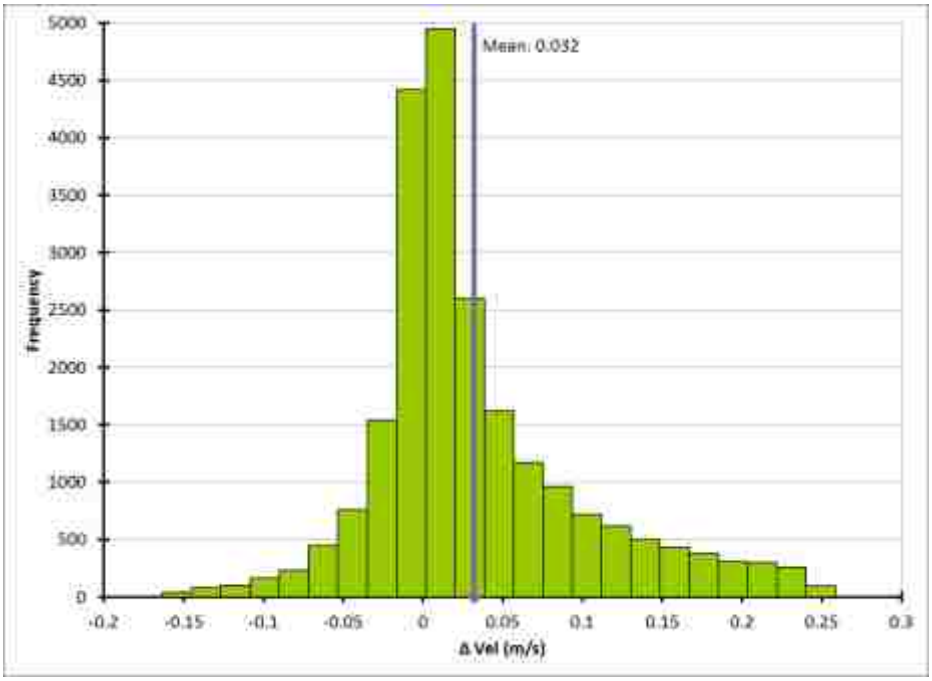

Figure 22: Change in velocity at 31.2 m^3/s between the calibrated model and the Baptist vegetation model

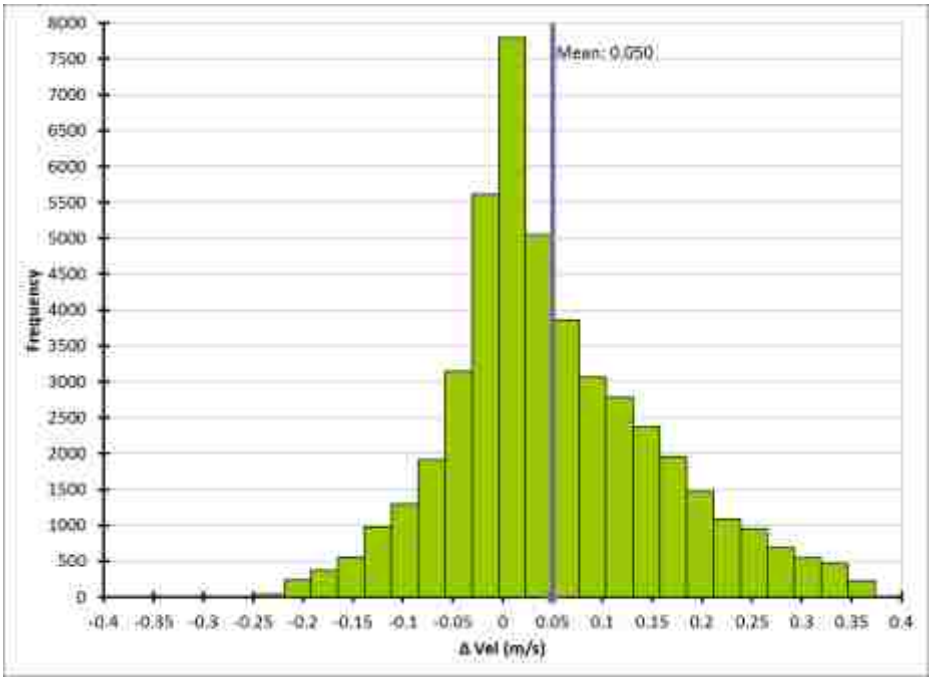

Figure 23: Change in velocity at 212.4 m^3/s between the calibrated model and the Järvelä vegetation model

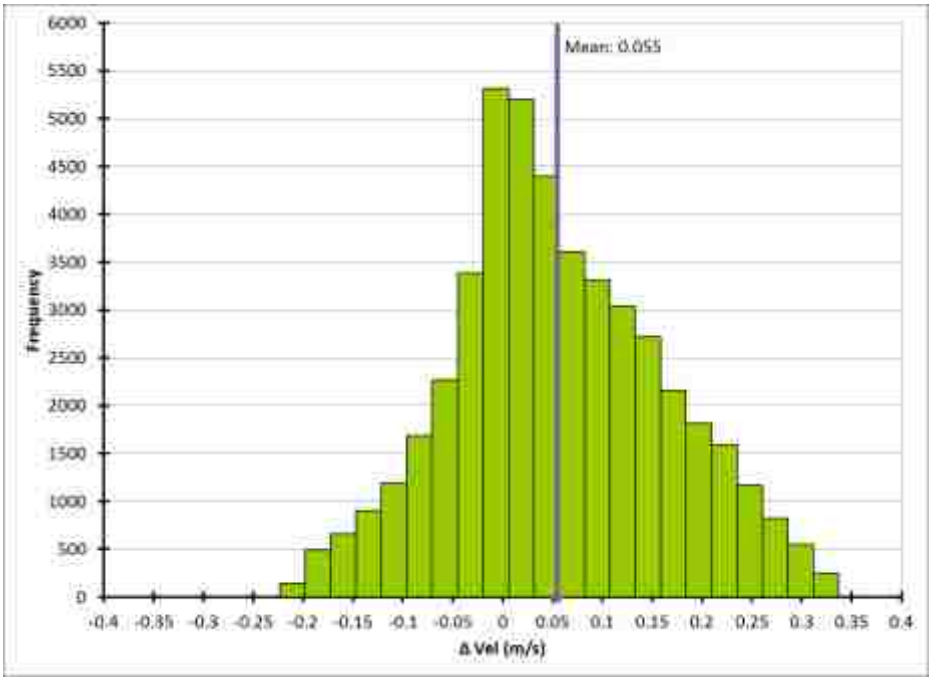

Figure 24: Change in velocity at 212.4 m^3/s between the calibrated model and the Baptist vegetation model

The tables below summarize the results of the change in water surface elevations and change in velocity magnitudes for each discharge and approach. The mean and standard deviation are represented in each table. Table 7 represents the 31.2, 70.8, 113.3, and 212.4 m3/s models for both the Järvelä and Baptist approaches, while Table 8 represents the sensitivity analyses for both approaches at 113.3 m3/s, by varying $C_{d\chi}$ and χ for Järvelä and varying C_D for Baptist.

Table 7: Summary of the change in water surface elevation and velocity between the vegetation models and the calibrated models

Flow (m^3/s)		ΔWSE (m)		ΔVelocity (m/s)	
		Järvelä	Baptist	Järvelä	Baptist
31.2	Mean	-0.113	-0.122	0.030	0.032
	Standard Deviation	0.064	0.062	0.067	0.066
70.8	Mean	-0.209	-0.209	0.041	0.043
	Standard Deviation	0.107	0.106	0.084	0.085
113.3	Mean	-0.232	-0.225	0.044	0.045
	Standard Deviation	0.142	0.130	0.095	0.096
212.4	Mean	-0.231	-0.231	0.050	0.055
	Standard Deviation	0.184	0.188	0.105	0.107

Table 8: Summary of the change in water surface elevation and velocity between the vegetation models and the calibrated models with a sensitivity analysis at 113.3 m^3/s discharge

Approach	113.3 m^3/s		ΔWSE (m)	ΔVelocity (m/s)
Järvelä	$C_{d\chi}$=0.5 χ=-0.45	Mean	-0.232	0.044
		Standard Deviation	0.142	0.095
	$C_{d\chi}$=0.4 χ=-0.45	Mean	-0.290	0.054
		Standard Deviation	0.146	0.109
	$C_{d\chi}$=0.6 χ=-0.45	Mean	-0.179	0.036
		Standard Deviation	0.140	0.086
	$C_{d\chi}$=0.5 χ=-0.35	Mean	-0.157	0.034
		Standard Deviation	0.136	0.082
	$C_{d\chi}$=0.5 χ=-0.55	Mean	-0.302	0.055
		Standard Deviation	0.150	0.113
Baptist	C_D=1.0	Mean	-0.225	0.045
		Standard Deviation	0.130	0.096
	C_D=1.5	Mean	-0.124	0.032
		Standard Deviation	0.123	0.080
	C_D=0.5	Mean	-0.364	0.069
		Standard Deviation	0.141	0.127

Changes in water surface elevations of the vegetation models compared to the calibrated models were also mapped. Both techniques at 31.2 m^3/s and 212.4 m^3/s are mapped at the location below. This first location is at the upstream end of reach 1B near Highway 99, displaying field sites 2 and 3 with pink and black squares respectively. A second location was also mapped downstream near State Route 145 approximately 14,800 meters downstream of the Reach 1B mesh inlet displaying field sites 4 and 5. For the remaining maps not displayed below, see Appendix E. The negative values represent the distance water surface elevation of the calibrated models, while the positive values represent distance above. The yellow nodes represent no change in water surface elevation.

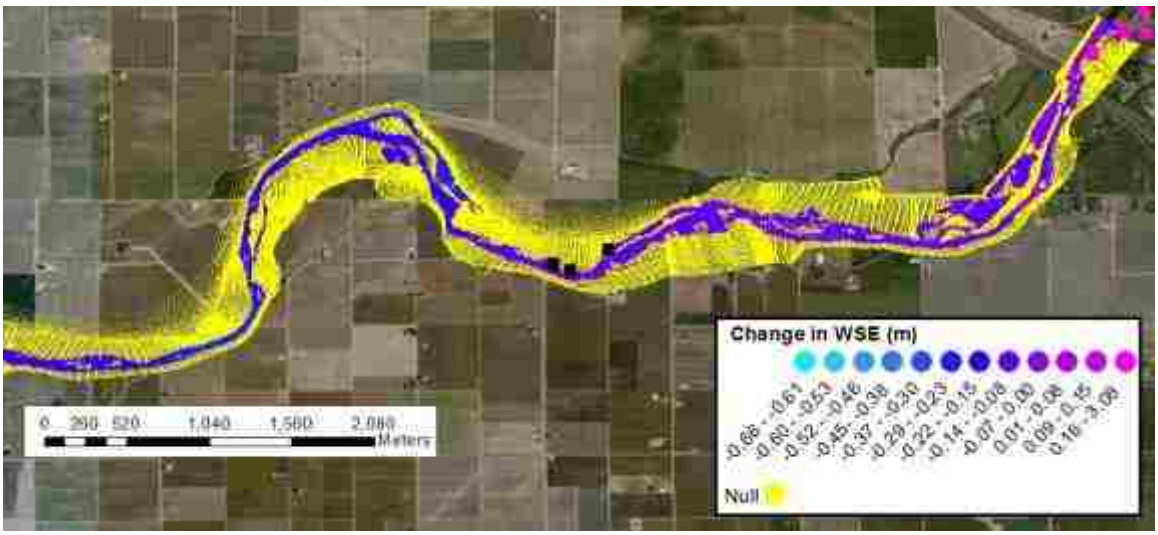

Figure 25: Change in water surface elevation at 31.2 m^3/s using the Järvelä approach near field sites 2 and 3

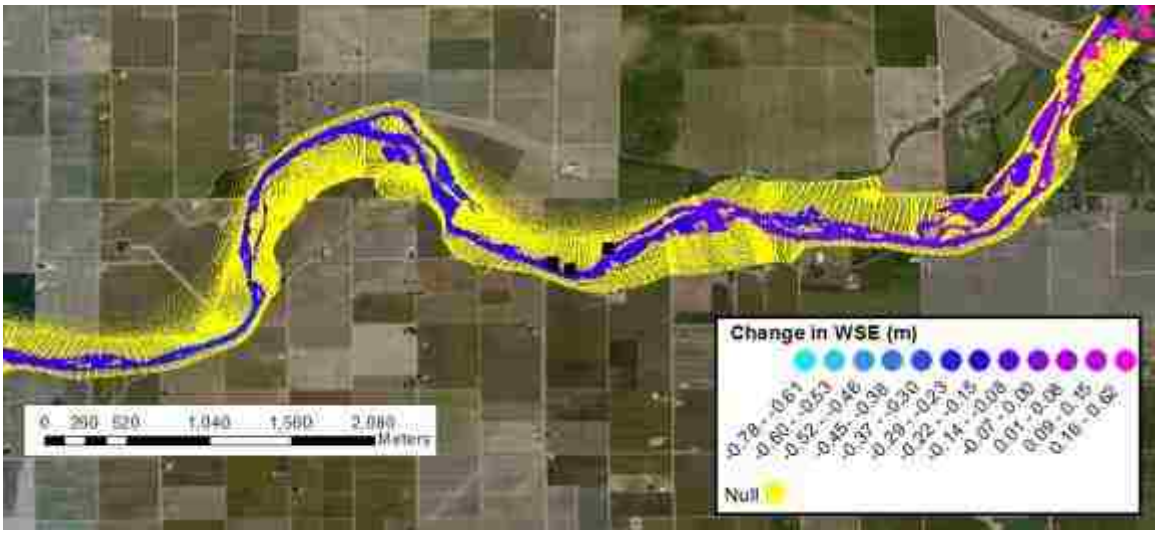

Figure 26: Change in water surface elevation at 31.2 m^3/s using the Baptist approach near field sites 2 and 3

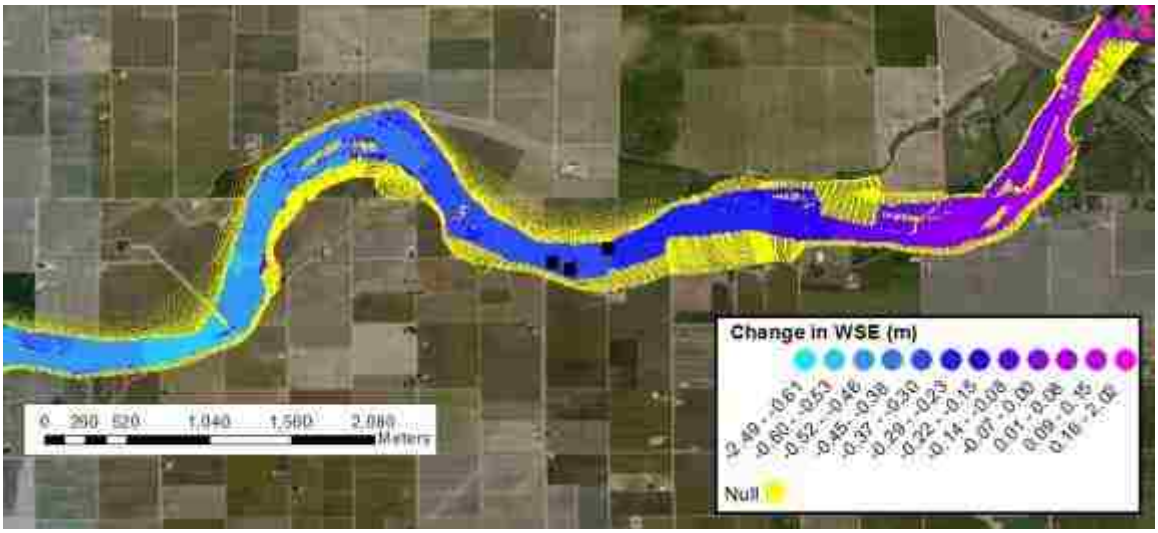

Figure 27: Change in water surface elevation at 212.4 m^3/s using the Järvelä apporach near field sites 2 and 3

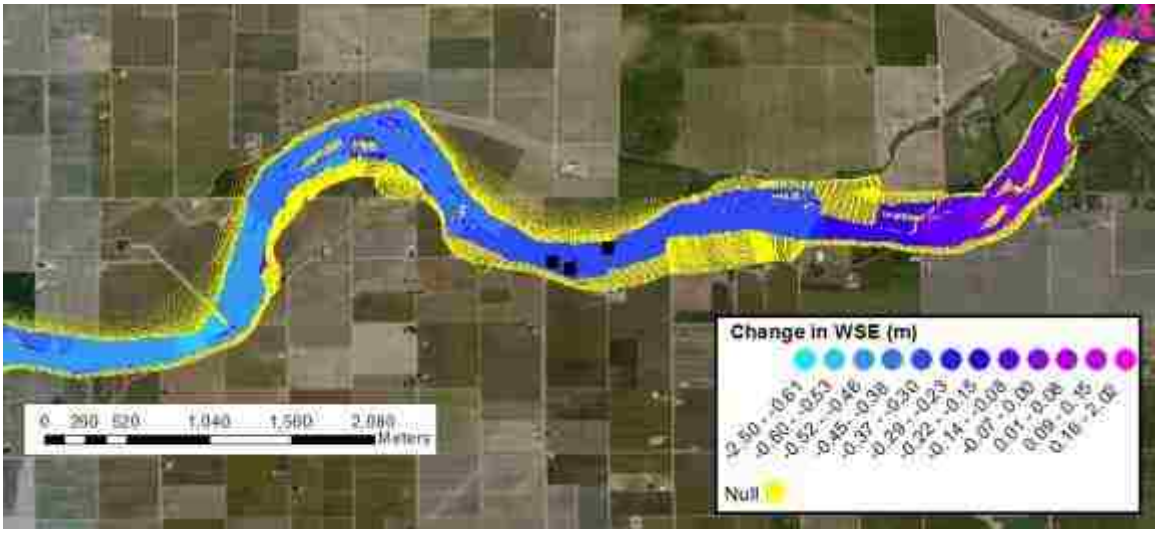

Figure 28: Change in water surface elevation at 212.4 m^3/s using the Baptist approach near field sites 2 and 3

Changes in velocities were also mapped for both techniques in comparison with the calibrated models. Maps for discharges at 31.2 and 212.4 m^3/s are displayed below. See Appendix E for maps at 70.8 and 113.3 m^3/s. These maps are located near field site 4 as indicated by the red dots. Negative values represent velocities less than the calibrated models, while positive represents values greater than those found in the

calibrated models. Yellow nodes represent no change in velocity between the vegetation and calibrated models.

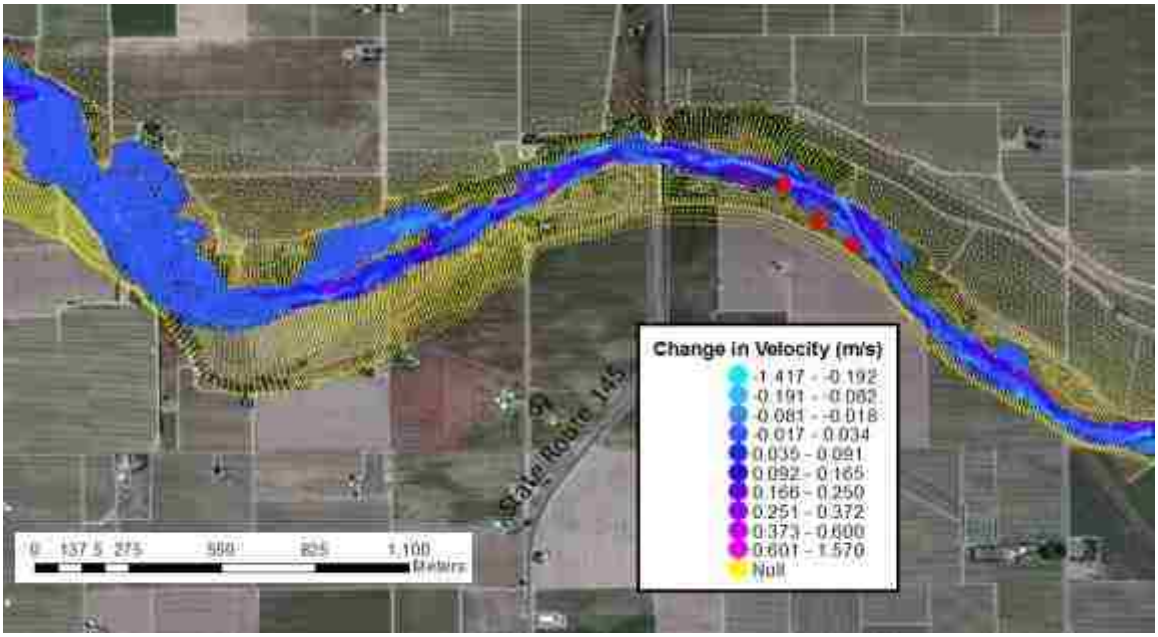

Figure 29: Change in velocity at 31.2 m^3/s with the Järvelä apporach near field site 4

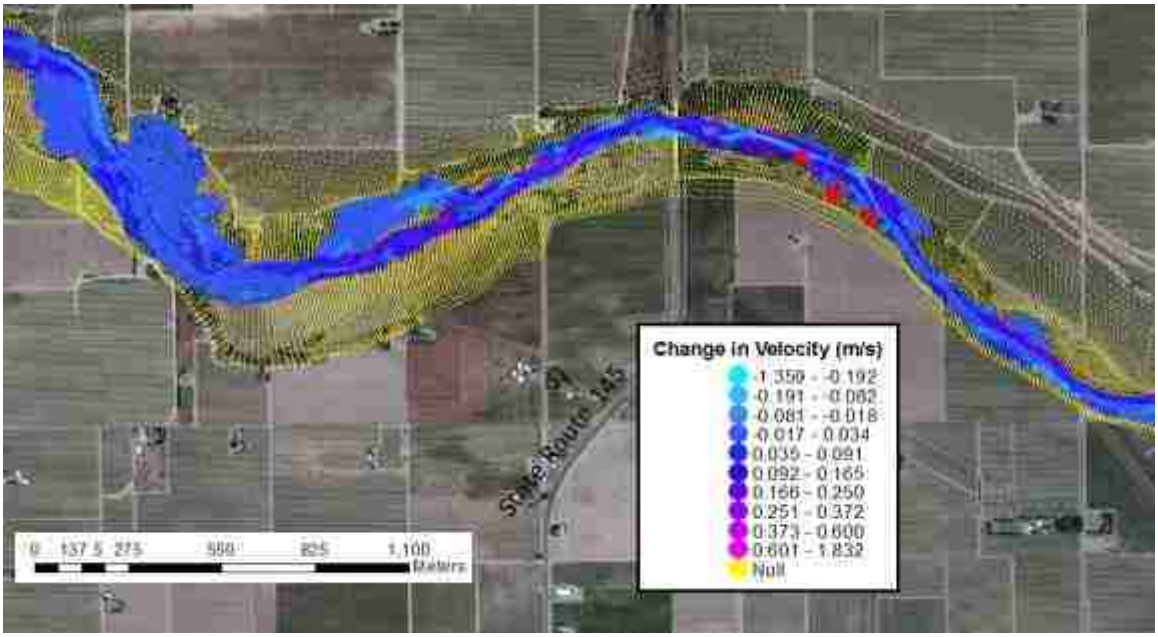

Figure 30: Change in velocity at 31.2 m^3/s with the Baptist approach near field site 4

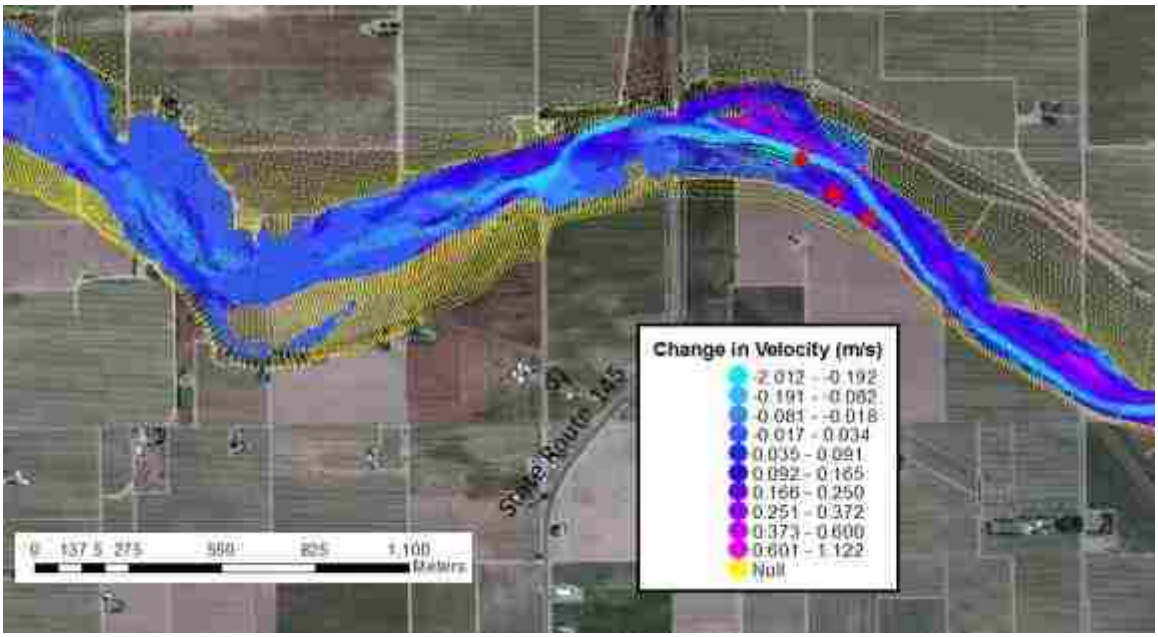

Figure 31: Change in velocity at 212.4 m^3/s with the Järvelä approach near field site 4

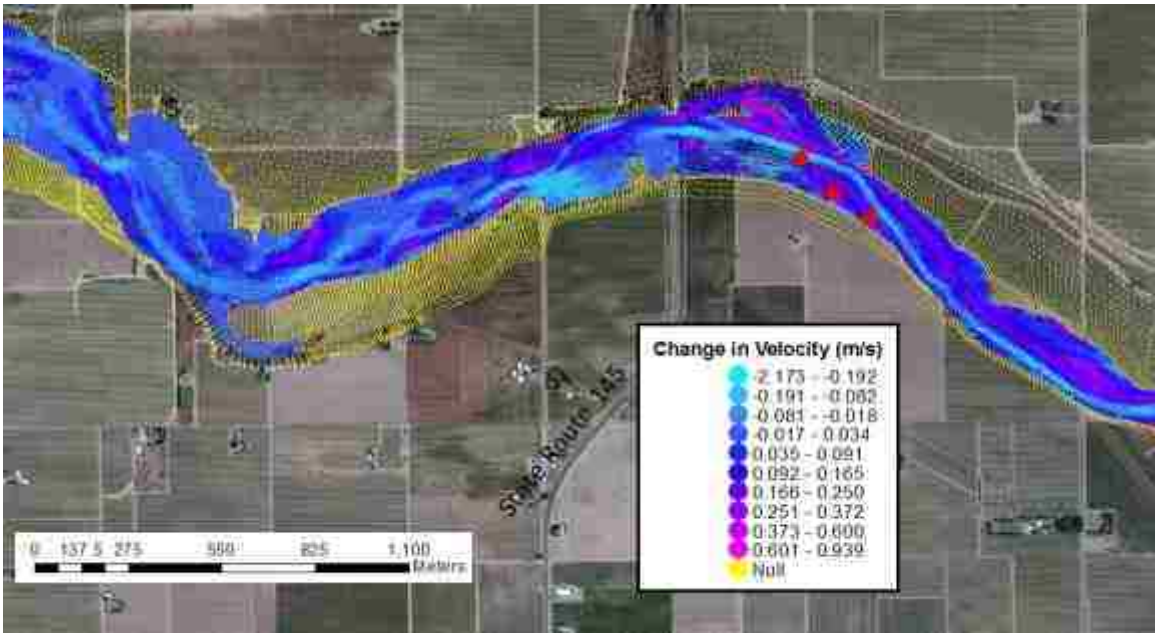

Figure 32: Change in velocity at 212.4 m^3/s with the Baptist approach near field site 4

Discussion

The purpose of this research was to: 1) develop a technique to measure vegetation parameters in the field to be implemented into hydraulic modeling software, in order to access how vegetation roughness affects flows in the floodplain, 2) assess how well the new SRH-2DV models with the implementation of dynamic roughness values work, in comparison to previously developed SRH-2D calibrated models, 3) determine which vegetation roughness approach, Järvelä or Baptist, is better suited for easily and accurately calculating vegetation roughness.

This study has shown that roughness imparted by vegetation is a function of the hydrodynamics of the system. The broad range of minimum and maximum n_e values in Table 3 and Table 4 indicate that the roughness varies with velocity and flow depth. The n_e values calculated show that a single value assigned to a land use does not accurately represent the roughness for an entire reach length. The maps of calculated roughness values show a general increase in roughness as flows increase, meaning that higher velocities induce greater roughness. This can be seen by comparing Figure 6 and Figure 7 to Figure 8 and Figure 9, and noticing the increase near the center of the channel from the lighter blue colored nodes at 31.2 m^3/s to the darker purple/pink colored nodes at 212.4 m^3/s. It should also be noted that at lower discharges the model has a tendency to default to the original *n* values specified at the model setup. This is due to low flows often not penetrating far into the floodplain where the majority of the vegetation resides. This can be seen by again comparing Figure 6 and Figure 7 to Figure 8 and Figure 9. Figure 6 and Figure 7 show much of the floodplain being covered in blue nodes (0.049 – 0.062 *n* values). This is due to the flow not reaching this area and the model displays the

default *n* value of 0.056 as shown in Figure 5. At higher discharges, water surface penetrates much further into the floodplain and thus dynamic roughness values were calculated.

Smaller roughness values resulted in lower water surface elevations for the vegetation models. The relative difference in water surface elevations varied depending on the discharge. This phenomenon can be seen in the plots of the water surface elevation along the river starting with Figure 10. These plots also show that difference between the models' water surface elevations is greatest in the middle of the reach length due to boundary conditions set in the model. At the upstream end the calibrated models and vegetation models are close, due to limited length of channel bed to affect water surface elevation by means of roughness. Moving away from the boundary conditions, roughness dominates the hydraulics and the depth decreases with decreased roughness. Near the downstream end, the calibrated models and vegetation models converge at the specified water surface elevation boundary condition. This can be seen in the aerial maps of Figure 25 to Figure 28.

The root mean square errors between the measured data and the models indicate that as discharge increases, both approaches decrease in accuracy. Although the calibrated models performed better at higher discharges when compared to the roughness approaches, the range of RMSE values for the calibrated show that applying a single roughness value for multiple flows is not effective. Rather than having to calibrate the roughness values for every discharge, it would be more effective to utilize the roughness approaches that take changing hydrodynamics into account.

The changes in velocities are harder to characterize. Average velocities were overpredicted in all of the vegetation models due to the decreased roughness values. The lower roughness values in the floodplain resulted in increased velocity in those areas. In areas where vegetation is not present, primarily the center of channel, the model assumes the default roughness value specified resulting in a decrease in velocity in those areas due to an increase in velocity in vegetated areas. Figure 29 to Figure 32 displays this phenomenon.

The differences between the Järvelä and Baptist approaches are minimal. For the scope of this research, they performed equally in terms of calculating the hydraulics of the system. The difference between these two techniques comes down to the vegetation parameters required for each, where limitations occur. Järvelä requires leaf area index and vegetation height to be measured in the field. This is relatively easy to do with a Hypsometer for height and AccuPar for LAI, both of which were used for this study. Techniques to determine height and LAI have also been developed using LiDAR data (Jensen et al. 2008; Riaño et al. 2004; Zimble et al. 2003). The uncertainty lies in determining species specific values of $C_{d\chi,}$and χ due to the limited research for these variables (Manoochehr Fathi-Moghadam 1996). For Baptist, stem diameter and stem density are measured in the field. Stem diameter can be derived fairly easily by measuring a small sample of vegetation and applying an average value to the species. Stem density is much more difficult to measure due to local areas of vegetation being heavily populated with stems. Local areas of densely populated stems are often spaced at large distances from each other, and as a result make it hard to define where the average stem density should be taken for the species. Determining C_D is also difficult due to the

requirement of velocity and geometric measurements of the vegetation. Using a single value of C_D to represent all stems is often practiced with success (Baptist et al. 2007; Nehal et al. 2012; Petryk and Bosmajian 1975). Unfortunately this does not accurately represent the vegetation and a unique value for each vegetation class would increase accuracy.

The sensitivity analysis showed that the parameters in question play an important role in affecting the roughness and hydraulic analysis, and therefore further research of these values is vital to improving the models' accuracy. The models were affected the most by altering χ for Järvelä and C_D for Baptist. Research being conducted at the time of this experiment, suggested that the relationship between the drag force $C_{d\chi}$ and the velocity U are linear, correlating to a χ value of -1 for all vegetation species (Jalonen et al. 2013). Jalonen et al. (2013) also suggested that *LAI* is the primary controlling factor for the Järvelä approach. If this is proven to be true, the uncertainty of the parameter χ will be eliminated, resulting in better calibration of the approach. A presentable solution to accurately representing C_D is to alter the model code to internally solve for the parameter based on measured vegetation dimensions and shear stresses.

This study has shown that both approaches yield similar results overall and therefor the decision of which approach to use should be based on efficiency of field measurements and the corresponding parameters. The Järvelä approach is more appropriate to use in areas of high density leafy vegetation due to LAI being the controlling factor in these areas. The Baptist approach is better used in areas of low vegetation density where stem density is more easily and accurately measured.

Conclusion

This study has established techniques for implementing field measured vegetation parameters into two-dimensional hydraulic models for the purpose of measuring dynamic vegetation roughness, in an effort to understand how this affects the hydraulics of an open channel system. This study focused on the San Joaquin River near Fresno, California, where field measurements of vegetation: height, stem diameter, stem density, and leaf area index were taken for 12 different vegetation classes and applied to a broader set of 42 different classes. Vegetation roughness computational techniques were developed based on research by Järvelä (2004) and Baptist et al. (2007) and implemented into a new version of SRH-2D. Hydraulic models were built in the newly developed SRH-2DV to utilize both the Järvelä and Baptist approaches to compare to non-dynamic roughness calibrated models already developed in SRH-2D for the San Joaquin reach in question (Reclamation 2012).

This study has given insight on how variable dynamic roughness can affect open channel flow. The models indicate that roughness changes dynamically with the hydraulics of the system and can vary greatly for a particular land use. When compared to traditional calibrated models, the roughness models underpredicted water surface elevations and overpredicted velocities due to calculating smaller roughness values. The Järvelä and Baptist approaches performed the same, in terms of hydraulic calculations. The approaches differ in regards to required field work and vegetation parameters. The sensitivity analysis performed showed that the uncertain parameters of χ, $C_{d\chi}$, and C_D are significant in calculating roughness and that further research is required for better understanding and assignment of these values. Currently the Järvelä approach is best

suited in areas of high density where leaf area index dominates and the Baptist approach is better suited for low density areas where stem density is easily acquired in absence of a high leaf area index.

Accurately describing vegetation roughness is crucial to understanding the hydraulics of the river system. Dynamic roughness not only affects water surface elevation, but also physical processes such as velocity distribution, shear stress, and momentum exchange, all of which are difficult to describe on a macro scale using a single non-dynamic roughness value (Vermaas et al. 2011). The ability to describe local values of dynamic roughness in areas of interest greatly enhances the understanding of the system and allows for better planning and engineering in problem areas. Both approaches discussed in this study are promising techniques for future hydraulic modeling.

References

Aberle, J., and Järvelä, J. (2013). “Flow resistance of emergent rigid and flexible floodplain vegetation.” *Journal of Hydraulic Research*, 51(1), 33–45.

Arcement, G. J., Jr., and Schneider, V. R. (1989). "Guide for selecting Manning’s roughness coefficients for natural channels and flood plains." *Rep. No. FHWA-TS-84-204*, U.S.D.T., Federal Highway Administration, Washington, D.C.

Baptist, M. J., Babovic, V., Rodriguez, J., Keijzer, M., Uittenbogaard, R. E., Mynett, A., and Verwey, A. (2007). “On inducing equations for vegetation resistance.” *Journal of Hydraulic Research*, 45(4), 435–450.

Chow, V. T. (1959). *Open-Channel Hydraulics.* McGraw-Hill Co., New York.

Darby, S. E. (1999). “Effect of riparian vegetation on flow resistance and flood potential.” *Journal of Hydraulic Engineering*, 125(5), 443–454.

Fathi-Maghadam, M., and Kouwen, N. (1997). “Nonrigid, nonsubmerged, vegetative roughness on floodplains.” *Journal of Hydraulic Engineering*, 123(1), 51–57.

Fathi-Moghadam, M. (1996). “Momentum absorption in non-rigid, non-submerged, tall vegetation along rivers.” University of Waterloo, Canada. (Doctoral thesis.)

Fischenich, C. (2000). "Robert Manning (a historical perspective)." *EMRRP Technical Notes Collection* (ERDC TN-EMRRP-SR-10), U.S. Army Engineer Research and Development Center, Vicksburg, MS.

Fischenich, C., and Dudley, S. (1999). “Determining drag coefficients and area for vegetation.” *EMRRP Technical Notes Collection* (ERDC TN-EMRRP-SR-08), U.S. Army Engineer Research and Development Center, Vicksburg, MS.

Holland, R. F. (1986). *Preliminary description of the terrestrial natural communities of California.* Sacramento, CA, Nongame-Heritage Program, California Department of Fish and Game.

Jalonen, J., Järvelä, J., and Aberle, J. (2013). “Leaf area index as vegetation density measure for hydraulic analyses.” *Journal of Hydraulic Engineering*, 139(5), 461–469.

Jarvela, J. (2004). “Determination of flow resistance caused by non-submerged woody vegetation.” *International Journal of River Basin Management*, 2(1), 61–70.

Jensen, J., Humes, K., Vierling, L., and Hudak, A. (2008). "Discrete return lidar-based prediction of leaf area index in two conifer forests." *Remote Sensing of Environment*, 112(10), 3947–3957.

Julien, P. Y. (2002). *River Mechanics.* Cambridge University Press, Cambridge.

Kouwen, N., and Fathi-Moghadam, M. (2000). "Friction factors for coniferous trees along rivers." *Journal of Hydraulic Engineering*, 126(10), 732–740.

Lai, Y. G. (2008). *SRH-2D version 2: Theory and User's Manual. Sedimentation and River Hydraulics–Two-Dimensional River Flow Modeling.* US Bureau of Reclamation, Technical Service Center, Denver, CO.

Moise, G. W., and Hendrickson, B. (2002). *Riparian vegetation of the San Joaquin River.* State of California Department of Water Resources, Technical Information Record SJD-02-1

Munson, B. R., Young, D. F., Okiishi, T. H., and Huebsch, W. W. (2009). *Fundamentals of Fluid Mechanics.* Wiley, New York.

Mussetter Engineering Inc. (2008). San Joaquin HEC-RAS model documentation technical memorandum prepared for California Dept. of Water Resources, Fresno, California, June 2.

Nehal, L., Yan, Z., Xia, J., and Khaldi, A. (2012). "Flow through non-submerged vegetation: A flume experiment with artificial vegetation." *Sixteenth International Water Technology Conference*, Istanbul, 1–12.

Nepf, H. M. (1999). "Drag, turbulence, and diffusion in flow through emergent vegetation." *Water Resources Research*, 35(2), 479–489.

Petryk, S., and Bosmajian, G. (1975). "Analysis of flow through vegetation." *Journal of the Hydraulics Division*, 101(7), 871–884.

Poff, N. L., Allan, J. D., Bain, M. B., Karr, J. R., Prestegaard, K. L., Brian, D., Sparks, R. E., Stromberg, J. C., and Richter, B. D. (1997). "The natural flow regime: A paradigm for river conservation and restoration." *BioScience*, 47(11), 769–784.

Reclamation. (2012). *Hydraulic Studies For Fish Habitat Analysis*. Technical Report No. SRH-2012-15. Prepared for San Joaquin River Restoration Project, Mid-Pacific Region, US Bureau of Reclamation, Technical Service Center, Denver, CO.

Riaño, D., Valladares, F., Condés, S., and Chuvieco, E. (2004). "Estimation of leaf area index and covered ground from airborne laser scanner (Lidar) in two contrasting forests." *Agricultural and Forest Meteorology*, 124(3-4), 269–275.

SJRRP. (2008). Annual Report 2008. 522–530.

SJRRP. (2010). Annual Technical Report, Appendix G "Surveys."

SJRRP. (2011). Annual Technical Report, Appendix G "Surveys."

Thompson, G., and Roberson, J. (1976). "A theory of flow resistance for vegetated channels." *Transactions of the ASAE*, 19(2), 288–293.

Wilson, C. (2007). "Flow resistance models for flexible submerged vegetation." *Journal of Hydrology*, 342(3-4), 213–222.

Vermaas, D. A., Uijttewaal, W. S. J., and Hoitink, A. J. F. (2011). "Lateral transfer of streamwise momentum caused by a roughness transition across a shallow channel." *Water Resources Research*, 47, W02530, doi:10.1029/2010WR010138.

Zimble, D. a., Evans, D. L., Carlson, G. C., Parker, R. C., Grado, S. C., and Gerard, P. D. (2003). "Characterizing vertical forest structure using small-footprint airborne LiDAR." *Remote Sensing of Environment*, 87(2-3), 171–182.

Appendices

Appendix A- Field Work

Six sites along the San Joaquin were chosen for this study. In these sites, data were measured in 10 meter by 10 meter areas. These areas were chosen based on the predominant vegetation that was required to be measured. Measurements included vegetation height, stem diameter, density, and leaf area index (LAI). Vegetation height was measured by use of a Hypsometer. The machine works by measuring the distance from the machine to the bottom of the vegetation and the distance from the machine to the top of the vegetation. It then measures the angle between the two distance lines and uses basic trigonometry to calculate the height. Vegetation stem diameter was measured at breast height using precision calipers for small branches, and a diameter tape for bigger stems. The small branches were tallied in bins of small sizes, similar to classifying data for a histogram. Small branches were tallied in one of the following categories; less than 0.5 cm, 0.5 cm to 1 cm, 1 cm to 2 cm, 2 cm to 3 cm, etc. This allowed for quicker field measurements of both stem diameter and density. Large branches were measured and recorded as measured. The density was measured by counting the total number of tallies recorded for every diameter bin at each site. LAI was measured by using the AccuPAR LP-80. The AccuPAR works by taking both above and below canopy measurements of direct sun radiation. The machine calculates LAI by taking the difference of the two. Two measurements were taken at breast height along the diagonal lines of the square area. These values were averaged to generate a LAI value. Figure 33, Figure 34, and Figure 35 are images of the field work performed. Figure 36 displays the locations of the field sites along the San Joaquin River.

Figure 33: Stem diameter being measured with precision calipers

Figure 34: Vegetation stems being counted and recorded in field book

Figure 35: LAI being measured with AccuPAR

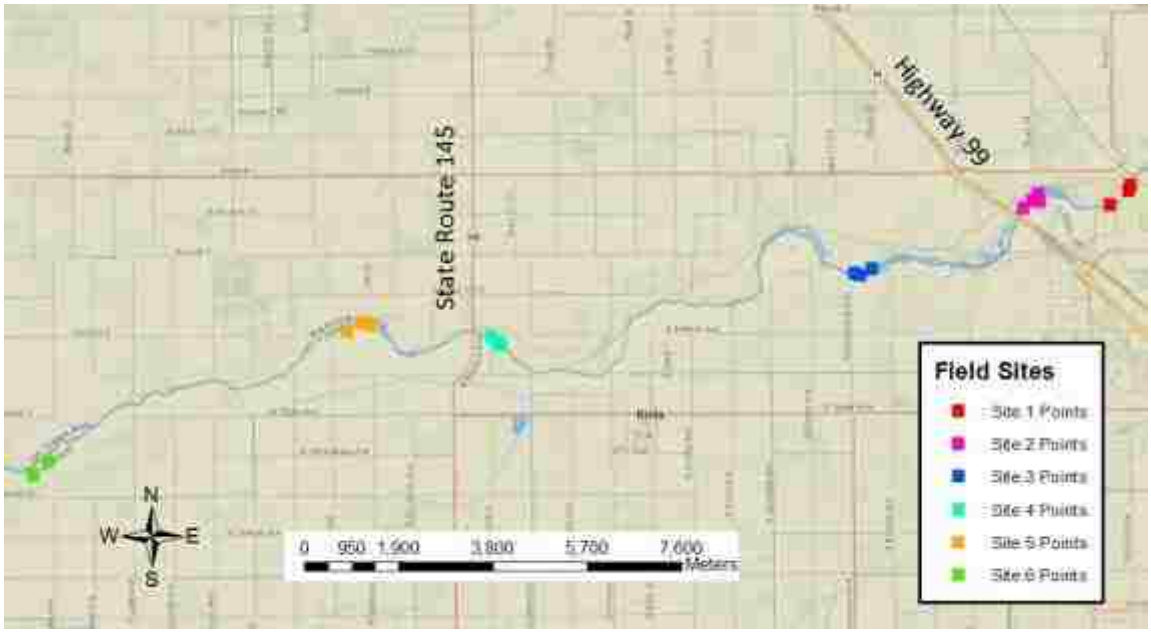

Figure 36: Locations of field data sites

Site 1 consisted of mixed riparian 3, willow scrub low density 6, willow riparian 3, and riparian scrub. Field measurements were not taken for riparian scrub due to excessive burning that left the vegetation near nonexistent. Site 2 consisted of

herbaceous, mixed riparian low density 6, cottonwood low density 4, and willow riparian 4. Site 3 consisted of mixed riparian 3, willow scrub 5, and willow riparian 3. Site 4 consisted of mixed riparian 1, willow scrub low density 6, and willow scrub 5. Site 5 consisted of herbaceous, cottonwood low density 4, and willow scrub 6. Site 6 consisted of cottonwood 3 and riparian scrub.

Figure 37: Site 1 mixed riparian 3

Site 1 mixed riparian 3 consisted of a number of different vegetation types including willows, shrubs, and elderberrys. The average height of all the species was 10.8 feet. There were a total of 138 stems counted with an average of 0.75 inches. Stems were generally small. Average LAI was calculated to be 0.91.

Figure 38: Site 1 willow scrub low density 6

The next site, willow scrub low density 6 consisted mostly of small willows with a large distance between species. The average height of the willows was 6.53 feet, contained an average LAI of 0.55, and had an average small stem diameter of 0.49 inches. 71 stems were counted in the area and were on the small side in regards to diameter.

Figure 39: Site 1 willow riparian 3

The willow riparian 3 site consisted of denser willow vegetation amongst a few other species. The average height of species was 12.2 feet with a density of 197 stems in the 100 meter area. The average LAI was 2.95 and consisted mostly of small stems with an average diameter of 0.98 inches.

Figure 40: Site 2 herbaceous

The first location in site 2 contained sparse herbaceous species of vegetation. The density was low at 68 stems in the area with an average diameter of 0.28 inches and a LAI of 0.1. The average height was 5.36 feet.

Figure 41: Site 2 mixed riparian low density 6

The next location in site 2 consisted of mostly low density willow. The average height of the trees was 7.22 feet. The species were mostly small with an average diameter of 0.69 inches and a LAI of 0.075. The density was low at 95 stems in the area.

Figure 42: Site 2 willow riparian 3

The willow riparian 3 vegetation at site 2 was slightly denser vegetation than the previous location. The willows had an average height of 11.98 feet, LAI of 0.96, average stem diameter of 0.49 inches, and a density of 77 stems in the 100 square meter area.

Figure 43: Site 2 cottonwood low density 4

The last species investigated in site 2 was the cottonwood low density 4. It contained the lowest stem density at 4 stems in the 100 square meter area. The stems had a large average diameter of 21.2 inches. The LAI was 2.48 for the trees.

Figure 44: Site 3 mixed riparian 3

The first location at site 3 consisted of mixed riparian similar to site 1. The stem density was similar at 137 stems in the area while the average stem diameter was slightly higher at 1.5 inches and contained numerous larger stems. The average height and LAI were much greater at 48.23 feet and 3.38, respectively.

Figure 45: Site 3 willow scrub 5

The willow scrub 5 location consisted of small willows with an average height of 7.55 feet, a low LAI at 0.12, a density of 134 stems in the area, and an average stem diameter of 0.49 inches.

Figure 46: Site 3 willow riparian 3

Willow riparian 3 consisted of large trees amongst willow riparian vegetation. The LAI and stem diameter were high at 3.9 and 178 stems, respectively. The average diameter was 1.07 and the average height was 23.29 feet.

Figure 47: Site 4 mixed riparian 1

The first species at site 4 was the mixed riparian 1. The species consisted mostly of small stems with an average diameter of 0.961 inches. The density was counted as 184 stems, while the LAI and average height were 2.52 and 26.8 feet respectively.

Figure 48: Site 4 willow scrub low density 6

Contrary to its name, this species ended up being very densely populated at 310 stems in the 100 square meter area. The LAI was low at 0.35. The average height was 8.41 feet while the average stem diameter was 0.55 inches.

Figure 49: Site 4 willow scrub 5

The last species in site 4 consisted of densely populated willow scrub consisting of 186 in the 100 square meter area. The LAI was low at 0.78. The average stem diameter was 0.65 inches and the average height was 7.22 feet.

Figure 50: Site 5 herbaceous

This location consisted of cheat grass throughout with an average height of 0.66 feet. There were no woody vegetation and therefore no other measurements were taken.

Figure 51: Site 5 willow scrub 6

Willow scrub 6 was fairly sparse. The density was counted to be 114 stems in the 100 square meter area. The average height was 8.42 feet. The LAI was 0.56 and the average diameter was 0.57 inches.

Figure 52: Site 5 cottonwood low density 4

This site consisted of more willows than cottonwoods. The average height was 12.69 feet. The LAI was 1.78 and the average diameter was 0.78 inches. The stem density was low at 101 stems.

Figure 53: Site 6 cottonwood 3

The first species investigated in site 6 was cottonwood 3. The average height was 15.09 feet. The LAI was fairly high at 3.04. The average stem diameter was 0.847 inches. The density was low at 80 stems in the area.

Figure 54: Site 6 riparian scrub

Riparian scrub at site 6 consisted of low density vegetation with a stem count of 136. The average height was 8.53 feet, while the average LAI and stem diameter were 0.48 and 0.54 inches respectively.

Appendix B - Field Data Processing

Field data was processed before development of the hydraulic models. The measured parameters for each vegetation type were averaged to give a representative value for stem diameter, LAI, stem density, and height of each vegetation class. Representative values for Vegetation height and LAI were derived by taking the arithmetic mean of the measurements. Average stem diameter was calculated by averaging values of the large stems and the small stems measured. An arithmetic mean of the large stems was taken. The small stems were averaged by a 50% passing method. This was done by determining the two diameter classes, in which the value of diameter that half of the measurements are less than, lies between. This number was then determined by linearly interpolating between the two classes' median values to locate the number in which 50% of the measurements are smaller. The final average stem diameter was calculated by taking a weighted average of the arithmetic mean of the large stem diameters and the 50% passing value of the small stem diameters, based on the number of stems counted for large and small classes. For the purpose of the model, everything was expressed in English units. Height and stem diameter were expressed in feet. Stem density was expressed in stems per square feet. LAI is unitless.

Vegetation classes that were not were not measured in the field, were assigned values of measured data based on what was considered similar vegetation. Table 9 shows the vegetation parameters measured in the field that were used for each class in the hydraulic models. The yellow cells indicate classes that were measured in the field. Classes that contain "Default" as a parameter do not contain vegetation and therefore the default n value is used in in lieu of calculating a n_e values.

Table 9: Summary of vegetation parameters used for models

Code	Description	Height (ft)	LAI	Stem Diameter (ft)	m (stems/ft^2)
AG	Ag Field	7.22	0.08	0.057	0.088
AR	Arundo	15.09	3.04	0.071	0.076
AS	Alkali Sink	Default	Default	Default	Default
CW1	Cottonwood Riparian	15.09	3.04	0.071	0.076
CW2	Cottonwood Riparian	15.09	3.04	0.071	0.076
CW3	Cottonwood Riparian	15.09	3.04	0.071	0.076
CW4	Cottonwood Riparian	15.09	3.04	0.071	0.076
CW5	Cottonwood Riparian	15.09	3.04	0.071	0.076
CWLD2	Cottonwood Low Density	28.49	2.13	0.926	0.051
CWLD4	Cottonwood Low Density	28.49	2.13	0.926	0.051
CWLD6	Cottonwood Low Density	28.49	2.13	0.926	0.051
D	Disturbed	Default	Default	Default	Default
EB	Savannah	17.75	3.42	0.086	0.179
EXO	Exotic Tree	17.75	3.42	0.086	0.179
H	Herbaceous	3.01	0.05	0.023	0.063
MR1	Mixed Riparian	26.79	2.52	0.080	0.178
MR2	Mixed Riparian	26.79	2.52	0.080	0.178
MR3	Mixed Riparian	29.53	2.15	0.094	0.134
MR4	Mixed Riparian	29.53	2.15	0.094	0.134
MRLD2	Mixed Riparian Low Density	7.22	0.08	0.057	0.088
MRLD4	Mixed Riparian Low Density	7.22	0.08	0.057	0.088
MRLD6	Mixed Riparian Low Density	7.22	0.08	0.057	0.088
OAK1	Riparian Oak Tree	15.09	3.04	0.071	0.076
OAK2	Riparian Oak Tree	15.09	3.04	0.071	0.076
OAK3	Riparian Oak Tree	15.09	3.04	0.071	0.076
OAK4	Riparian Oak Tree	15.09	3.04	0.071	0.076
RS	Riparian Scrub	2.60	0.48	0.045	0.126
RW	Riverwash	Default	Default	Default	Default
URB	Urban	Default	Default	Default	Default
WA	Open Water	Default	Default	Default	Default
WET	Wetland/Marsh	7.22	0.08	0.057	0.088
WR1	Willow Riparian	11.98	0.96	0.041	0.072
WR2	Willow Riparian	11.98	0.96	0.041	0.072
WR3	Willow Riparian	17.75	3.42	0.086	0.179
WR4	Willow Riparian	11.98	0.96	0.041	0.072
WRLD	Willow Riparian Low Density	11.98	0.96	0.041	0.072
WRLD2	Willow Riparian Low Density	11.98	0.96	0.041	0.072
WRLD3	Willow Riparian Low Density	11.98	0.96	0.041	0.072
WRLD4	Willow Riparian Low Density	11.98	0.96	0.041	0.072
WS5	Willow Scrub	7.38	0.45	0.048	0.149
WS6	Willow Scrub	8.42	0.56	0.047	0.106
WSLD6	Willow Scrub Low Density	7.47	0.45	0.043	0.177

Appendix C- SRH-2D Equations

SRH-2D and SRH-2DV hydraulically model open channel river systems by solving the two-dimensional depth-averaged dynamic wave equations, otherwise known as the St. Venant equations. The St. Venant equations are derived from the three-dimensional Navier-Stokes equations by averaging the vertical component. This is possible because open channels often flow with minimal depth and therefore effects of vertical flows are negligible.

The Navier-Stokes equations represent a complete physical description of flow for incompressible Newtonian fluids (Munson et al. 2009).

$$\rho\left(\frac{\partial u}{\partial t}+u\frac{\partial u}{\partial x}+v\frac{\partial u}{\partial y}+w\frac{\partial u}{\partial z}\right)=-\frac{\partial p}{\partial x}+\rho g_x+\mu\left(\frac{\partial^2 u}{\partial x^2}+\frac{\partial^2 u}{\partial y^2}+\frac{\partial^2 u}{\partial z^2}\right)$$

$$\rho\left(\frac{\partial v}{\partial t}+u\frac{\partial v}{\partial x}+v\frac{\partial v}{\partial y}+w\frac{\partial v}{\partial z}\right)=-\frac{\partial p}{\partial y}+\rho g_y+\mu\left(\frac{\partial^2 v}{\partial x^2}+\frac{\partial^2 v}{\partial y^2}+\frac{\partial^2 v}{\partial z^2}\right)$$

$$\rho\left(\frac{\partial w}{\partial t}+u\frac{\partial w}{\partial x}+v\frac{\partial w}{\partial y}+w\frac{\partial w}{\partial z}\right)=-\frac{\partial p}{\partial z}+\rho g_z+\mu\left(\frac{\partial^2 w}{\partial x^2}+\frac{\partial^2 w}{\partial y^2}+\frac{\partial^2 w}{\partial z^2}\right)$$

After depth and time averaging the Navier-Stokes equations, the 2D St. Venant equations are obtained below (Lai 2008).

$$\frac{\partial h}{\partial t}+\frac{\partial hU}{\partial x}+\frac{\partial hV}{\partial y}=e$$

$$\frac{\partial hU}{\partial t}+\frac{\partial hUU}{\partial x}+\frac{\partial hVU}{\partial y}=\frac{\partial hT_{xx}}{\partial x}+\frac{\partial hT_{xy}}{\partial y}-gh\frac{\partial z}{\partial x}-\frac{\tau_{bx}}{\rho}+D_{xx}+D_{xy}$$

$$\frac{\partial hV}{\partial t}+\frac{\partial hUV}{\partial x}+\frac{\partial hVV}{\partial y}=\frac{\partial hT_{xy}}{\partial x}+\frac{\partial hT_{yy}}{\partial y}-gh\frac{\partial z}{\partial y}-\frac{\tau_{by}}{\rho}+D_{yx}+D_{yy}$$

In these equations, *t* is time, *x* and *y* are the streamwise and transverse coordinates, and *h* is flow depth. The time-averaged velocities in the *x* and y directions are represented by *U*

and V respectively, while e is equal to the excess rainfall rate. Acceleration due to gravity is represented by g, ρ is water density, z is water surface elevation, and T_{xx}, T_{xy}, and T_{yy} are the depth averaged turbulent stresses. D_{xx}, D_{xy}, D_{yx}, and D_{yy} are terms representing dispersion. Bed friction is represented by τ_{bx} and τ_{by}.

The turbulent stresses and shear stresses are represented using the following equations (Lai 2008).

$$\tau_{bx} = \rho C_f U\sqrt{U^2 + V^2}$$

$$\tau_{by} = \rho C_f V\sqrt{U^2 + V^2}$$

$$C_f = \frac{gn^2}{h^{1/3}}$$

$$T_{xx} = 2(\nu + \nu_t)\frac{\partial U}{\partial x} - \frac{2}{3}k$$

$$T_{yy} = 2(\nu + \nu_t)\frac{\partial V}{\partial y} - \frac{2}{3}k$$

$$T_{xy} = 2(\nu + \nu_t)(\frac{\partial U}{\partial y} + \frac{\partial V}{\partial x})$$

In these equations, ν, ν_t, and k represent the kinematic viscosity of water, turbulent eddy viscosity, and the turbulent kinetic energy. Manning's roughness is represented with n. The turbulent eddy viscosity is represented by the following equation,

$$\nu_t = \alpha U^* h$$

where α is a constant ranging from 0.3 to 1.0 but typically chosen as 0.7, U^* is the bed frictional velocity (Lai 2008).

Appendix D- Model Development

Every model created was made in similar fashion, varying only a few parameters in each simulation involving vegetation characteristics or flow already discussed above. Every model was run in SRH-2D partial interface mode to provide the user more control (Lai 2008). In this mode, SMS is only required to generate the two-dimensional mesh. The user then uses SRH-2D preprocessor to generate an input file to run SRH-2D or SRH-2DV. The preprocessor prompts the user to define a number of conditions, the majority of which stayed the same for all models.

The preprocessor prompts the user to define the module selected. "FLOW" is chosen for all simulations in order to model the hydraulics for each run. Monitoring points must be defined for the purpose of checking solutions with respect to time. Five points were chosen as the same points used in the Reclamation (2012) study. Figure 55 shows the locations of these points.

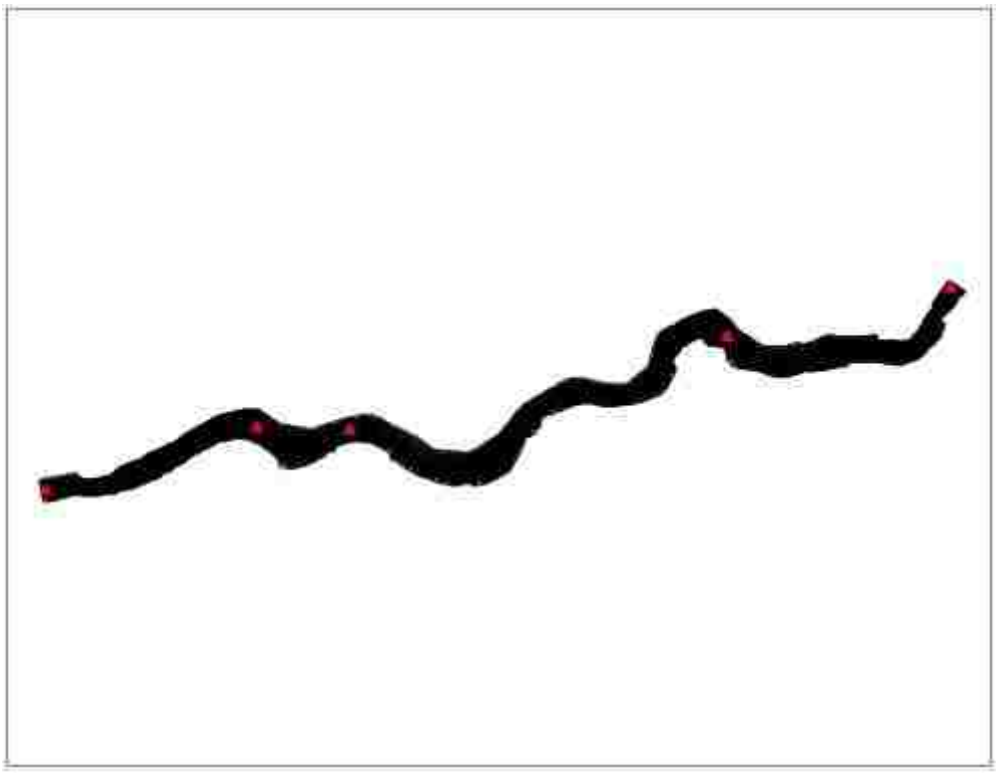

Figure 55: Locations of monitoring points along the 1B reach mesh

"STEADY" flow is chosen for all simulations. SRH-2D always runs in unsteady flow, but if "STEADY" flow is chosen, this means that the final solutions at the end of the run are the only solutions being considered when computing, therefore the intermediary solutions may be incorrect (Lai 2008). Every model was run at 10 second computation intervals. The initial dry simulations without vegetation computations were run from a "DRY" bed for a simulation time of 480 hours to ensure steady state of solutions. Every simulation runs with vegetation computations were run for 200 simulation hours. These runs were all started from ending conditions of the initial dry simulations. This was done in an effort to reduce computation time. The depth-averaged parabolic "PARA" turbulent model was selected for every model and a default value of 0.7 of α was chosen. These were chosen to stay consistent with the calibrated models developed by Reclamation. English units of feet for the output solutions were chosen for every model.

Initial Manning's roughness values were provided for the 7 material types defined in the mesh, for every model. See Table 2 and Figure 4 for values and display of roughness values throughout the mesh. Two boundary conditions were chosen at the upstream and downstream ends of the mesh. The upstream boundary condition is defined by a volumetric flow rate, while the downstream condition is specified as a known water surface elevation. See Table 1 for upstream and downstream boundary conditions. "SRHN" solutions output was chosen for every model. This displays solutions at every node in the mesh. Solutions are posted in a text file and easily imported into ArcGIS.

In addition to the regular SRH-2D preprocessor inputs, the new vegetation modules require a text file that specifies details required for the vegetation roughness calculations to occur. The same text file was used for every vegetation model. The user must specify the location of the folder containing the required vegetation shapefile. The comma separated values file must be kept in the same folder and must contain the same name as the shapefile. This folder must be kept in the same folder containing the SRH-2D executable in order to work properly. A column header in the comma separated file must be specified for the output solutions of each polygon. "ABBREV" was chosen. This is simply the abbreviation of the vegetation polygon in question and acts as a quick description. For example "MR3" stands for Mixed Riparian 3. Vegetation computational time step must also be specified in seconds. This is how frequently the program calculates the new roughness values. 10 seconds was chosen, as this was the same time step chosen for the hydraulic calculations. Results output time step must also be specified in seconds. This is how often, in simulation time, the program generates a solution file. 3600 seconds was specified.

The vegetation roughness simulations were defined by parameters that were specific to the Baptist and Järvelä techniques. Table 10 below summarizes the simulations performed with their corresponding parameters. These are the parameters that remained constant with every vegetation class.

Table 10: Summary of parameters that do not vary between species for all vegetation simulations performed

Flow (m^3/s)	Method	$C_{D\chi}$	χ	U_χ (m/s)	C_b	C_D
31.2	Jarvela	0.5	-0.45	0.1	Null	Null
70.8	Jarvela	0.5	-0.45	0.1	Null	Null
113.3	Jarvela	0.5	-0.45	0.1	Null	Null
113.3	Jarvela	0.4	-0.45	0.1	Null	Null
113.3	Jarvela	0.6	-0.45	0.1	Null	Null
113.3	Jarvela	0.5	-0.55	0.1	Null	Null
113.3	Jarvela	0.5	-0.35	0.1	Null	Null
212.4	Jarvela	0.5	-0.45	0.1	Null	Null
31.2	Baptist	Null	Null	Null	80	1
70.8	Baptist	Null	Null	Null	80	1
113.3	Baptist	Null	Null	Null	80	1
113.3	Baptist	Null	Null	Null	80	1.5
113.3	Baptist	Null	Null	Null	80	0.5
212.4	Baptist	Null	Null	Null	80	1

Appendix E- Model Results

The following figures represent results at 70.8 and 113.3 m^3/s for the Järvelä and Baptist approaches. The tables represent the n_e minimum, maximum, and average values using both approaches, in regards to five land uses established by Reclamation for the default *n* values. The mapped n_e values focus on field site 4 near State Route 145. The histograms displayed represent change in water surface elevations and velocities from the calibrated models developed by Reclamation. The sensitivity analysis results for 113.3 m^3/s are also shown in the histograms. Values at the 70.8 and 113.3 m^3/s values are represented in these figures. Maps of the change in water surface elevation are also provided below. The first set focuses on the upstream end of the reach near field sites 2 and 3 showing both techniques at 70.8 and 113.3 m^3/s. The next set of figures focuses on the downstream end near field sites 4 and 5, representing both approaches at flows of 31.2, 70.8, 113.3, and 212.4 m^3/s.

Table 11: Summary of n_e values calculated by the vegetation models at 70.8 m^3/s

		Järvelä			Baptist		
Land Use Type	**Default n**	**Minimum n_e**	**Maximum n_e**	**Average n_e**	**Minimum n_e**	**Maximum n_e**	**Average n_e**
Agriculture	0.056	0.004	0.135	0.047	0.007	0.095	0.048
Open/Bare Ground/ Scattered Brush-Weeds	0.056	0.006	0.124	0.050	0.010	0.095	0.053
Scattered Trees/ Light Brush	0.075	0.004	0.135	0.056	0.009	0.090	0.056
Medium Density Trees/ Brush	0.1	0.009	0.145	0.067	0.012	0.100	0.055
Dense Trees/Brush	0.125	0.006	0.148	0.069	0.009	0.125	0.058

Table 12: Summary of n_e values calculated by the vegetation models at 113.3 m^3/s

		Järvelä			Baptist		
Land Use Type	**Default n**	**Minimum n_e**	**Maximum n_e**	**Average n_e**	**Minimum n_e**	**Maximum n_e**	**Average n_e**
Agriculture	0.056	0.003	0.137	0.045	0.008	0.100	0.046
Open/Bare Ground/ Scattered Brush-Weeds	0.056	0.008	0.120	0.049	0.010	0.100	0.054
Scattered Trees/ Light Brush	0.075	0.006	0.144	0.043	0.010	0.101	0.045
Medium Density Trees/ Brush	0.1	0.003	0.165	0.069	0.009	0.117	0.052
Dense Trees/Brush	0.125	0.003	0.165	0.071	0.009	0.139	0.060

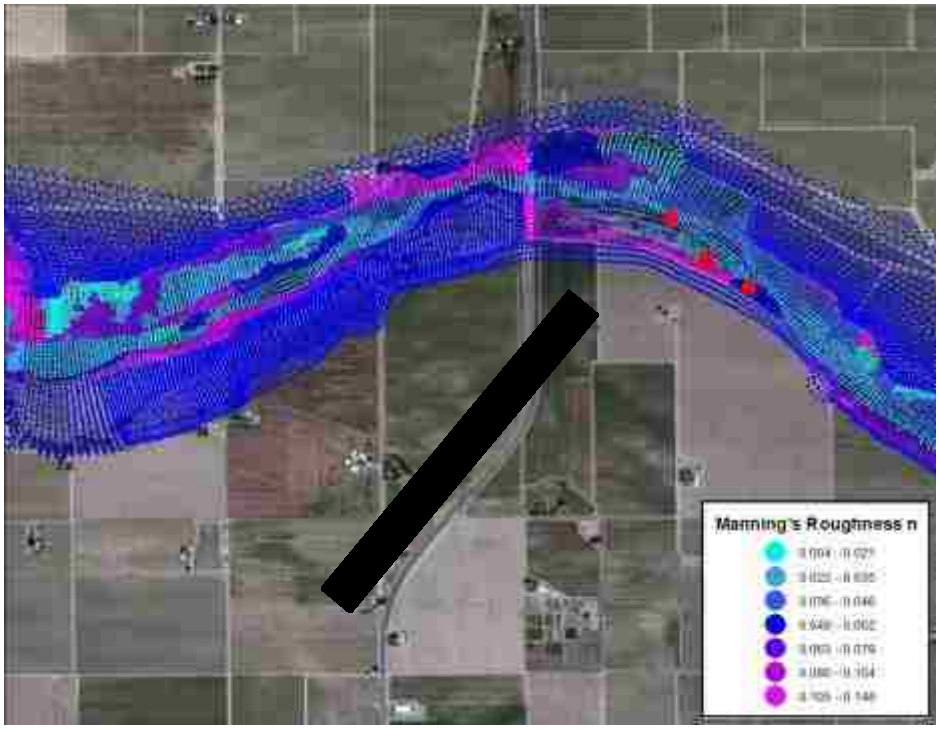

Figure 56: Manning's *n* near field site 4 using the Järvelä approach at 70.8 m^3/s

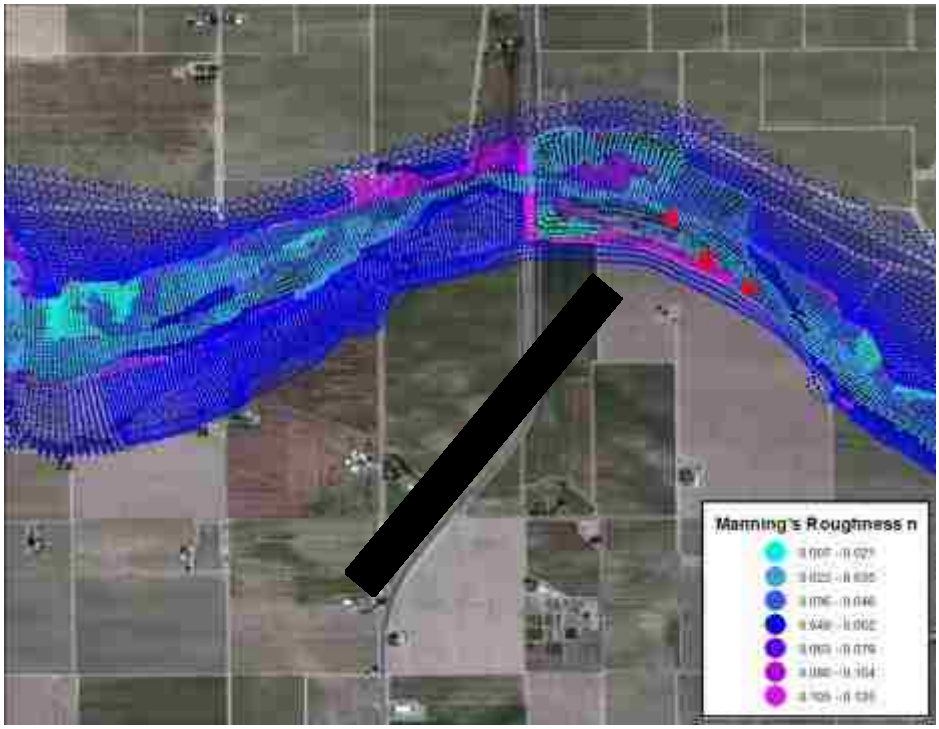

Figure 57: Manning's *n* near field site 4 using the Baptist approach at 70.8 m^3/s

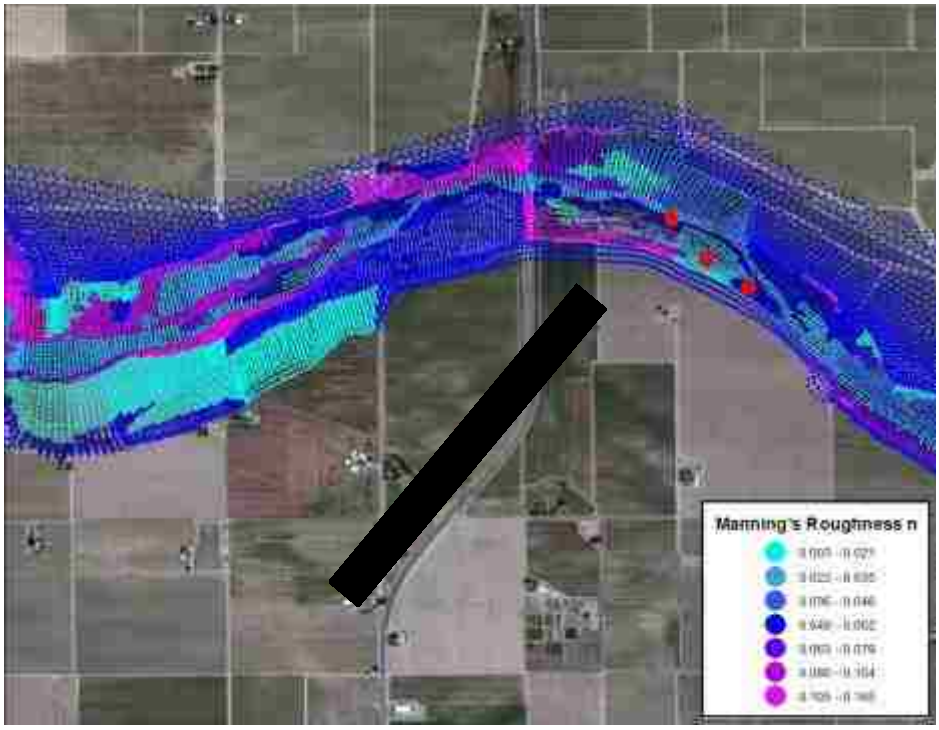

Figure 58: Manning's *n* near field site 4 using the Järvelä approach at 113.3 m^3/s

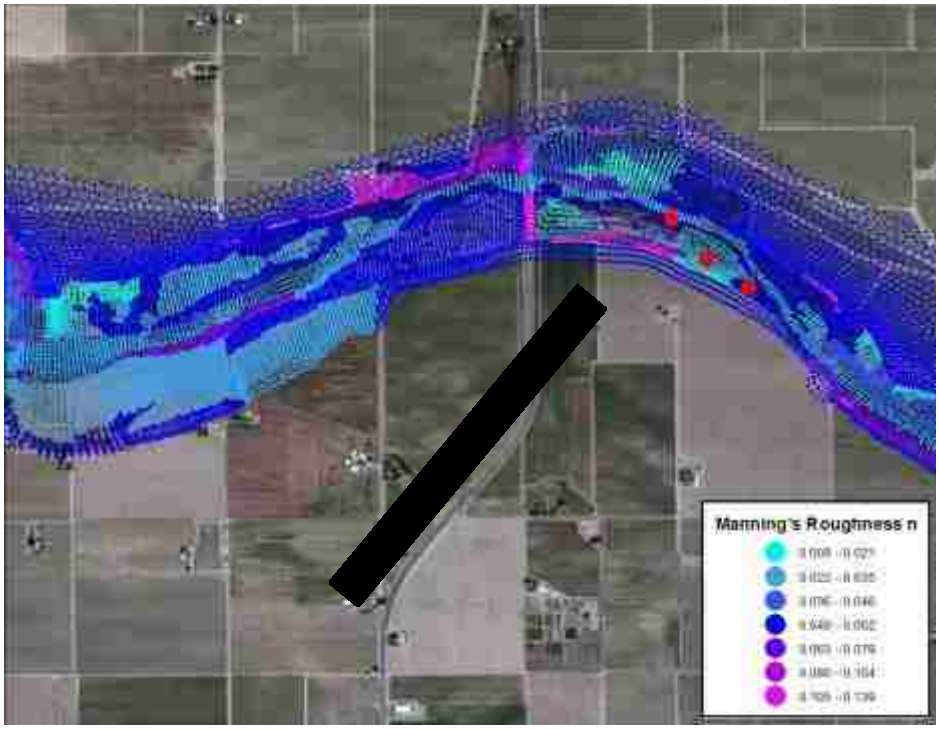

Figure 59: Manning's *n* near field site 4 using the Baptist approach at 113.3 m^3/s

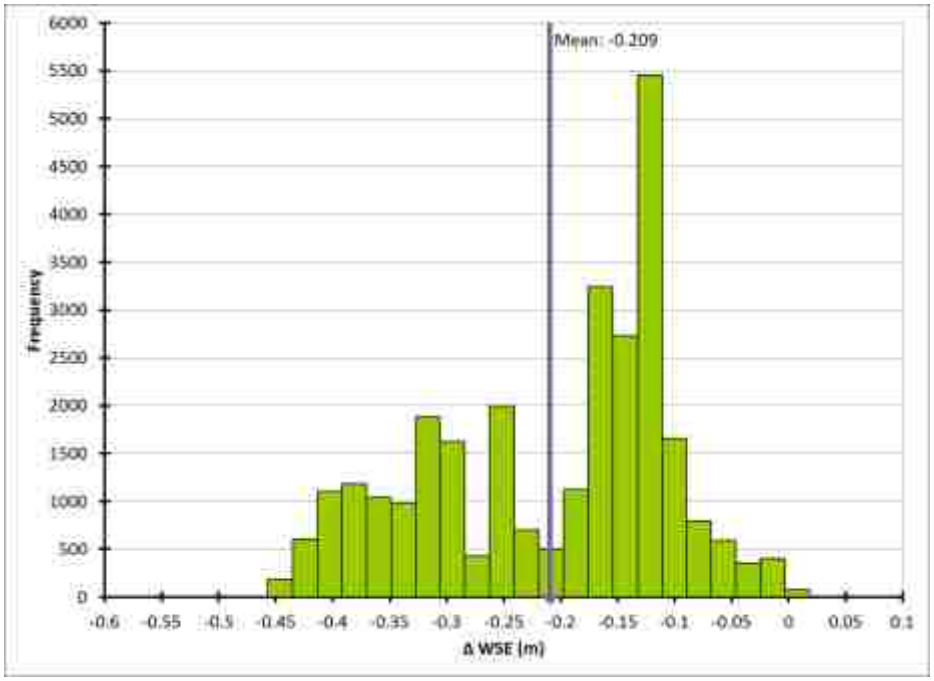

Figure 60: Change in water surface elevation at 70.8 m^3/s between the calibrated model and the Järvelä vegetation model

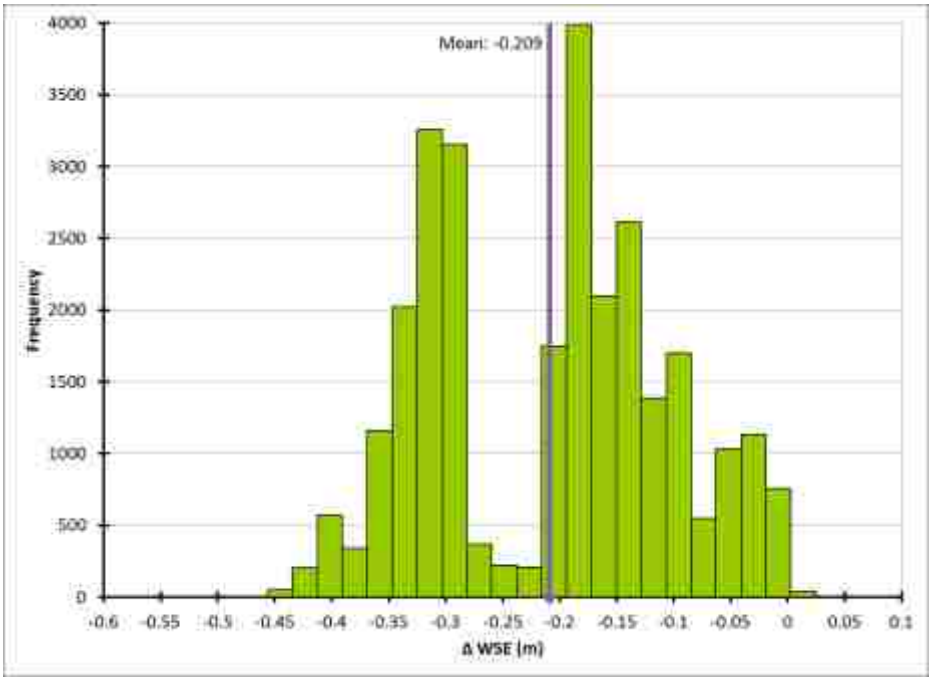

Figure 61: Change in water surface elevation at 70.8 m^3/s between the calibrated model and the Baptist vegetation model

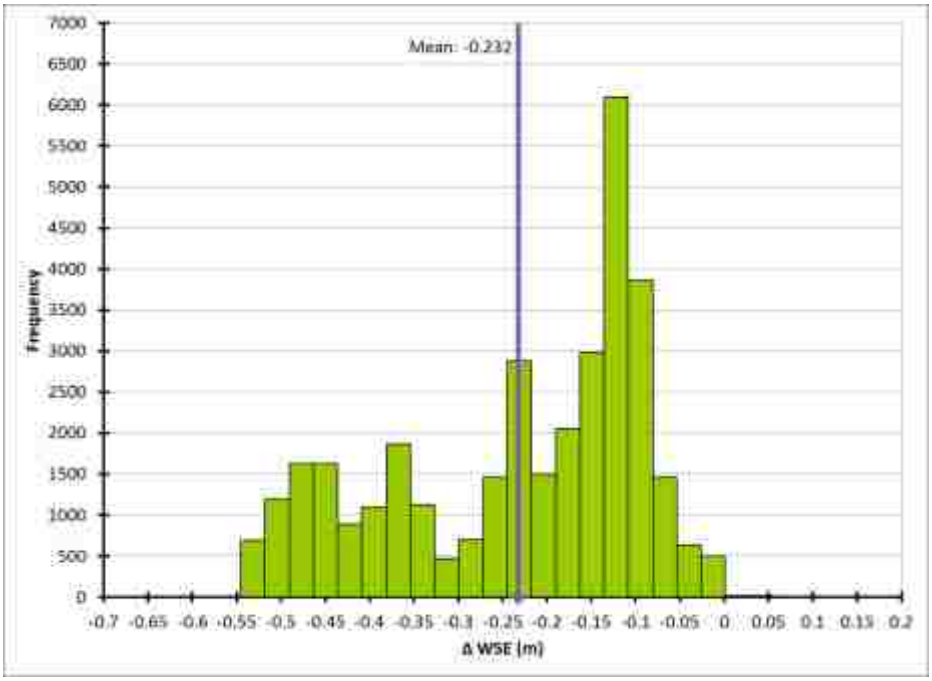

Figure 62: Change in water surface elevation at 113.3 m^3/s between the calibrated model and the Järvelä vegetation model

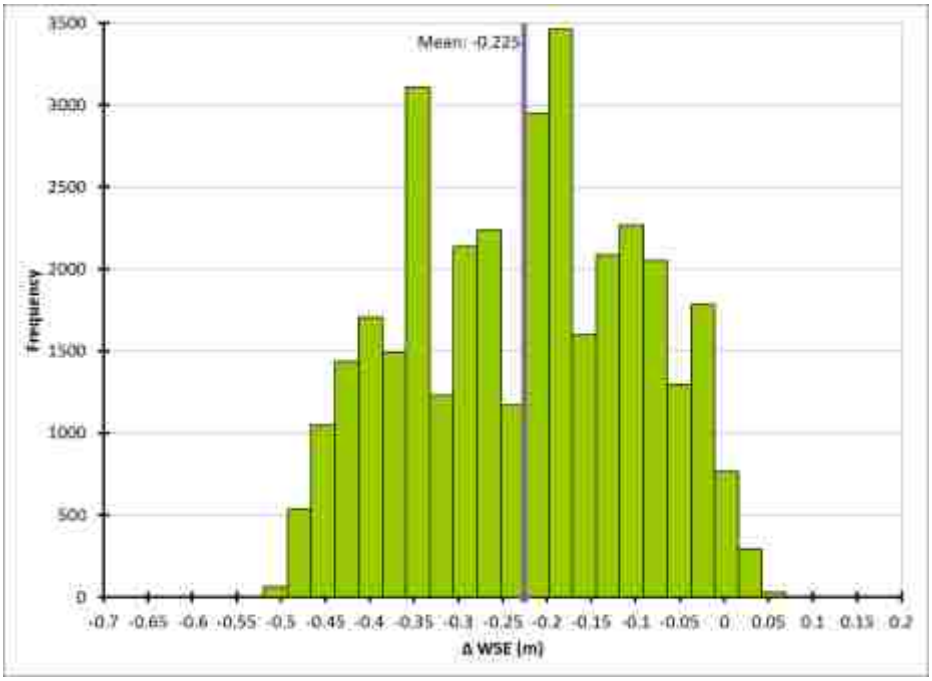

Figure 63: Change in water surface elevation at 113.3 m^3/s between the calibrated model and the Baptist vegetation model

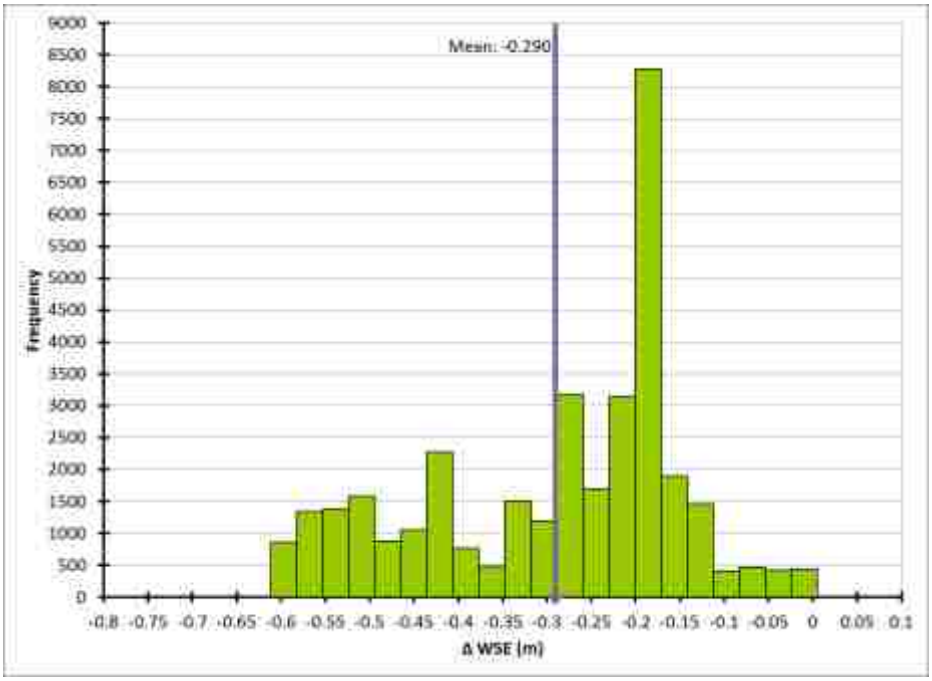

Figure 64: Change in water surface elevation at 113.3 m^3/s using the Järvelä method decreaing $C_{d\chi}$ from 0.5 to 0.4

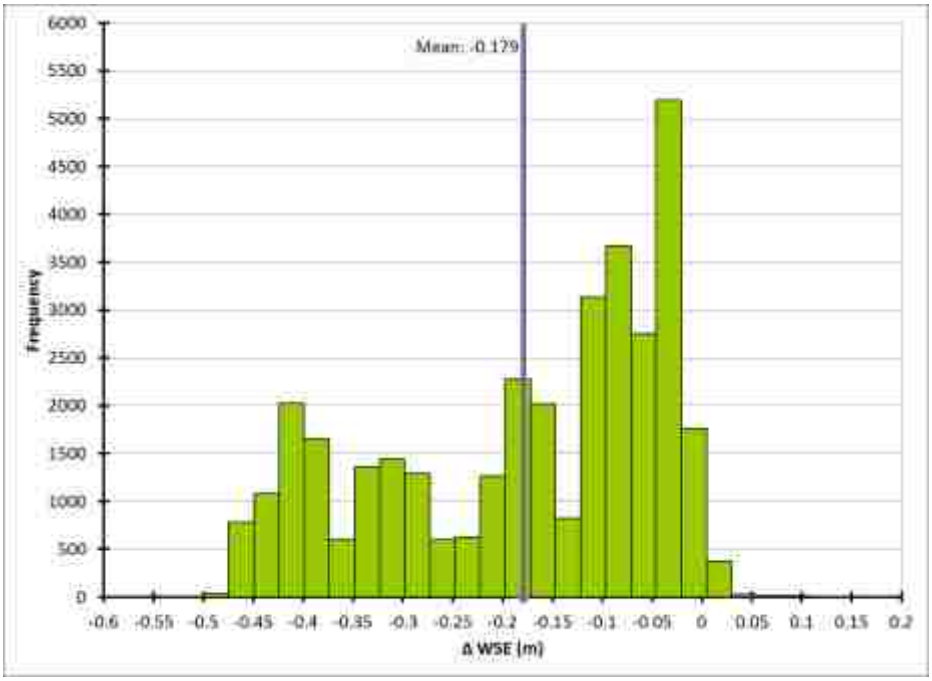

Figure 65: Change in water surface elevation at 113.3 m^3/s using the Järvelä method increaing $C_{d\chi}$ from 0.5 to 0.6

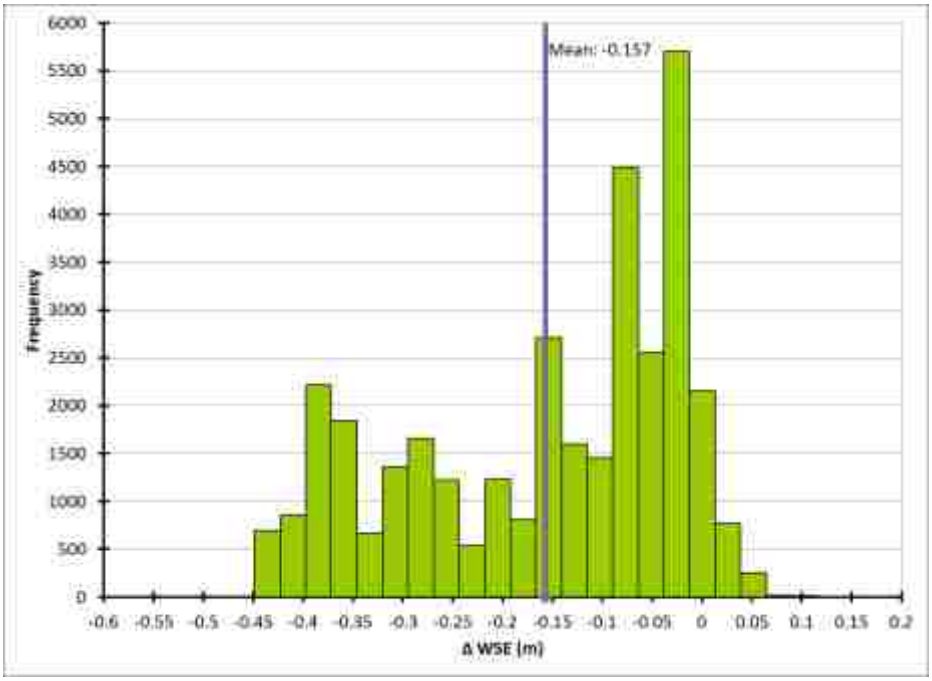

Figure 66: Change in water surface elevation at 113.3 m^3/s using the Järvelä method increaing χ from -0.45 to -0.35

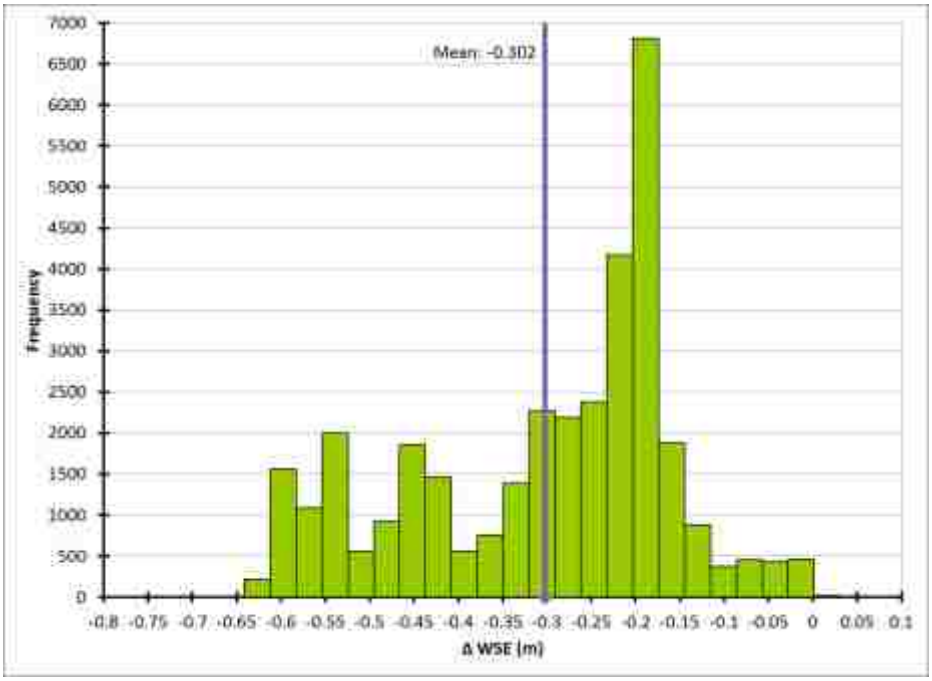

Figure 67: Change in water surface elevation at 113.3 m^3/s using the Järvelä method decreaing χ from -0.45 to -0.55

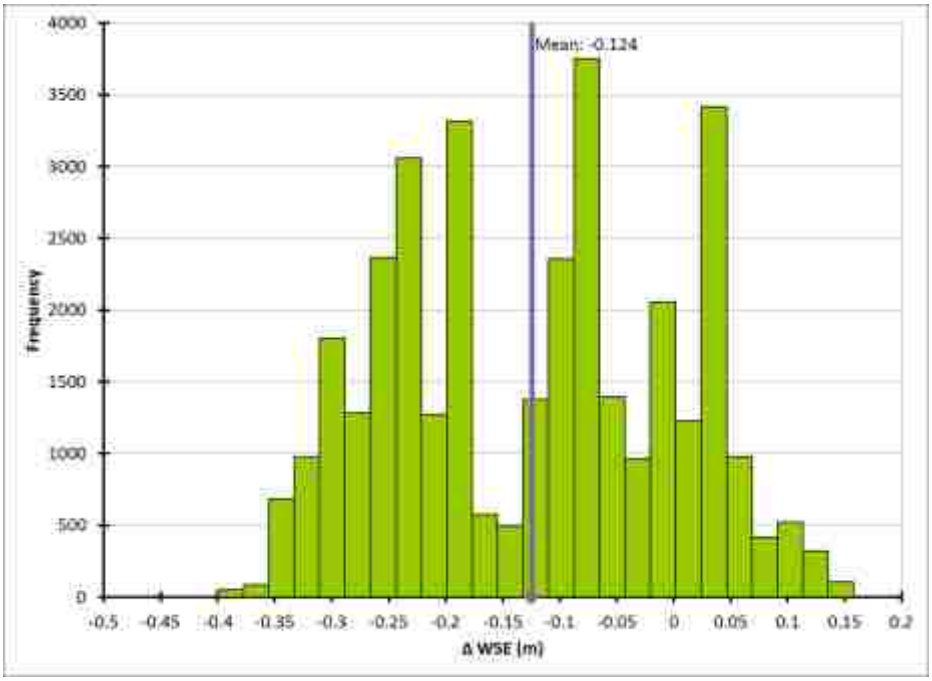

Figure 68: Change in water surface elevation at 113.3 m^3/s using the Baptist method increaing C_D from 1.0 to 1.5

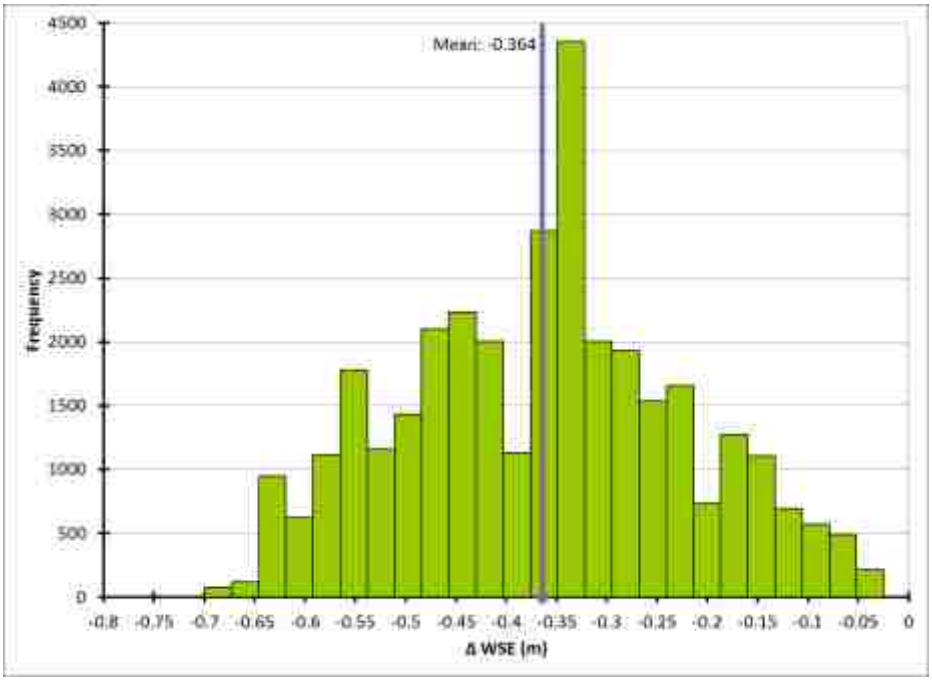

Figure 69: Change in water surface elevation at 113.3 m^3/s using the Baptist method decreaing C_D from 1.0 to 0.5

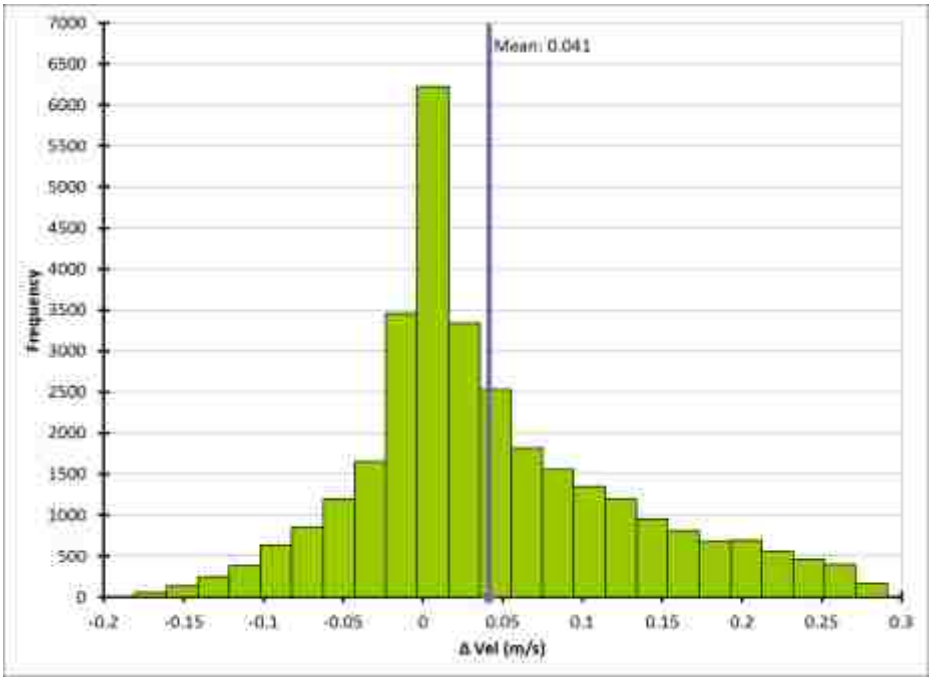

Figure 70: Change in velocity at 70.8 m^3/s between the calibrated model and the Järvelä vegetation model

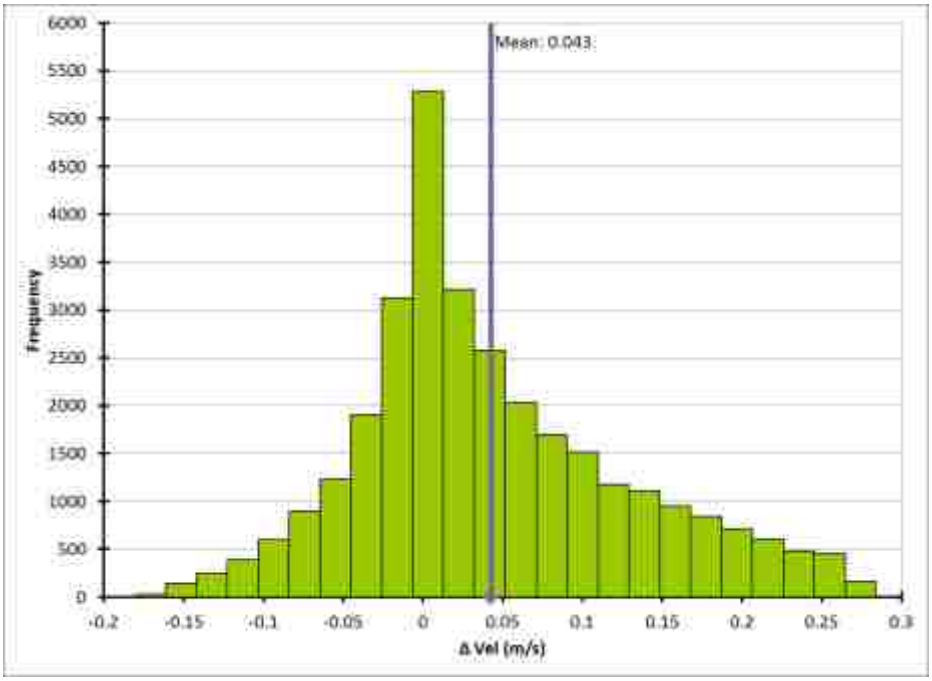

Figure 71: Change in velocity at 70.8 m^3/s between the calibrated model and the Baptist vegetation model

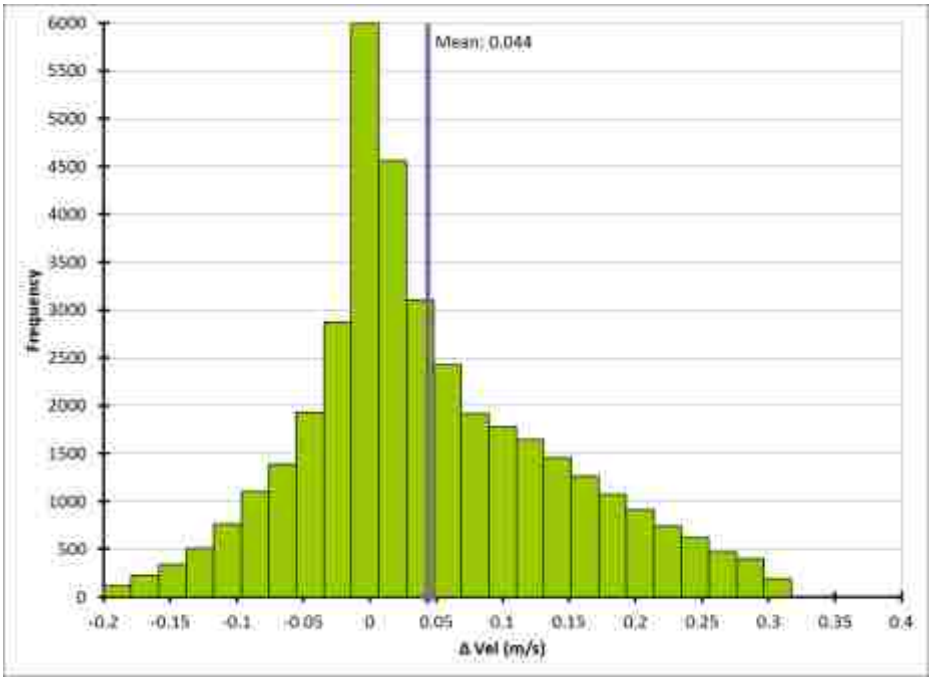

Figure 72: Change in velocity at 113.3 m^3/s between the calibrated model and the Järvelä vegetation model

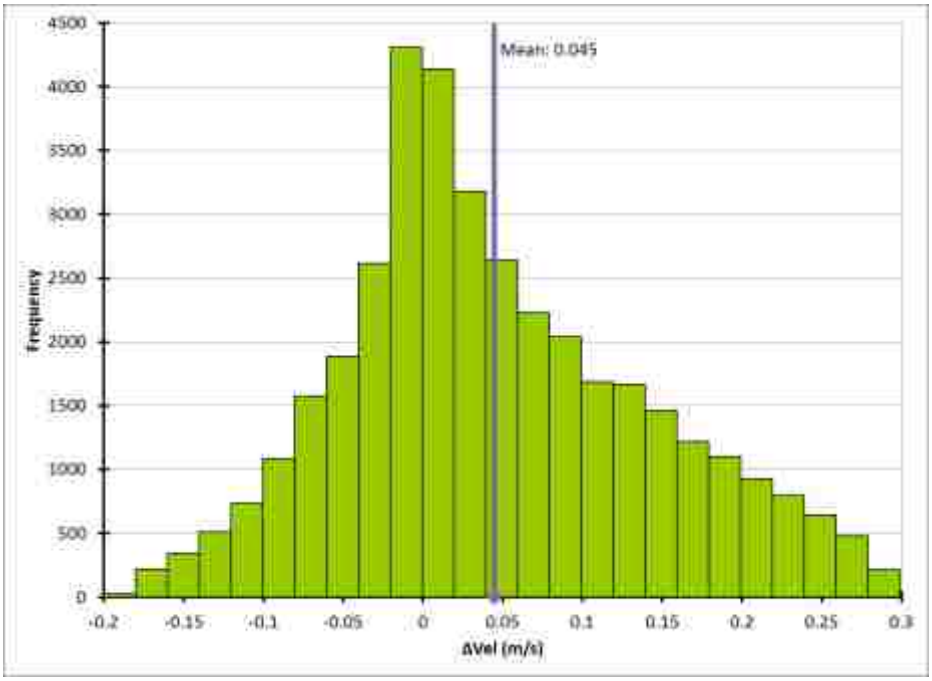

Figure 73: Change in velocity at 113.3 m^3/s between the calibrated model and the Baptist vegetation model

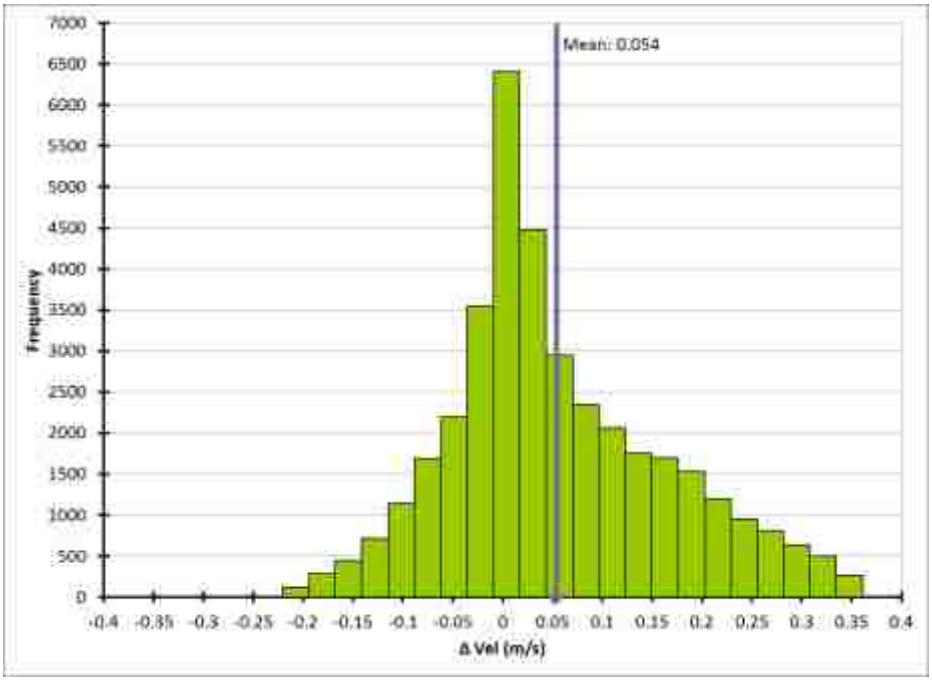

Figure 74: Change in velocity at 113.3 m^3/s using the Järvelä method decreasing $C_{d\chi}$ from 0.5 to 0.4

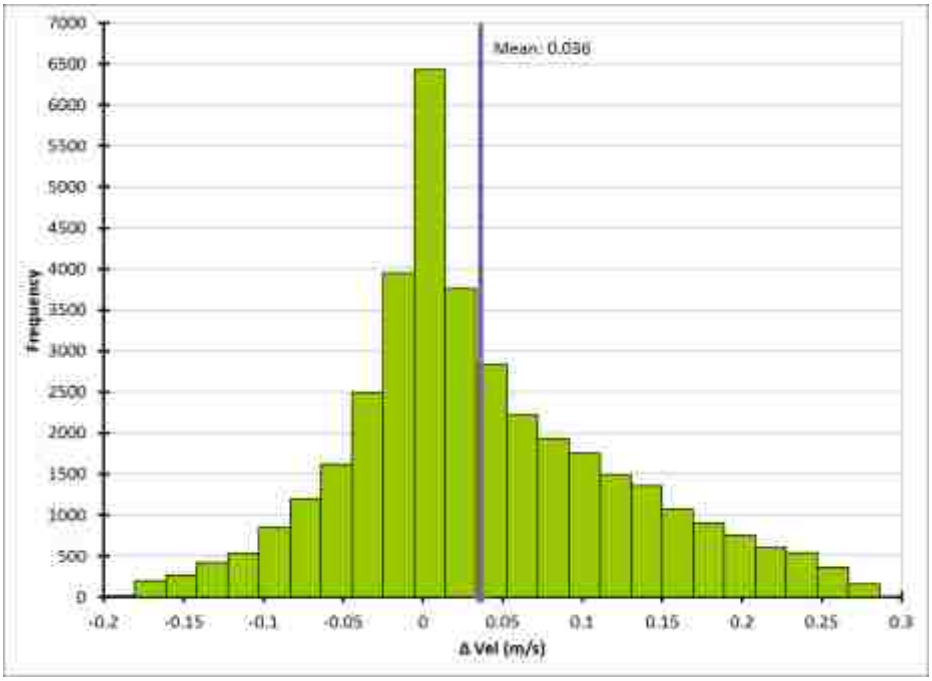

Figure 75: Change in velocity at 113.3 m^3/s using the Järvelä method increasing $C_{d\chi}$ from 0.5 to 0.6

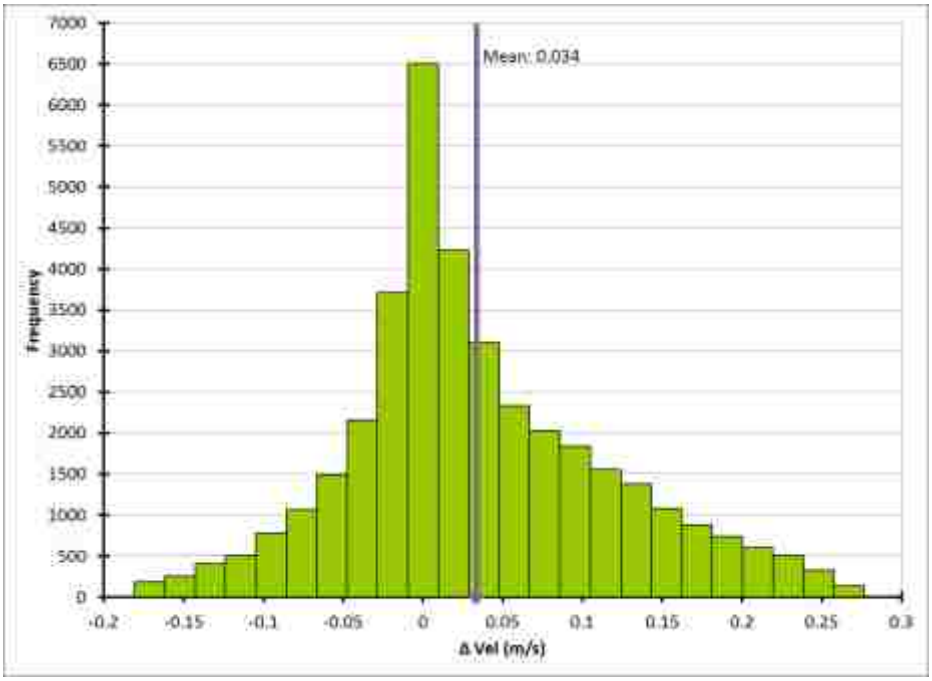

Figure 76: Change in velocity at 113.3 m^3/s using the Järvelä method increasing χ from -0.45 to -0.35

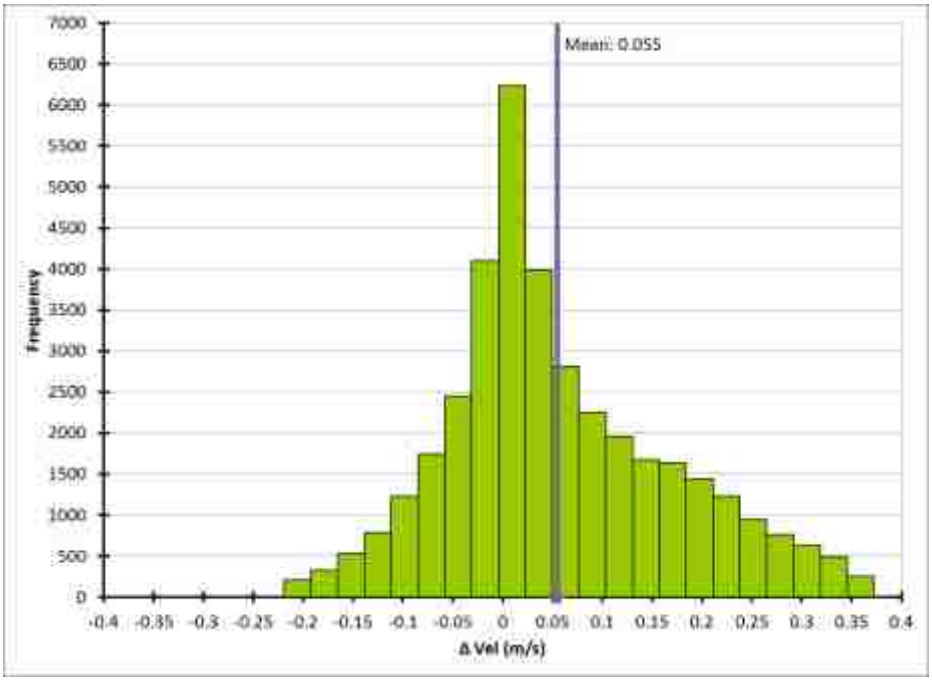

Figure 77: Change in velocity at 113.3 m^3/s using the Järvelä method decreasing χ from -0.45 to -0.55

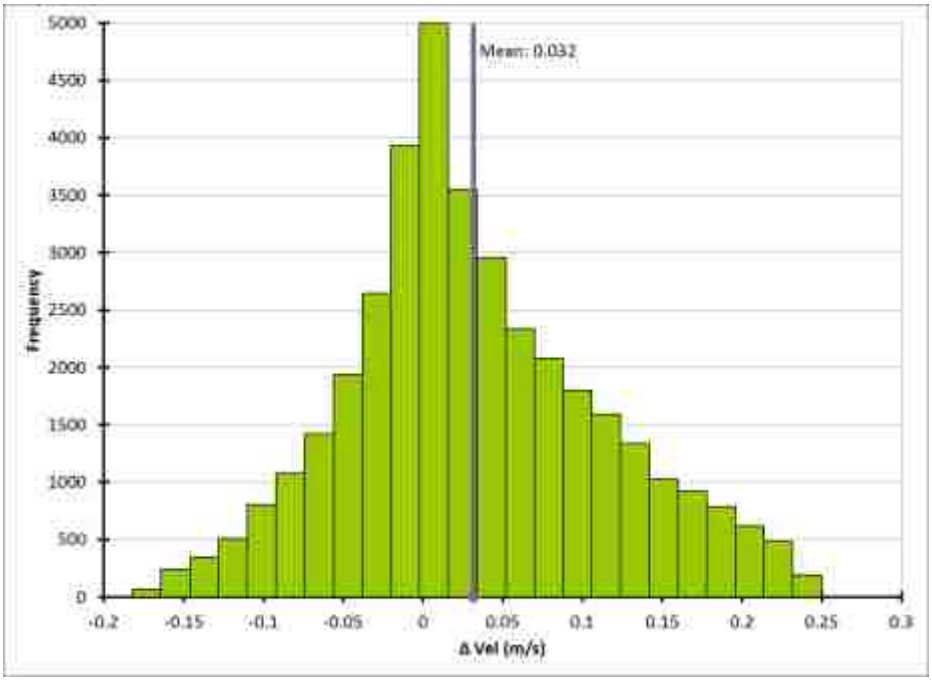

Figure 78: Change in velocity at 113.3 m^3/s using the Baptist method increasing C_D from 1.0 to 1.5

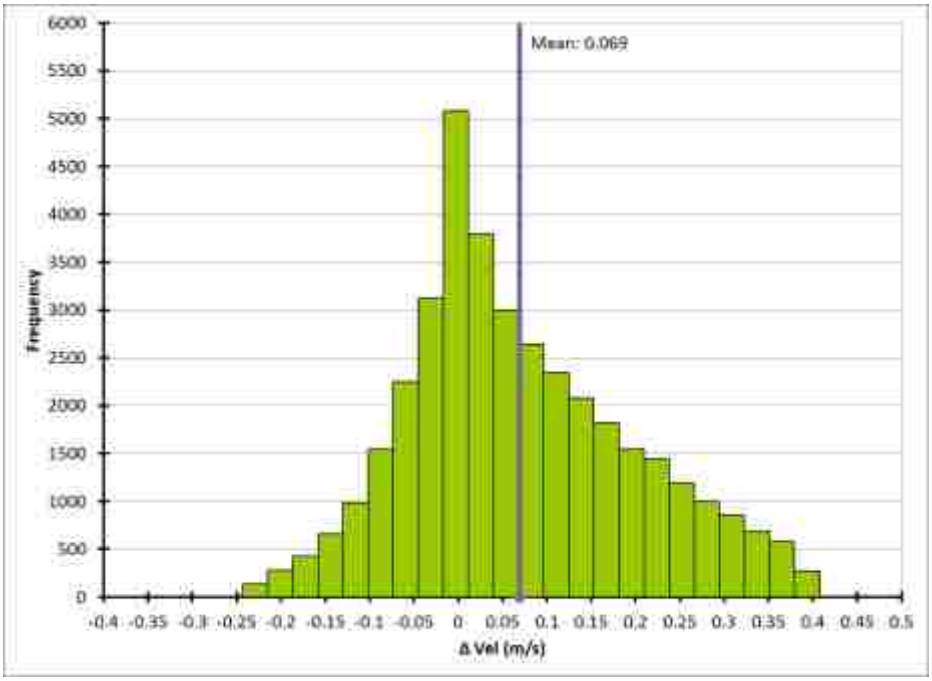

Figure 79: Change in velocity at 113.3 m^3/s using the Baptist method decreasing C_D from 1.0 to 0.5

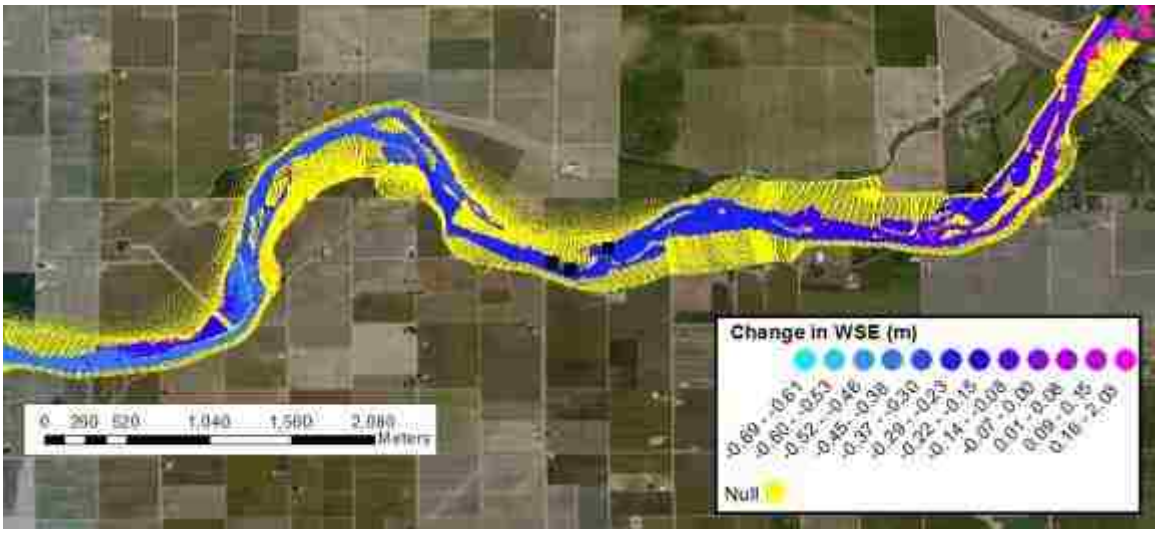

Figure 80: Change in water surface elevation at 70.8 m^3/s using the Järvelä approach near field sites 2 and 3

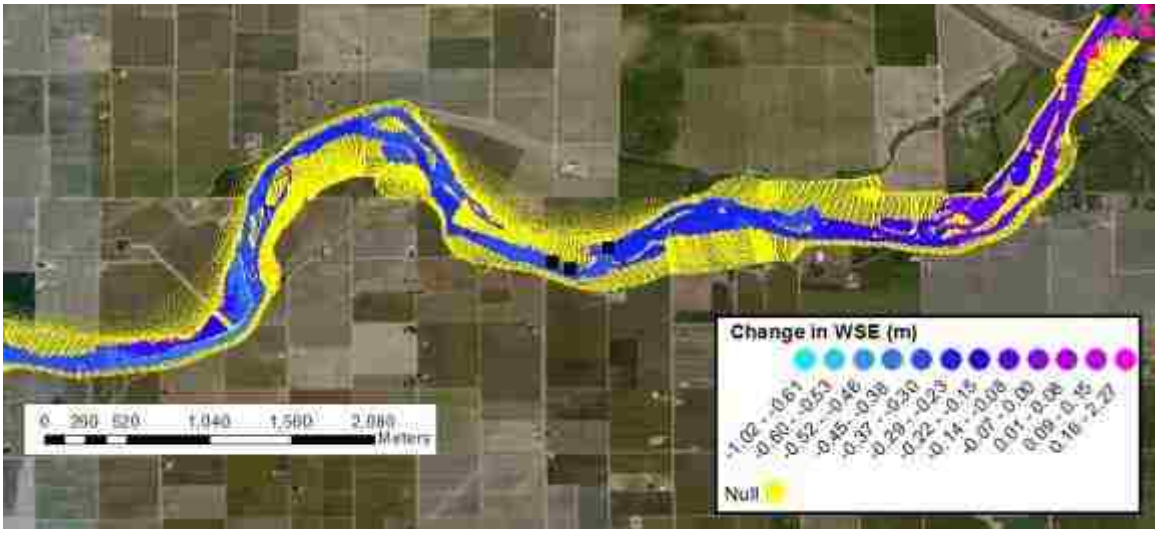

Figure 81: Change in water surface elevation at 70.8 m^3/s using the Baptist approach near field sites 2 and 3

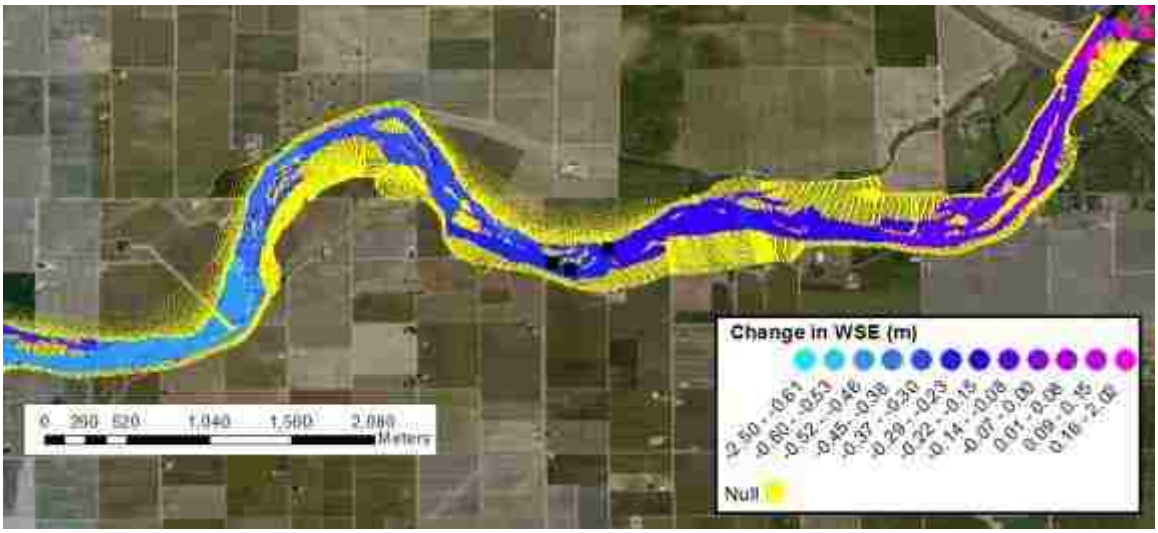

Figure 82: Change in water surface elevation at 113.3 m^3/s using the Järvelä approach near field sites 2 and 3

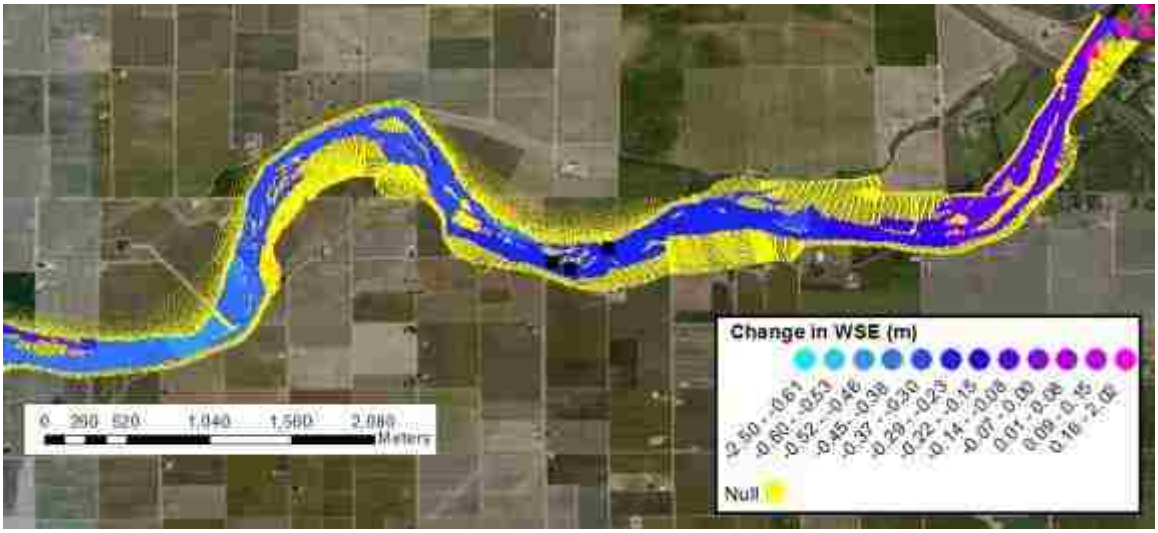

Figure 83: Change in water surface elevation at 113.3 m^3/s using the Baptist approach near field sites 2 and 3

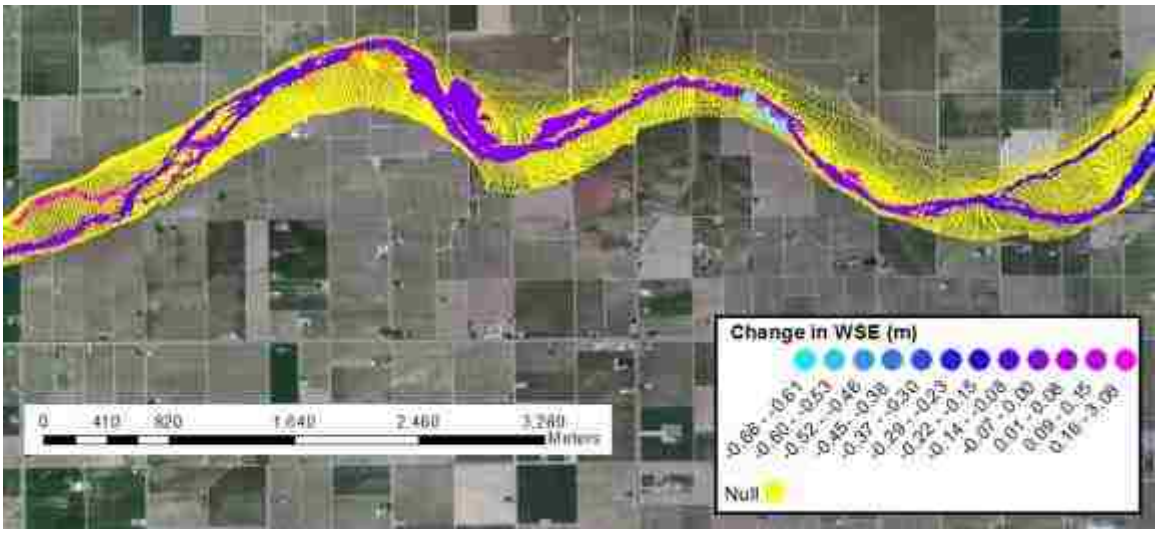

Figure 84: Change in water surface elevation at 31.2 m^3/s using the Järvelä approach near field sites 4 and 5

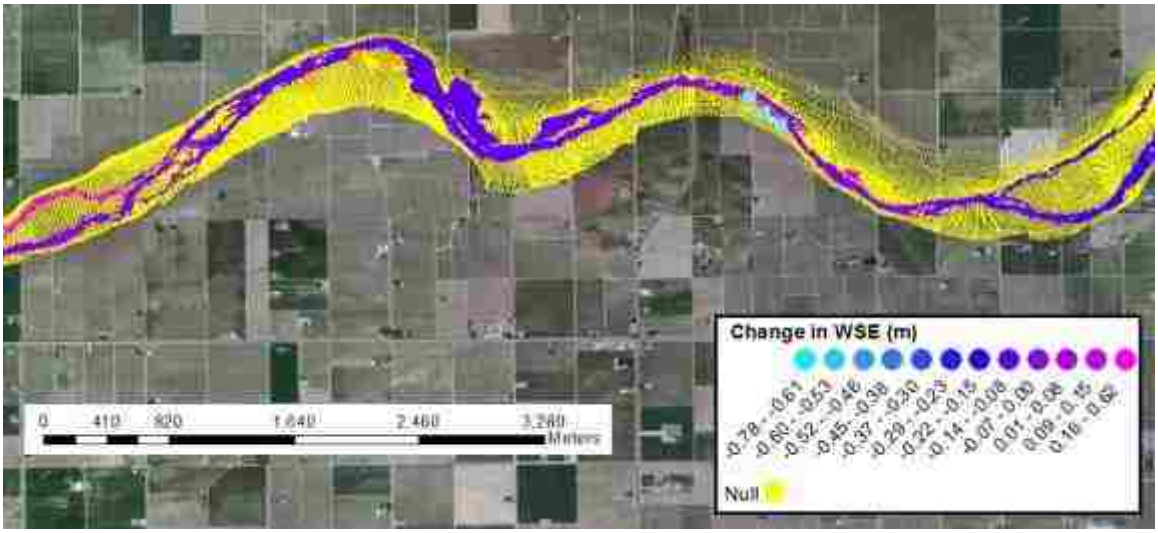

Figure 85: Change in water surface elevation at 31.2 m^3/s using the Baptist approach near field sites 4 and 5

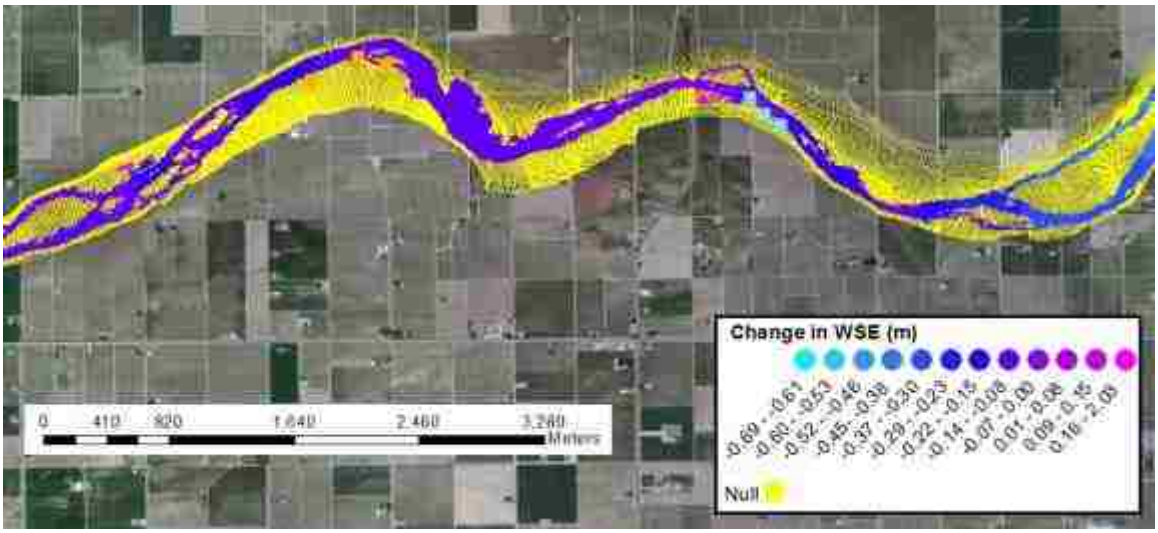

Figure 86: Change in water surface elevation at 70.8 m^3/s using the Järvelä approach near field sites 4 and 5

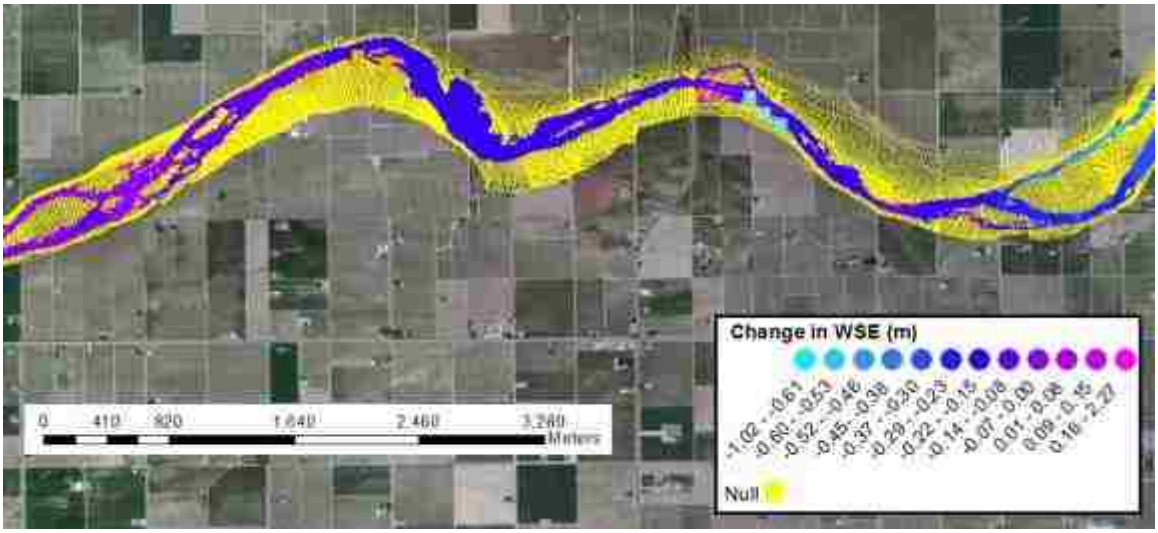

Figure 87: Change in water surface elevation at 70.8 m^3/s using the Baptist approach near field sites 4 and 5

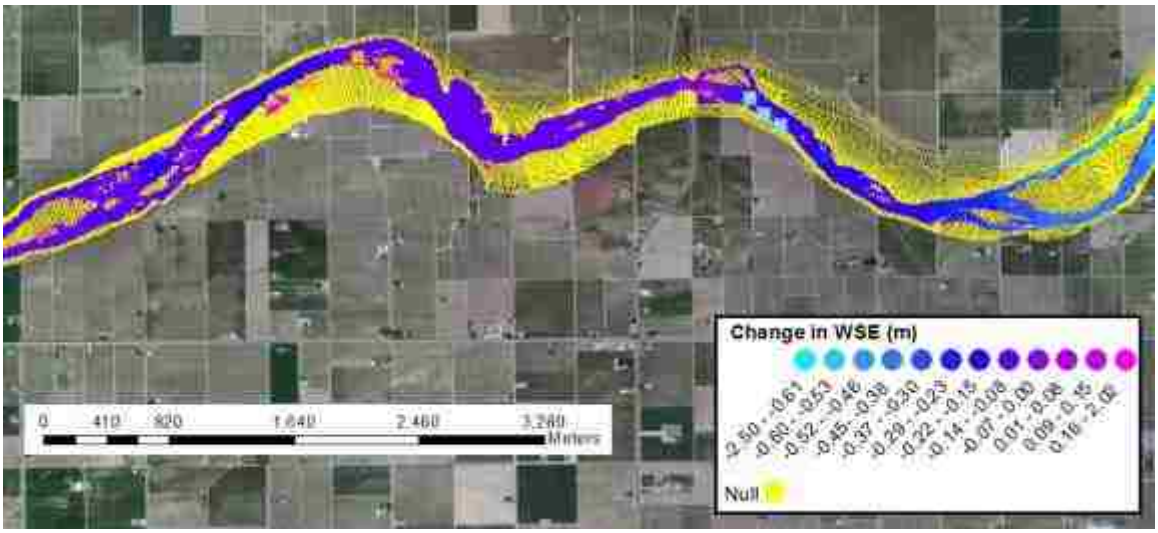

Figure 88: Change in water surface elevation at 113.3 m^3/s using the Järvelä approach near field sites 4 and 5

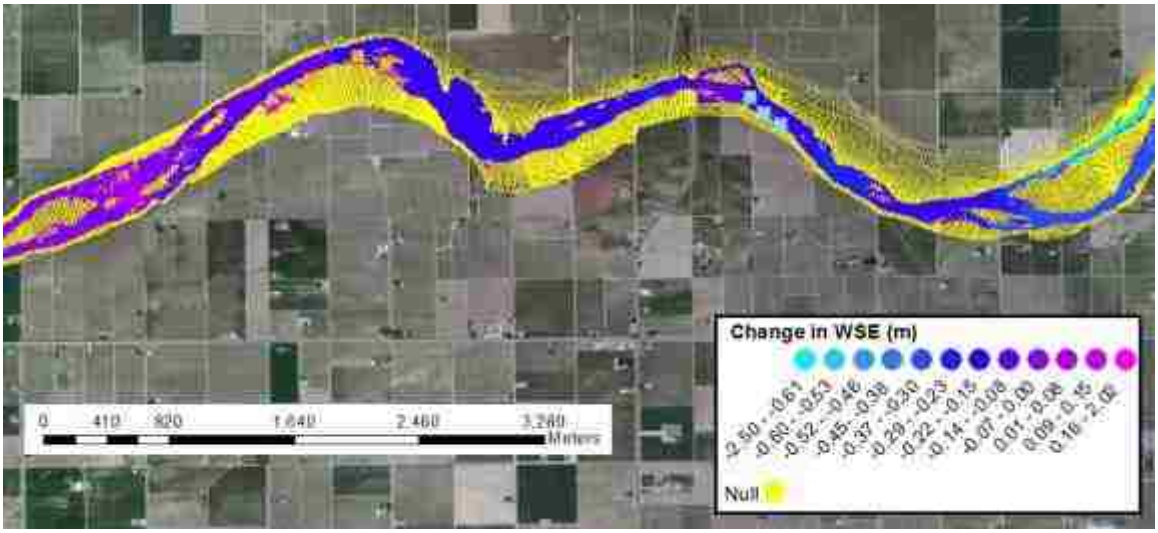

Figure 89: Change in water surface elevation at 113.3 m^3/s using the Baptist approach near field sites 4 and 5

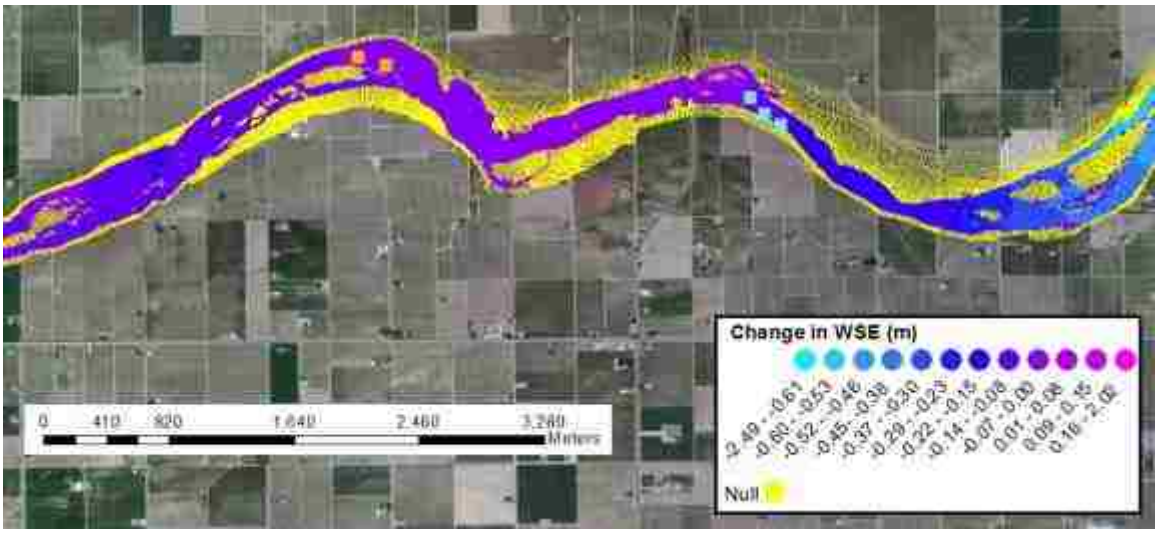

Figure 90: Change in water surface elevation at 212.4 m^3/s using the Järvelä approach near field sites 4 and 5

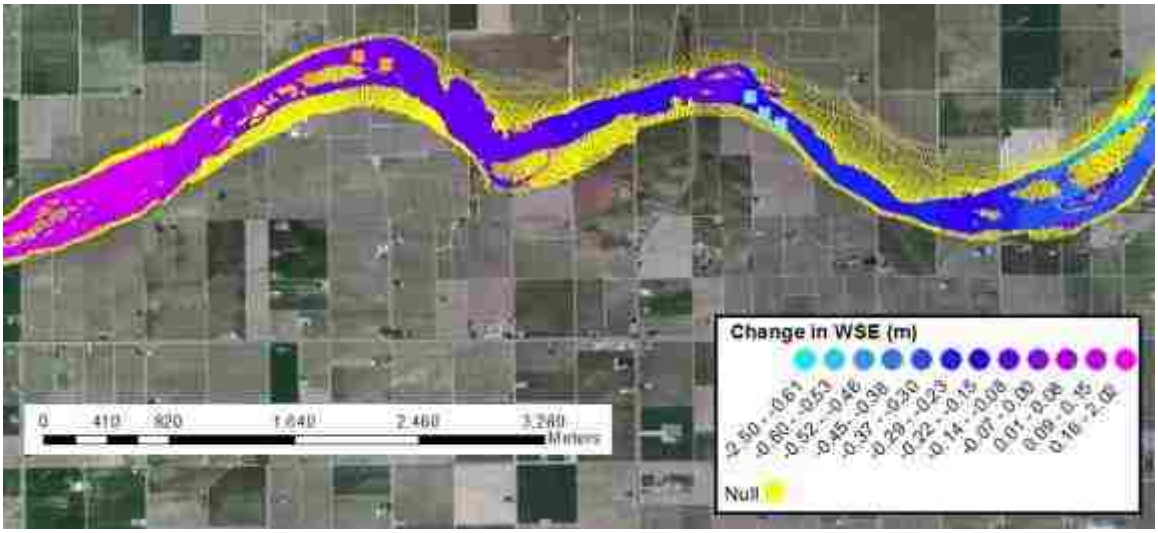

Figure 91: Change in water surface elevation at 212.4 m^3/s using the Baptist approach near field sites 4 and 5

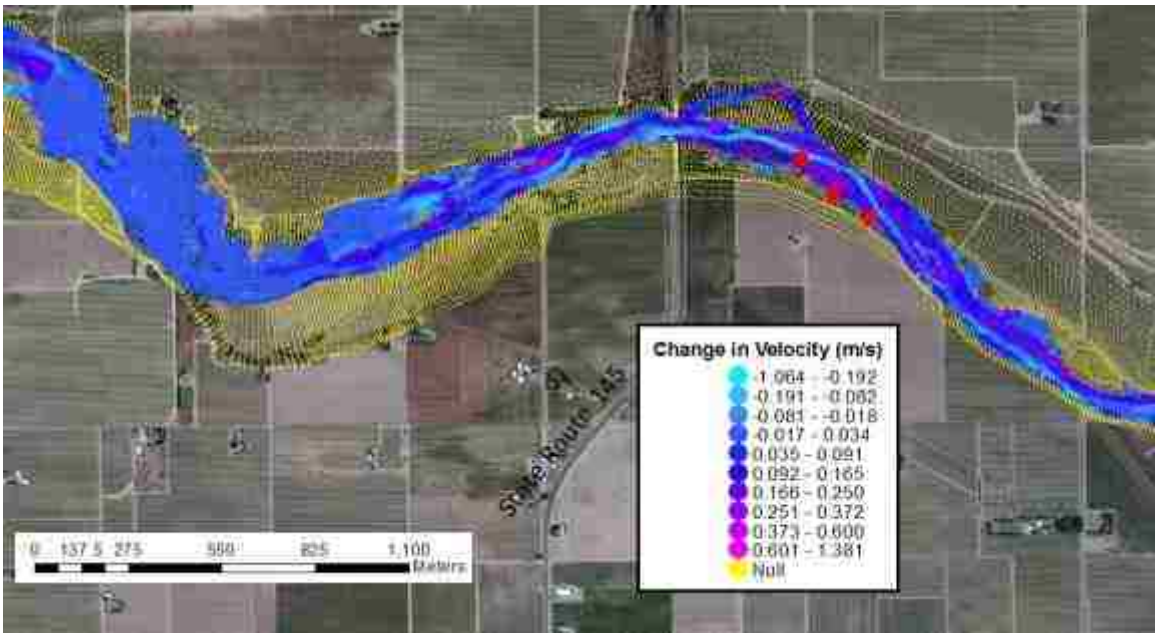

Figure 92: Change in velocity at 70.8 m^3/s using the Järvelä approach near field site 4

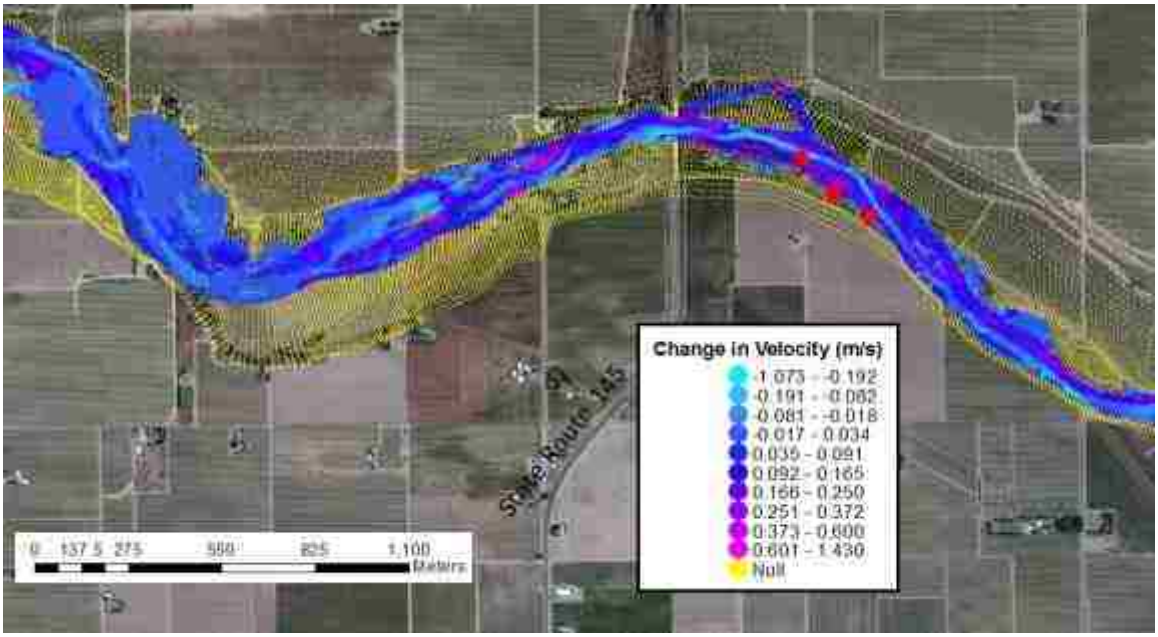

Figure 93: Change in velocity at 70.8 m^3/s using the Baptist approach near field site 4

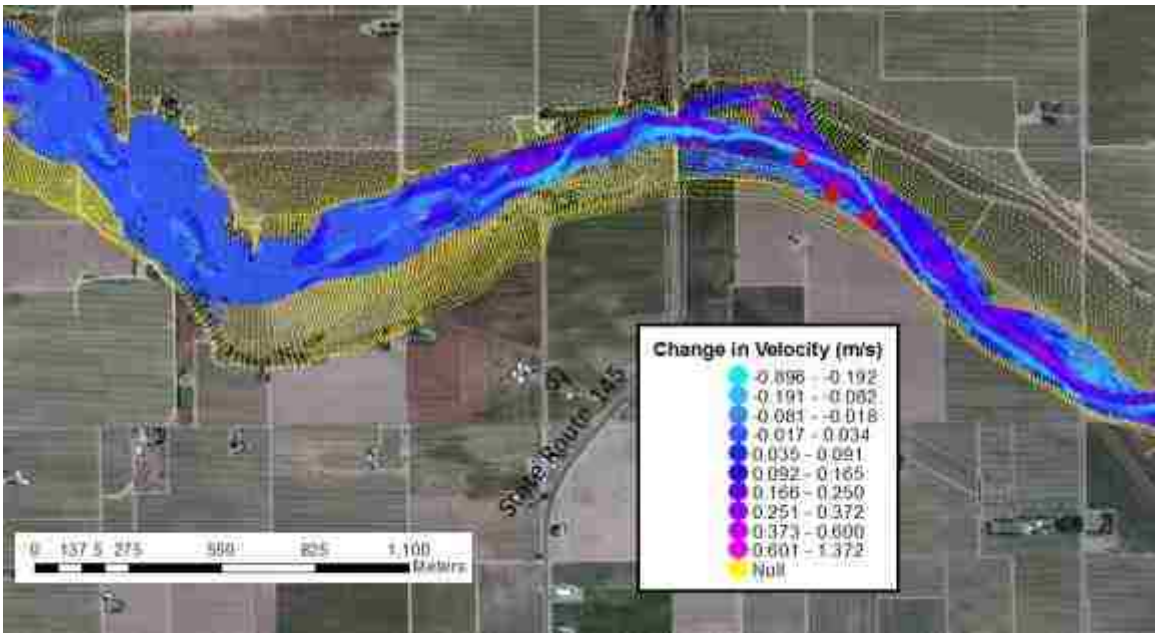

Figure 94: Change in velocity at 113.3 m^3/s with the Järvelä approach near field site 4

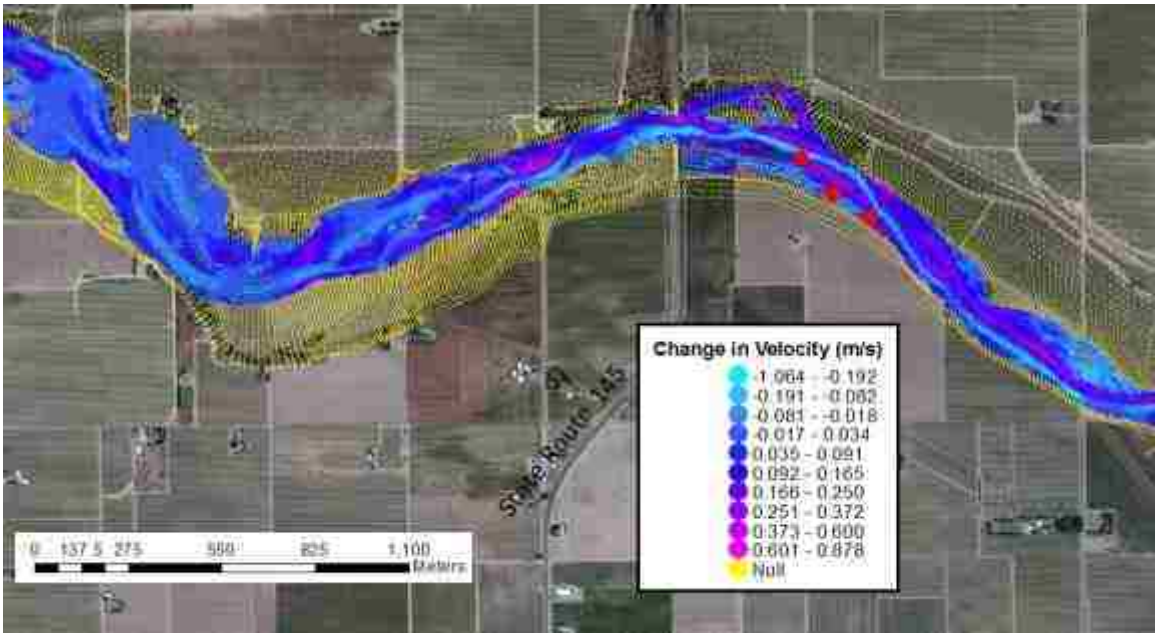

Figure 95: Change in velocity at 113.3 m^3/s with the Baptist approach near field site 4